DECEMBER 1968

EMPIRICAL DETERMINATION OF RADIATION INTERCHANGE FACTORS

Authors: R. P. Bobco and J. E. Rogers

Prepared for
NATIONAL AERONAUTICS AND SPACE ADMINISTRATION
MANNED SPACECRAFT CENTER
Houston, Texas

HUGHES
HUGHES AIRCRAFT COMPANY
SPACE SYSTEMS DIVISION

FINAL REPORT

NASA CONTRACT NAS 9-7548

NASA CR-101945

DECEMBER 1968

EMPIRICAL DETERMINATION OF RADIATION INTERCHANGE FACTORS

Authors: R. P. Bobco and J. E. Rogers

Prepared for
NATIONAL AERONAUTICS AND SPACE ADMINISTRATION
MANNED SPACECRAFT CENTER
Houston, Texas

HUGHES
HUGHES AIRCRAFT COMPANY
SPACE SYSTEMS DIVISION

FINAL REPORT

NASA CONTRACT NAS 9-7980

Principal Investigator R. P. Bobco
R. P. Bobco

Technical Monitor: R. E. Durkee

Hughes Project Manager Leo J. Nolte
Leo J. Nolte

CONTENTS

1.0 INTRODUCTION AND SUMMARY

Thermal design of spacecraft has been an art and a science based on computer analysis and space simulation tests. The analysis is reasonably straightforward insofar as conduction and radiation are the dominant modes of heat transfer. Conduction is well understood and most thermal designers have available to them both reams of data on physical properties and access to modest laboratory facilities for measuring analytically intractable coefficients for joint or contact conductances. Radiative heat transfer played a secondary role in thermal design until the mid-50's when space exploration became a reality. The notation and jargon of radiative transfer have always been arcane so that without a strong motivation based on design application, the study of radiation phenomena received scant attention among engineers. Even after a decade of intensive study, the analytical construction of radiation interchange factors remains as a tedious and irksome prelude to nodal analysis.

Many thermal designers have regarded radiative phenomena either with distaste or distrust or both. The distaste may be attributed to the difficulty of computing or measuring shape factors, finding surface properties, and inverting matrices. The distrust arises from the uncertainties associated with analytical models for emission/reflection (diffuse, specular, directional?), the accuracy of surface property measurements, and the difficulty of visualizing radiative transfer. As a group, spacecraft thermal designers have felt that it would be desirable to have a capability for measuring radiation interchange factors.

The measurement of radiation phenomena has been common practice for many years in the several technologies of applied optics: photography, illumination, and infrared detection. A recent application of optics technology to

spacecraft solar radiation measurements is reported in Reference 1 (see Appendix). In that paper, Bobco describes a technique for measuring local solar irradiation in a shirt-sleeve environment using scale models of spacecraft having real (prototype) surface finishes. Earlier studies by Bevans, el al (Reference 2) and Viskanta, et al (Reference 3) were concerned with the measurement of radiation phenomena, but their experiments were conducted in cold-walled vacuum chambers. These earlier experiments served to provide a basis for evaluating several analytical surface finish models, but their techniques were not convenient for measuring the radiant interchange between two surfaces in a multisurface enclosure.

The results reported here are an extension of the experimental procedure described in Reference 1. The discussion starts with the derivation of the analytical basis for measuring radiation interchange factors. It is shown that the script-F factor depends upon the ratio of energy absorbed at one surface to the energy emitted from another surface.

$$\mathcal{F}_{ki} = \frac{\tilde{\epsilon}_k \, \tilde{\epsilon}_i \, \tilde{G}_k^{(i)}}{\tilde{J}_{oi}}$$

where $\tilde{G}_k^{(i)}$ is the hemispherical flux incident at a surface A_k and which originates at A_i; $\tilde{J}_{oi}$ is the hemispherical flux originating at A_i (before interreflection); and $\tilde{\epsilon}_k$, $\tilde{\epsilon}_i$ are apparent hemispherical emittances. The results of a technology survey are presented in which procedures were sought for exciting and measuring radiant fluxes at surfaces. It is concluded that the only practicable procedure is one in which a surface, A_i, is excited remotely and the irradiation at another surface, A_k, is measured remotely.

The remaining discussion emphasizes the implementation of remote excitation/remote detection for measuring long wave (thermal) interchange factors because the feasibility of solar measurements is established in Reference 1. A procedure is described whereby local surface emission may be simulated by irradiating a small diffusely reflecting target with a beam (pencil) of long wave energy. More analysis is presented to show that single point or local excitation is adequate for many geometrical arrangements; the validity of superposition is proved for cases where multiple point excitation is required.

Off-the-shelf, commercially available equipment is described for implementing remote excitation/remote detection measurements of both thermal and solar radiation interchange factors. The remote excitation/remote detection concept is shown schematically in Figure 1.

Analysis is developed to examine the possibility of a spectral mismatch arising from the use of a beam of 1100°C blackbody energy to simulate surface excitation at 100°F. The analysis shows that a potential spectral mismatch may occur when two conditions exist simultaneously: 1) the direct view shape factor (e.g. F_{ki}) is less than or comparable to the "reflected view factor" (e.g. $F_{kj}F_{ji}$), 2) the reflecting surface (e.g. A_j) has a ratio of solar to thermal reflectances, $\tilde{\rho}_j^*/\tilde{\rho}_j$, which is appreciably different than unity (e.g., greater than two or less than one-half). A potential spectral mismatch can be identified and circumvented by using infrared lasers in addition to a blackbody source to excite a target area.

The rudiments of a facility are described for making reliable measurements of radiation interchange factors using scale models of spacecraft. A model holding fixture with three degrees of rotational freedom (e.g., roll, pitch, yaw) and a co-ordinate system scribed on a laboratory floor provide all of the dimensional data needed to obtain repeatable measurements. Finally, a two-phase development program is recommended to explore the accuracy and utility of the remote excitation/remote detection concept and to establish guidelines for a fully automated laboratory suitable for making "production line" measurements of radiative interchange factors.

It is recommended that the next phase be concerned with equipment procurement, exploratory measurements, and prototype demonstration. Experiments should be conducted with geometrically simple models with idealized surface finishes which are analytically tractable so that empirical results can be compared with predicted values without recourse to sophisticated analysis. Such a study would serve to develop laboratory techniques and procedures and define the limits of accuracy and application. A second experimental phase would apply the developed procedures to spacecraft models having more realistic geometries and surface finishes. This phase should be completed with detailed error analysis and documentation sufficient to establish the role of radiation interchange measurements as a useful thermal design tool.

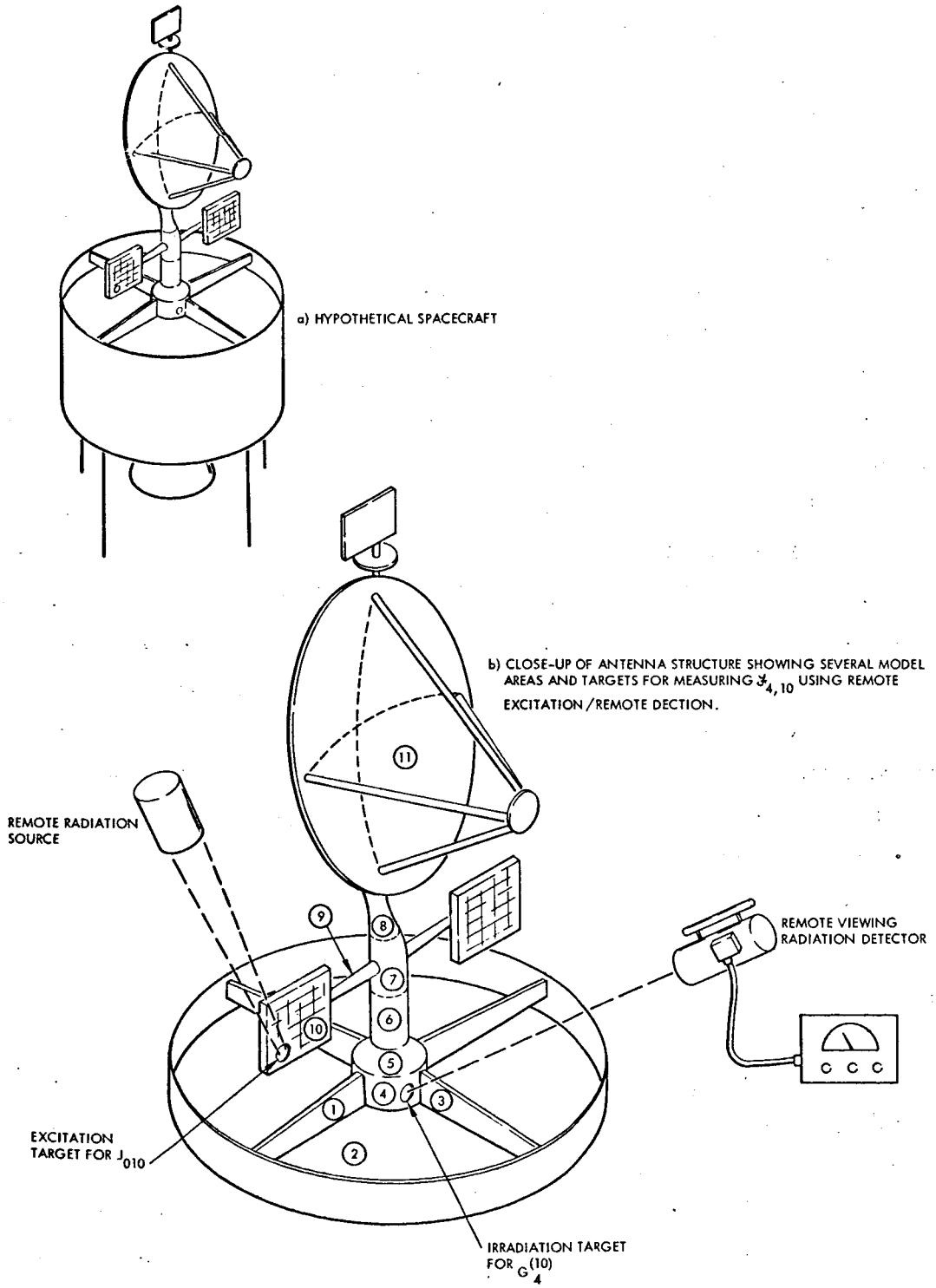

Figure 1. Remote Excitation/Remote Detection Concept

2.0 ANALYTICAL BASIS FOR RADIATION INTERCHANGE MEASUREMENTS

A procedure for obtaining radiative interchange factors from experimental measurements is described below. The analytical basis for the measurements is developed first for a conceptually simple enclosure in which all surfaces emit and reflect diffusely. The analysis is extended to enclosures which emit diffusely and reflect in a diffuse-plus-specular manner and finally to a system of surfaces which emit directionally and reflect bidirectionally. The analysis assumes gray surface properties, uniform irradiation, and uniform emission.

2.1 DIFFUSE ENCLOSURES

Consider an enclosure containing N surfaces which emit and reflect diffusely. The gross radiant flux leaving any surface is commonly called the radiosity and consists of emitted plus reflected energy. The radiosity is expressed as

$$J_k = J_{ok} + \rho_k G_k \quad \text{, power/unit area} \tag{1}$$

$$= J_{ok} + \rho_k \sum_{j=1}^{N} J_j F_{kj} \tag{2}$$

Inasmuch as "k" represents any surface in the enclosure, Equation 2 represents a linear set of algebraic equations which may be written as

$$\sum_{j=1}^{N} (\delta_{kj} - \rho_k F_{kj}) J_j = J_{ok} \quad , \quad k=1, 2, \ldots, N \tag{3}$$

in which the response vector J_j can be found in terms of the excitation vector J_{ok} and the inverted transfer matrix whose elements are β_{kj}. The solution of Equation 3 may be expressed as

$$J_k = \sum_{j=1}^{N} J_{oj}\, \beta_{kj} \tag{4}$$

where β_{kj} is the (kj)th element of the inverted transfer matrix.

Radiosity is not a convenient parameter for thermal designers who use nodal computer programs. It is possible to use the definition of net heat flux

$$q_{k,net} = J_k - G_k \quad , \text{ power/unit area} \tag{5}$$

to define a radiative interchange factor, $\mathcal{H}_{kj}$, so that

$$q_{k,net} = \sigma \sum_{j=1}^{N} \mathcal{H}_{kj} \left(T_k^4 - T_j^4\right) \quad , \text{ power/unit area} \tag{6}$$

The interchange factor may be computed as

$$\mathcal{H}_{kj} = \frac{\epsilon_k\, \epsilon_j}{\rho_k}\, \beta_{kj} \quad , \text{ dimensionless} \tag{7}$$

The diffuse (hemispherical) emittances ϵ_k, ϵ_j and the diffuse reflectance ρ_k are surface properties which are assumed known.

Although radiosity is not convenient as a thermal design parameter, it is a measurable quantity. By combining Equations 4 and 7 to eliminate β_{kj}, find

$$J_k = \frac{\rho_k}{\epsilon_k} \sum_{j=1}^{N} \frac{1}{\epsilon_j}\, J_{oj}\, \mathcal{H}_{kj} \tag{8}$$

a relationship between measurable quantities, J_k and J_{oj}, and a thermal design parameter, $\mathcal{H}_{kj}$. The interchange factor to some surface of interest, say A_i, may be found by setting

$$J_{oj} = 0 \quad , \begin{cases} j = 1, 2 \ldots, N \\ j \neq i \end{cases} \tag{9}$$

then from Equation 8

$$\mathcal{F}_{ki} = \left[\frac{\epsilon_k \epsilon_i}{\rho_k}\right] \frac{J_k}{J_{oi}} \tag{10}$$

Inasmuch as $J_{ok} = 0$, it follows from Equation 1 that

$$J_k = \delta_{ki} J_{oi} + \rho_k G_k^{(i)} \tag{11}$$

The superscript on the irradiation is used to denote that all of the energy incident at A_k originates at A_i. The interchange factor requires measuring the excitation, J_{oi}, and the irradiation $G_k^{(i)}$:

$$\mathcal{F}_{ki} = \epsilon_k \epsilon_i \left[\frac{G_k^{(i)}}{J_{oi}} + \frac{\delta_{ki}}{\rho_k}\right] \tag{12}$$

2.2 DIFFUSE-PLUS-SPECULAR ENCLOSURE, $\rho_k = \rho_k^d + \rho_k^m$

As a better approximation to real surface properties, it is sometimes assumed that surfaces emit diffusely and reflect in a diffuse-plus-specular manner. The concept of radiosity may be retained by limiting it to the gross <u>diffuse</u> radiant flux leaving a surface:

$$J_k = J_{ok} + \rho_k^d G_k \tag{13}$$

The irradiation must take into account both diffusely and specularly directed energy toward A_k. Instead of the shape factor, F_{kj}, it is necessary to use the exchange factor, ϕ_{kj} to account for specular incidence:

$$J_k = J_{ok} + \rho_k^d \sum_{j=1}^{N} J_j \phi_{kj} \quad , \quad k = 1, 2, \ldots, N \tag{14}$$

This equation represents a linear set which may be solved for the radiosity to obtain an expression equivalent to Equation 4. The only difference is that the transfer matrix contains ϕ_{kj} in place of F_{kj}.

The interchange factor of interest to designers may be expressed as

$$\mathcal{I}_{kj} = \frac{\epsilon_k \epsilon_j}{\rho_k^d} \beta_{kj} \tag{15}$$

The technique of single surface excitation may be used to measure the interchange factor to obtain a result comparable to Equation 12.

$$\mathcal{I}_{ki} = \epsilon_k \epsilon_i \left[\frac{G_k^{(i)}}{J_{oi}} + \frac{\delta_{ki}}{\rho_k^d} \right] \tag{12a}$$

2.3 REAL ENCLOSURES

The analysis for real surfaces becomes much more complex because it is necessary to account for the emergent direction of emission, the incident direction of absorption, and both incident and emergent directions of reflection. Bevans and Edwards developed the analytical approach for real surfaces in terms of radiative intensity, directional emittance and absorptance, and bidirectional reflectance. The gross radiative flux leaving a surface A_k and directed toward a surface A_w consists of emitted and reflected components

$$\pi I_{kw} = \mathcal{J}_{okw} + \sum_{j=1}^{N} r_{jkw} \pi I_{jk} F_{kj} \tag{16}$$

A psuedo-radiosity, $\mathcal{J}_{kw}$, may be introduced to provide an analog to Equation 2:

$$\mathcal{J}_{kw} = \mathcal{J}_{okw} + \sum_{j=1}^{N} r_{jkw} \mathcal{J}_{jk} F_{kj} \quad , \begin{cases} k = 1, 2, \ldots, N \\ w = 1, 2, \ldots, N \end{cases} \tag{17}$$

where $\mathcal{J}_{kw} = \pi I_{kw}$, etc. The hemispherical flux leaving A_k may be thought of as radiosity

$$\tilde{J}_k = \sum_{w=1}^{N} \mathcal{J}_{kw} F_{kw} = \tilde{J}_{ok} + \tilde{\rho}_k \tilde{G}_k \tag{18}$$

where the tilde is used to denote that the parameters are not diffuse. That is

$$\tilde{J}_{ok} = \sum_{w=1}^{N} \varepsilon_{okw} F_{kw} \tag{19a}$$

$$\tilde{G}_{k} = \sum_{j=1}^{N} \alpha_{jk} F_{kj} \tag{19b}$$

$$\tilde{\rho}_{k} = \frac{\sum_{w=1}^{N} \sum_{j=1}^{N} r_{jkw} \alpha_{jk} F_{kj} F_{kw}}{\sum_{j=1}^{N} \alpha_{jk} F_{kj}} \tag{19c}$$

$$= \sum_{w=1}^{N} \rho_{kw} F_{kw} \tag{19d}$$

The hemispherical-directional reflectance, ρ_{kw}, is introduced in Equation 19d.

Equation 17 represents a set of N^2 linear equations which may be solved by inverting a transfer matrix whose elements are

$$\delta_k^{\ i} - r_{kwj} F_{wk} \delta_w^{\ j}$$

The Kronecker delta is written with superscripts and subscripts. The pair of indices (ij) refer to a row, while (kw) identify a column in the transfer matrix. The solution may be expressed as

$$\varepsilon_{kw} = \sum_{p=1}^{N} \sum_{\ell=1}^{N} \varepsilon_{op\ell} \beta_{kw}^{\ p} \tag{20}$$

where $\beta_{kw}^{\ p}$ is an element in the inverted transfer matrix occupying the (kw)th row and (pℓ)th column.

The net heat flux may be expressed as the difference between the emergent flux (apparent radiosity) and the incident flux

$$q_{k,net} = \tilde{J}_k - \tilde{G}_k \tag{21}$$

or the difference between hemispherically emitted flux ($\tilde{J}_{ok}$) and absorbed flux

$$q_{k,net} = \tilde{J}_{ok} - \tilde{\alpha}_k \tilde{G}_k \tag{22}$$

where

$$\tilde{\alpha}_k \tilde{G}_k = \sum_{j=1}^{N} \alpha_{kj} \vartheta_{jk} F_{kj} \tag{23}$$

The gray body assumption yields

$$\alpha_{kj} = \epsilon_{kj} \tag{24}$$

Using thermodynamic arguments, the interchange factor may be found from either Equation 21 or 22. Equation 21 yields

$$\mathcal{F}_{kj} = \frac{\tilde{\epsilon}_k}{\tilde{\rho}_k} \sum_{w=1}^{N} F_{kw} \eta_{\substack{kw \\ j}} \tag{25a}$$

while Equation 22 gives

$$\mathcal{F}_{kj} = \sum_{w=1}^{N} \epsilon_{kw} F_{kw} \eta_{\substack{wk \\ j}} \tag{25b}$$

where

$$\eta_{\substack{ab \\ j}} = \sum_{p=1}^{N} \epsilon_{jp} \beta_{\substack{ab \\ jp}} \tag{26}$$

When the excitation, $\vartheta_{op\ell}$, occurs as a result of temperature, it is the product of directional emittance and the black body emissive power.

$$\vartheta_{ojp} = \epsilon_{jp} E_p \tag{27}$$

Equation 27 may be introduced in Equation 20 to obtain

$$\mathcal{J}_{wk} = \sum_{j=1}^{N} E_j \eta_{\substack{wk \\ j}} \tag{28}$$

where use was made of Equation 26.

When only a single surface, j = i, is excited, Equation 28 yields

$$\eta_{\substack{wk \\ i}} = \frac{{}^{(i)}_{wk}}{E_i} \tag{29}$$

which may be introduced in Equation 25b to give the result

$$\underset{\sim}{4}_{ki} = \frac{1}{E_i} \sum_{w=1}^{N} \epsilon_{kw} \, {}^{(i)}_{wk} \, F_{kw} \tag{30}$$

Making use of Equations 23 and 24 and the result implicit in 19a and 27 that

$$\tilde{J}_{oi} = \tilde{\epsilon}_i \, E_i \tag{31}$$

it follows that

$$\underset{\sim}{4}_{ki} = \frac{\tilde{\epsilon}_k \, \tilde{\epsilon}_i \, \tilde{G}^{(i)}_k}{\tilde{J}_{oi}} \tag{32}$$

If Equations 25a and 19 are used to relate fluxes and interchange factors, then the term $\tilde{\epsilon}_k^2 \, \delta_{ki}/\tilde{\rho}_k$ is added to the right side of 32 to obtain an expression corresponding to Equations 12 and 12a. The dual nature of the self-interchange factor has been observed before (Reference 6), and further discussion follows below with an important application shown in subsection 4.2.

2.4 SELF-EXCHANGE FACTORS

The self-interchange factor is ordinarily of no importance in thermal analysis because q_{kk} is necessarily zero. However, $\mathcal{G}^*_{kk}$ is vital to the computation of solar interchange; it also has an important role in the empirical determination of radiant interchange factors.

Two different self-interchange factors can be derived from the same expression for net heat flux. The analysis preceding Equation 32 above gives insight to the difference. This summary identifies the differences in more detail. A comparison of the factors is given below:

Radiosity Approach	Irradiation Approach
$q_{k,net} = \tilde{J}_k - \tilde{G}_k$	$q_{k,net} = \tilde{J}_k - \tilde{G}_k$
$= \frac{\tilde{\epsilon}_k}{\tilde{\rho}_k}\left(\sigma T_k^4 - \tilde{J}_k\right)$	$= \epsilon_k\left(\sigma T_k^4 - \tilde{G}_k\right)$
$\sum_{j=1}^{N} \mathcal{F}_{kj} = \tilde{\epsilon}_k/\rho_k$	$\sum_{j=1}^{N} \mathcal{F}_{kj} = \tilde{\epsilon}_k$
$\mathcal{F}_{kj} = \tilde{\epsilon}_k\,\tilde{\epsilon}_j\left[\frac{\tilde{G}_k^{(j)}}{\tilde{J}_{oj}}\right], \begin{cases} j=1,2,\cdots,N \\ j\neq k \end{cases}$	$\mathcal{F}_{kj} = \tilde{\epsilon}_k\,\tilde{\epsilon}_j\left[\frac{\tilde{G}_k^{(j)}}{\tilde{J}_{oj}}\right], \begin{cases} j=1,2,\cdots,N \\ j=k \end{cases}$
$\mathcal{F}_{kk} = \frac{\tilde{\epsilon}_k^2}{\tilde{\rho}_k}\left[\frac{\tilde{J}_{ok} + \tilde{\rho}_k\,\tilde{G}_k^{(k)}}{\tilde{J}_{ok}}\right], \; j = k$	

The two different self-interchange factors are related as

$$\mathcal{F}_{kk\,(\text{irradiation})} = \mathcal{F}_{kk\,(\text{radiosity})} - \frac{\tilde{\epsilon}_k^2}{\tilde{\rho}_k} \tag{33}$$

The radiosity self-interchange factor has been suggested for use in solar interreflection analysis (Reference 6) because the excitation term is

$$\tilde{J}_{ok} = \tilde{\rho}_k\, C_{s,k}\, S$$

and the radiosity $\mathcal{F}_{kk}$ accounts for both the direct solar irradiation and the hemispherically reflected solar flux. The irradiation self-interchange factor accounts for the hemispherically reflected flux only.

It should be observed that the radiosity self-interchange factor is always greater than unity, while the irradiation self-interchange factor is always less than unity. This disparity has been difficult to explain from purely algebraic considerations; with the physical interpretation presented above, it is obvious that both factors are correct and the laws of thermodynamics remain inviolate.

2.5 CONCLUDING REMARKS

This analysis has shown how a radiation interchange factor may be formulated in terms of two measurable quantities. In principle, it is possible to measure both the emergent flux at the single excited surface, $\tilde{J}_{oi}$, and the absorbed flux at any surface, $\tilde{\epsilon}_k \tilde{G}_k^{(i)}$. However, in practice, it is more convenient to measure an incident flux, $\tilde{G}_k^{(i)}$, than the absorbed flux. In deference to practicability, the experimental technique will be identified as "the $\tilde{G}_k^{(i)}/\tilde{J}_{oi}$ algorithm." The remainder of this report deals with problems that arise in implementing the algorithm.

Finally, it is important to note that, in a real surface enclosure, the product $\tilde{\epsilon}_k \tilde{G}_k$ represents a mean value with respect to direction. The apparent hemispherical absorptance, $\tilde{\epsilon}_k$, is defined as a mean value which has been "weighted" for radiant flux incident from all directions. The hemispherical absorptance which is commonly used in thermal analysis is based on uniform irradiation (i.e., equal weighting) from all directions. It is possible to imagine a surface, A_k, with strong directional absorptance irradiated in a small angular field so that "apparent" and "common" hemispherical absorptances could be different. The remaining discussion will not make any distinction among the several interpretations of hemispherical properties; it will be assumed that the differences are of second-order importance.

3.0 TECHNOLOGY SURVEY

A simple algorithm was developed in the preceding section that provides the basis for measuring radiation interchange factors. The result may be interpreted in terms of either gray (total) or monochromatic interchange. In order to apply the $\tilde{G}_k^{(i)}/\tilde{J}_{oi}$ algorithm to the thermal design of spacecraft, a technology survey was made of several scientific and engineering disciplines to identify procedures for exciting radiation and measuring radiant flux at surfaces. Any given scheme was judged feasible if it were capable of being carried out and practicable if the implementation and execution could be done easily and conveniently for an experimentalist.

In assessing the utility of any given scheme, it was assumed that model spacecraft would be used that were both geometrically and radiatively similar to some functional spacecraft of interest. It was assumed that the models would range in scale from 0.1 to 1.0 of full size, the models might have a maximum dimension in the range 1.0 to 10 feet, and they might weigh between 1.0 and 500 pounds. Ideally, measurements should be made in a shirt-sleeve environment and the data should be in terms of total rather than spectral (monochromatic) fluxes. Recognition was given also to the thermal designers need for both thermal and solar radiant interchange factors. Finally, it was postulated that extreme precision was not required for most thermal design applications; the accuracy of a measured value of $\tilde{G}_k^{(i)}/\tilde{J}_{oi}$ should be comparable to the accuracy of measuring reflectance in an integrating sphere or heated hohlraum (Reference 1), or of measuring a shape factor with a globoscope.

3.1 SURVEY OR EXPERIMENTAL TECHNIQUES

Two approaches were considered in the survey of experimental techniques for the empirical determination of radiation interchange factors:

1) Analog methods

2) Electromagnetic radiation methods

The survey of analog methods was based on the application of Fredholm's integral equation of the second kind to physical disciplines not directly related to radiative transfer. The survey of experimental techniques used in nonthermal radiative transfer encompasses the full spectrum from particulate radiation to radio-wave propagation.

Analog Methods

A brief literature search was made of various fields of mathematical physics in an attempt to learn of applications of linear integral equations to problems not related to radiative transfer. There are a number of problems in which the propagation of a field depends on the values of the field at some distance from a location of interest, not just on values at neighboring points. Governing principles for such fields may be formulated in terms of integral equations or integrodifferential equations which may be reduced to integral equations. Several examples are given in Reference 4 from molecular transport theory, acoustics, and quantum mechanics. In addition to these cases, many differential equations may be expressed as integral equations by the introduction of Green's functions (e.g., the Sturm-Liouville problem).

In many instances, these equations of mathematical physics may be reduced to the form of a Fredholm integral equation of the second kind. Furthermore, most of the physical systems described by integral equations can be either simulated or duplicated in a laboratory. Unfortunately, no complete mathematical analog could be found to the radiant intensity equation,

$$I(\vec{r}, \vec{\Omega}) = \epsilon(\vec{r}, \vec{\Omega}) I_b(\vec{r}) + \int_{\Omega_i} f(\vec{r}, \vec{\Omega}, \vec{\Omega}_i) I(\vec{s}, \vec{\Omega}_i) \cos\theta_i \, d\omega$$

In the absence of a mathematical analog, the survey of experimental methods used in nonradiative problems of "action at a distance" was discontinued. It should not be construed that no analog exists, only that none could be identified in this study.

Electromagnetic Radiation Considerations

The survey of experimental methods used in electromagnetic propagation probed a variety of related disciplines in physics and engineering: 1) nuclear transport, 2) illumination, 3) photography, 4) infrared technology, 5) radiative heat transfer, 6) radio-wave propagation.

The $\tilde{G}_k^{(i)}/\tilde{J}_{oi}$ algorithm was used in an attempt to identify different techniques and equipment for exciting surfaces and measuring radiant energy absorbed or incident at surface while maintaining geometrical and emissive/reflective similarity of prototype and model enclosures.

The application of nuclear radiation (including X-rays) to the measurement of radiant interchange factors was judged not feasible for several reasons:

1) Nuclear particles would not interact with surfaces in a simple reflection or absorption mode. It would be necessary to account for particle transmission and secondary emission at all surfaces.

2) The spectral distribution of a beam of nuclear particles would occupy a narrow wave band which would not be a reasonable approximation of either the solar spectrum or a black-body spectrum of a surface in the temperature range -100 to +200°F.

3) The health hazard associated with nuclear radiation would create many problems in handling models and equipment.

Radio-wave radiation, lying at the opposite end of the spectrum from nuclear radiation, is also believed to be not feasible for measuring radiant interchange factors of interest to spacecraft thermal designers. The radio wavelengths span the spectrum from about 10^3 to 10^{11} microns. The primary reason for the lack of feasibility is the difficulty of simulating surface reflection characteristics (solar and thermal) to incident long wave ($>10^2$ microns)

radiation. Dielectric surfaces tend to transmit radio waves, while conductive surfaces tend to absorb them. When reflection does occur, radio waves tend to reflect specularly unless surface irregularities (roughness) are of the same magnitude as the wavelength of the incident energy. The monochromatic nature of radio transmission and problems of wave diffraction around surfaces are additional difficulties which make radio-wave radiation generally unattractive for thermal design applications. The single thermal application that might prove susceptible to radio-wave measurements is that of interchange between surfaces at extreme cryogenic temperatures (less than 100°R).

The field of applied optics dealing with illumination provided the techniques and equipment used in early studies of radiant interchange measurement at Hughes (1964). Although illumination is spectrally limited to the waveband of human visual response (about 0.4 to 0.7 micron), and many of the experimental methods and devices used to measure of solar radiation may be adapted to the measurement of solar radiation (about 0.2 to 4.0 microns) and thermal radiation (say, 1.0 to 30 microns). The results reported by Bobco (Reference 1) demonstrate the feasibility of using off-the-shelf equipment for measuring local solar irradiation on model spacecraft. A modification of the technique for measuring thermal radiant interchange is described below. It appears that the only technologies which can be used to measure thermal and solar radiant interchange parameters are those of applied optics (illumination, photography, infrared) and heat transfer.

A number of feasible measurement schemes are described below, but not all of them are practicable. It appears to be feasible to duplicate both boundary conditions and surface properties in order to obtain the absorbed to excited flux ratio $\tilde{\alpha}_k \tilde{G}_k^{(i)}/\tilde{J}_{oi}$. However, it is practicable to simulate boundary conditions or surface properties or both insofar as it is then more convenient to measure the fluxes of interest. It does not appear feasible to simulate surface properties. The remaining discussion distinguishes between thermal interchange factors, $\mathcal{F}_{ki}$, and solar interchange factors, $\mathcal{F}^*_{ki}$, because it does not appear to be possible to use the same experiments to make simultaneous measurements in the different wave bands.

Thermal Radiant Interchange

An experiment based on duplication of boundary conditions and surfaces is described by Viskanta, Schornhorst, and Toor (Reference 3). A model consisting of two plane surfaces was tested in a cold-walled vacuum chamber. The surfaces were heated electrically and temperatures were measured at both surfaces. Local irradiation was measured at one surface using calibrated radiometers mounted behind small apertures in the surface. In this regard, the experiment was not concerned with the absorbed flux which is the parameter of importance to the thermal designer.

It would be possible to use this same kind of test with a model spacecraft to obtain $\tilde{G}_k^{(i)}/\tilde{J}_{oi}$ data by heating one surface at a time and measuring local irradiation at all other surfaces. The experiment would require great care in design and fabrication of the model in order to eliminate (or account for) conduction and to minimize the time required to reach a steady state when changing from one excited surface to another. Other disadvantages of this type of duplication include the requirement of a cold-walled vacuum chamber and the associated difficulty of making minor changes to the model during the course of a test.

An experimental procedure exists in which surface finishes are duplicated but surface excitation is simulated: A small diffusely reflecting target lying on the surface of the excitation area is irradiated by a pencil of infrared energy to simulate diffuse emission from that location. The irradiation at other surfaces may be determined by using a second diffusely reflecting target on a surface of interest and measuring the reflected energy with a remote viewing radiometer. Insofar as the scheme is not based on measuring temperature, the experiment may be performed in a shirt-sleeve environment, and the model may be designed and fabricated without regard to conduction or convection heat losses. This scheme has the disadvantage of requiring multiple placement of the excitation target. The differences between diffuse reflection and directional emission may be reconciled by an analytical study and do not detract from the feasibility (or practicability) of the method.

This scheme of remote excitation/detection is well-suited to measuring radiant interchange phenomena between exterior surfaces of a spacecraft, and it appears feasible to adapt it between interior surfaces, as well. Interior model systems could be fabricated with a number of small removable panels in each nodal area. An excitation element (target) could be achieved by replacing a panel with a translucent diffuse material which would be irradiated externally. A reflecting irradiation target could be placed anywhere in the enclosure and viewed through a small aperture (a second removable panel) to obtain a measurement. Obvious variations to this procedure include the use of a reflecting target, instead of a transmitting target, irradiated through a small aperture or the elimination of a reflecting irradiation target by measuring the flux emerging from an irradiated aperture.

A third scheme combines features of the two procedures mentioned above and appears to be feasible. The diffuse excitation target used for external beam irradiation may be replaced by a small electric heating element whose radiating surface is identical to the excitation area material. The experiment could be performed in a one atmosphere environment under the following conditions:

1) The heater element must be insulated from the bulk area which constitutes the excited surface.

2) All model surfaces must be isothermal; only the small heated excitation area can be at an elevated temperature.

3) The background radiation must be suppressed in order to discriminate between signal (excitation area radiation) and noise (model and surroundings radiation).

Each of the three conditions requires a period of trial and error to develop workable components, techniques, and operational sequences. The problem of signal and noise discrimination represents the only conceptual impediment to the successful implementation of this scheme. For example, it may be impossible to distinguish between the signal from a low-emittance high-temperature source and a high-emittance low-temperature background.

There are numerous combinations of techniques and instruments available for exciting surfaces and measuring radiant flux, but all of them can be related to the three schemes described above.

Solar Radiant Interchange

The distinction between duplication and simulation is less severe insofar as measurement of solar interchange factors is concerned. That is, all surfaces may be duplicated and the simulation is confined to the choice of a collimated source of radiant energy. The radiant sources available to the thermal designer include the sun (Reference 1), various short arc lamps used for solar simulation, or common light sources used for illumination or photography. The basic procedure is described in Reference 1, where it is observed that there is no need to duplicate the zero air-mass solar flux because the measurements are based on relative flux rather than temperature. If the sun is used as the radiant source, it is necessary to use field stops and/or reflective optics to mask off the irradiation from all model regions except the excited surface. Signal and noise discrimination may be achieved by making successive measurements of signal plus noise and noise alone. If an artificial radiant beam is employed, it is still necessary to excite only one surface at a time, but a chopper may be used to discriminate between signal and noise. Whether the sun is real or simulated, the procedure requires direct excitation of a real surface rather than a diffusely reflecting target, as in the case of thermal interchange measurements.

The results reported in Reference 1 suggest that spectral duplication is not vital to measurement of solar interchange phenomena. Spectral matching is desirable, but the use of any radiant source that is essentially white in the visible waveband (0.4 to 0.7μ) should be suitable for most spacecraft surfaces.

3.2 SURVEY SUMMARY

At the start of this survey, it was hoped that two independent candidate techniques would be found to be practicable for the empirical determination of radiation interchange factors. Only one candidate emerged from the study — the technique of remote excitation and remote detection. This single technique is believed to be practicable for both thermal and solar measurements with different equipment required for the two wavebands.

The remaining discussion emphasizes the measurement of thermal, rather than solar, radiant interchange parameters. The results reported in Reference 1 virtually ensure that solar interchange can be measured to any degree of accuracy desired. The thermal interchange measurements require additional analysis and justification to demonstrate that the remote excitation/remote detection scheme is practicable.

4.0 REMOTE EXCITATION AND REMOTE DETECTION

A brief description of the remote excitation/remote detection technique is given in Section 3.0, but the practicability of the method can not be demonstrated without additional attention to details. This section develops a more detailed analytical basis for obtaining $\tilde{G}_k^{(i)}/\tilde{J}_{oi}$, discusses off-the-shelf hardware, and identifies some potential limitations associated with equipment characteristics.

The implementation of experimental methods for obtaining radiant interchange factors requires the following:

1) Knowledge of the hemispherical surface emittances of the various surfaces, $\tilde{\epsilon}_k$ and $\tilde{\epsilon}_i$.

2) A technique for measuring the hemispherical incident flux at any surface, $\tilde{G}_k$.

3) A technique for exciting one surface at a time and measuring the hemispherical emergent flux, $\tilde{J}_{oi}$.

The measurement and computation of hemispherical emittance is a science which has received considerable attention since the mid-'50's and will not be considered in this discussion. The measurement of hemispherical irradiation is conceptually straightforward; the only requirement is a detector which is both small relative to the nodal surface of interest and free of directional sensitivity. The term "free of directional sensitivity" is used here to identify a component of a detection system which is diffusely absorbing, transmitting, or reflecting. The smallness is required to prevent the detector from having a strong radiative interaction with the surroundings while the directional sensitivity must be avoided in order to obtain a diffuse (hemispherical)

measurement. A variety of detectors may be used depending on the waveband of interest; these include illuminometers, photographic film under a diffuse cover glass, diffuse targets viewed from remote locations by photometers or radiometers, photon sensitive devices such as solar cells or CdS wafers under diffuse cover glass, or even a small aperture in the surface backed by an integrating sphere and its associated detector.

The problem of single-surface excitation and its measurement represents the only conceptual impediment to obtaining a radiative interchange factor by experimental means. The nature of the problem differs with the waveband of interest insofar as solar excitation is conceptually different from thermal excitation. Solar excitation is proportional to the product of the collimated solar flux and an incidence factor, $SC_{s,k}$, while thermal excitation is proportional to the total blackbody emissive power, σT_k^4. Solar excitation of a single surface may be simulated with comparative ease using a collimating projection system and a lamp source with appropriate spectral characteristics. It is not necessary to duplicate the magnitude of the solar constant, S, for the measurement of interchange phenomena. Thermal excitation is more difficult to achieve because conduction and convective heat transfer can obscure the radiative exchange.

Thermal excitation of a single surface may be attained either by duplication or simulation. Duplication requires heating the surface of interest while cooling all other surfaces and controlling convection and conduction. Surface heating may be accomplished by bonding electric heater blankets or heat exchangers to the back of a surface. In principle, all other surfaces could be maintained at cryogenic temperatures to minimize "noise," but in practice, such a procedure would be difficult to implement. Convection could be eliminated by testing in a vacuum and conduction could be minimized by careful design and fabrication of surface interfaces. Alternately, it might be possible to make measurements in a shirtsleeve environment by making transient measurements of the excited surface temperature, the irradiation at other surfaces, and then correlate data on an instantaneous basis.

Thermal excitation by simulation can be accomplished in a variety of ways. Equation 1 is repeated for convenience

$$\mathcal{F}_{ki} = \frac{\tilde{\epsilon}_k \, \tilde{\epsilon}_i \, \tilde{G}_k^{(i)}}{\tilde{J}_{oi}} \tag{1}$$

The excitation, $\tilde{J}_{oi}$, is a hemispherical flux and should be associated with a spectral waveband; however, it is not necessary to associate $\tilde{J}_{oi}$ with the emittance $\tilde{\epsilon}_i$. If duplication is required then

$$\tilde{J}_{oi} = \tilde{\epsilon}_i \, \sigma T_i^4 \tag{2}$$

but a collimated input may be used instead as

$$\tilde{J}_{oi} = \tilde{\rho}_i \, \mathcal{S} C_{s,i} \tag{3}$$

Two obvious conditions must be fulfilled to make this type of simulated thermal excitation acceptable:

1) The collimated flux, $\mathcal{S}$, must have the same wavèband characteristics implied by σT_i^4.

2) The directional reflectance must have the same characteristics as directional emittance; that is

$$\tilde{\rho}_i = K \, \tilde{\epsilon}_i \quad , \quad \text{(hemispherical)} \tag{4}$$

and

$$\rho_{iw} = K \, \epsilon_{iw} \, , \quad \text{(directional)} \tag{5}$$

where

$$\tilde{\epsilon}_i = \frac{1}{\pi} \int_{(2\pi)_{\text{emergent}}} \epsilon_{i,\theta} \cos\theta \, d\omega$$

$$\tilde{\rho}_i = \frac{1}{\pi} \int_{(2\pi)_{\text{emergent}}} \rho_{i,\theta} \cos\theta \, d\omega$$

K = constant

The collimated input of $\mathcal{S}$ on A_i must be redistributed in the same directions as flux emitted from A_i. The type of simulation implied above amounts to virtual duplication and as such represents a nearly ideal situation which may not be attainable.

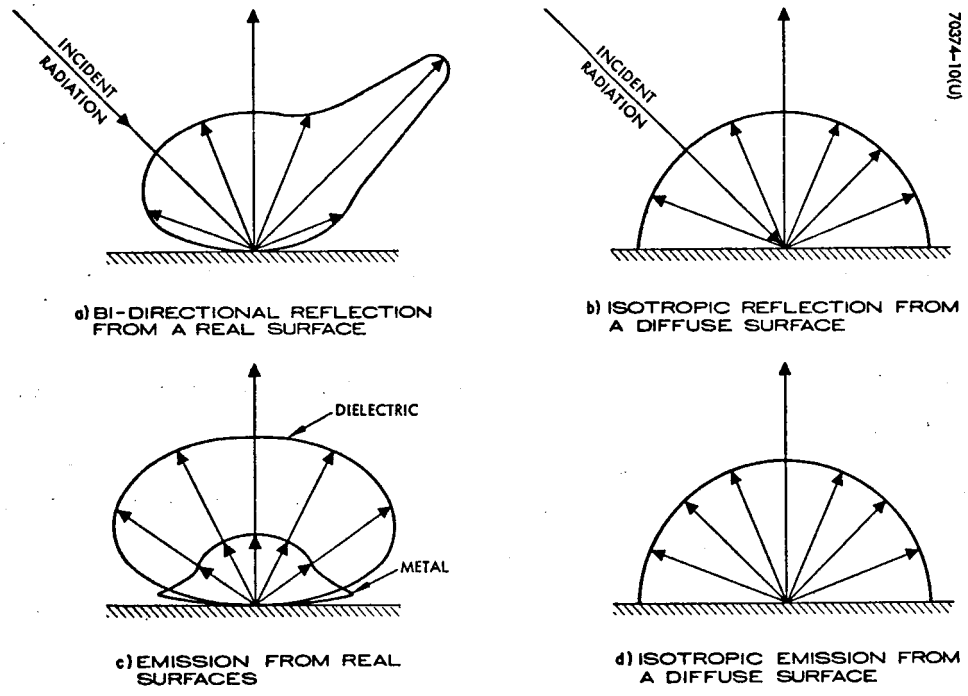

Figure 2. Schematic Comparison of Reflection and Emission From Real and Ideal (Diffuse) Surfaces

The virtual duplication of thermal excitation by use of a collimated IR input serves as a point of departure for purposes of engineering design simulation. As the next step, it may be observed that

1) If A_i were a diffuse emitter and a diffuse reflector, Equation 1 would be satisfied.

2) The emittance of real surfaces tends to be diffuse.

Directional characteristics of real and ideal surfaces appear in Figure 2. From these observations, it is tempting to conclude that the surface A_i should be made a diffuse reflector in order to approximate the directional emittance of its real prototype. This type of surface simulation appears to represent a reasonable compromise with virtual duplication; it has the advantage of completely eliminating the product $\tilde{\rho}_i \, C_{s,i}$ from both numerator and denominator of Equation 1. Its greatest disadvantage is that the true bidirectional reflective character of A_i may be destroyed even if the magnitude of hemispherical reflectance is preserved.

The error induced in substituting a diffusely reflecting surface for a real (bidirectional) surface is an analytically tractable quantity. A geometry of interest may be postulated and solved for real surface properties and for one surface having a diffuse reflectance. Unfortunately, such an error analysis is beyond the scope of the present study.

Another compromise for the sake of implementing single surface excitation with a collimated input involves the use of a small portion of A_i as a diffuse reflector while preserving the real reflective properties everywhere else. This approach violates the assumption of uniform excitation, but the error may be eliminated by repeating measurements with the source moved to several locations on A_i. [NOTE: A double integration over a source area and a sink area is required to change "local" exchange factors to "area mean" exchange factors. The assumption of uniform irradiation and excitation eliminates the mathematical details, but these same details must be recovered when local excitation and/or local irradiation are measured.] This technique of local excitation is susceptible of error analysis and a simple case is examined below for a diffuse-plus-specular enclosure.

4.1 COMPARISON OF POINT AND UNIFORM EXCITATION

An enclosure of three definite surfaces is shown in the sketch below. An incremental area, δA_k, is shown lying at the centroid of one of the areas, A_1. If the reflective properties of all surfaces are known and all dimensions are specified, a formal problem may be identified as follows: What is the error in assuming $\mathcal{F}_{k2} = \mathcal{F}_{12}$ and $\mathcal{F}_{k3} = \mathcal{F}_{13}$? If δA_k lies at the centroid of A_2, what is the error in assuming $\mathcal{F}_{k1} = \mathcal{F}_{21}$ and $\mathcal{F}_{k3} = \mathcal{F}_{23}$?

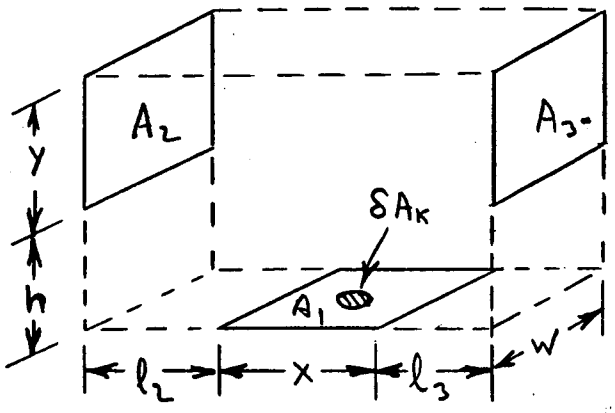

$\delta A_K << A_1$

$\rho_i = \rho_i^d + \rho_i^m$

$i = 1, 2, 3$

$\rho_K = \rho_K^d$ ONLY

The transfer matrix for this enclosure is

$$D = \begin{vmatrix} (1 - \rho_1^d \phi_{11}) & - \rho_1^d \phi_{12} & - \rho_1^d \phi_{13} & 0 \\ - \rho_2^d \phi_{21} & (1 - \rho_2^d \phi_{22}) & - \rho_2^d \phi_{23} & 0 \\ - \rho_3^d \phi_{31} & - \rho_3^d \phi_{32} & (1 - \rho_3^d \phi_{33} & 0 \\ - \rho_k \phi_{k1} & - \rho_k \phi_{k2} & - \rho_k \phi_{k3} & 1 \end{vmatrix}$$

The several interchange factors of interest may be evaluated in closed form as follows:

$$\mathcal{F}_{12} = \frac{\epsilon_1 \epsilon_2}{D} \left[\phi_{12}(1-\rho_3^d \phi_{33}) + \rho_3^d \phi_{13} \phi_{32} \right]$$

$$\mathcal{F}_{13} = \frac{\epsilon_1 \epsilon_3}{D} \left[\phi_{13}(1-\rho_2^d \phi_{22}) + \rho_2^d \phi_{12} \phi_{23} \right]$$

$$\mathcal{F}_{21} = \frac{\epsilon_2 \epsilon_1}{D} \left[\phi_{21}(1-\rho_3^d \phi_{33}) + \rho_3^d \phi_{23} \phi_{31} \right]$$

$$\mathcal{F}_{23} = \frac{\epsilon_2 \epsilon_3}{D} \left[\phi_{23}(1-\rho_1^d \phi_{11}) + \rho_1^d \phi_{21} \phi_{13} \right]$$

$$\mathcal{J}_{k1} = \frac{\epsilon_k \epsilon_1}{D}\Big[\phi_{k1}(1-\rho_2{}^d\phi_{22})(1-\rho_3{}^d\phi_{33}) + \rho_2{}^d\phi_{k2}\phi_{21}(1-\rho_3{}^d\phi_{33}) + \rho_3{}^d\phi_{k3}\phi_{31}(1-\rho_2{}^d\phi_{22})$$
$$+ \rho_2{}^d\rho_3{}^d(\phi_{k2}\phi_{23}\phi_{31} + \phi_{k3}\phi_{32}\phi_{21} - \phi_{k1}\phi_{23}\phi_{32})\Big]$$

$$\mathcal{J}_{k2} = \frac{\epsilon_k \epsilon_2}{D}\Big[\phi_{k2}(1-\rho_1{}^d\phi_{11})(1-\rho_3{}^d\phi_{33}) + \rho_1{}^d\phi_{k1}\phi_{12}(1-\rho_3{}^d\phi_{33}) + \rho_3{}^d\phi_{k3}\phi_{32}(1-\rho_1{}^d\phi_{11})$$
$$+ \rho_1{}^d\rho_3{}^d(\phi_{k1}\phi_{13}\phi_{32} + \phi_{k3}\phi_{31}\phi_{12} - \phi_{k2}\phi_{13}\phi_{31})\Big]$$

$$\mathcal{J}_{k3} = \frac{\epsilon_k \epsilon_3}{D}\Big[\phi_{k3}(1-\rho_1{}^d\phi_{11})(1-\rho_2{}^d\phi_{22}) + \rho_1{}^d\phi_{k1}\phi_{13}(1-\rho_2{}^d\phi_{22}) + \rho_2{}^d\phi_{k2}\phi_{23}(1-\rho_1{}^d\phi_{11})$$
$$+ \rho_1{}^d\rho_2{}^d(\phi_{k1}\phi_{12}\phi_{23} + \phi_{k2}\phi_{21}\phi_{13} - \phi_{k3}\phi_{12}\phi_{21})\Big]$$

If δA_k lies on A_1 and $\rho_k = \rho_1$, then the percentage error in $\mathcal{J}_{12}$ is

$$\frac{100}{\mathcal{J}_{12}}(\mathcal{J}_{12} - \mathcal{J}_{k2})$$

When $A_1 \perp A_2$ and $A_2 \,//\, A_3$, then $\phi_{11} = 0$ and $\phi_{k1} = 0$ so that

$$\frac{\Delta\mathcal{J}_{12}}{\mathcal{J}_{12}} \times 100 = \frac{(\phi_{12}-\phi_{k2})(1-\rho_3{}^d\phi_{33}) + (\phi_{13}-\phi_{k3})(\rho_3{}^d\phi_{32}) - \rho_1{}^d\rho_3{}^d(\phi_{k3}\phi_{31}\phi_{12} - \phi_{k2}\phi_{13}\phi_{31})}{\phi_{12}(1-\rho_3{}^d\phi_{33}) + \rho_3{}^d\phi_{13}\phi_{32}} \times 100$$

If dA_k is on A_2, then $\phi_{11} = 0$, but $\phi_{k2} \neq 0$,

$$\frac{\Delta\mathcal{J}_{23}}{\mathcal{J}_{23}} \times 100 = \left\{\frac{\left[\phi_{23}-\phi_{k3}(1-\rho_2{}^d\phi_{22})\right] + \left[\phi_{21}-\phi_{k1}(1-\rho_2{}^d\phi_{22})\right](\rho_1{}^d\phi_{13}) - \rho_2{}^d\phi_{k2}\phi_{23} - \rho_1{}^d\rho_2{}^d\left[\phi_{k1}\phi_{12}\phi_{23}\phi_{k2}\phi_{21}\phi_{13} - \phi_{k3}\phi_{12}\phi_{21}\right]}{\phi_{23} + \rho_1{}^d\phi_{21}\phi_{13}}\right\} \times 100$$

These expressions suggest that the errors will be small if the surface-to-surface exchange factors ϕ_{12}, ϕ_{23}, etc., are of comparable value as the point-to-surface factors, ϕ_{k2}, ϕ_{k3}, etc. The equations above have a simpler appearance in fully specular enclosures for which all $\rho_i{}^d = 0$, $i = 1, 2, 3$:

$$\frac{\Delta\mathcal{J}_{12}}{\mathcal{J}_{12}} \times 100 = \frac{\phi_{12} - \phi_{k2}}{\phi_{12}} \times 100 \qquad \left\{\begin{matrix}\delta A_k \text{ on } A_1 \\ A_i \text{ specular}\end{matrix}\right\}$$

$$\frac{\Delta\mathcal{J}_{23}}{\mathcal{J}_{23}} \times 100 = \frac{\phi_{23} - \phi_{k3}}{\phi_{23}} \times 100 \qquad \left\{\begin{matrix}\delta A_k \text{ on } A_2 \\ A_i \text{ specular}\end{matrix}\right\} \qquad i = 1, 2, 3$$

The closed form expressions above also serve to illustrate that the error in equating local excitation with uniform excitation is a strong function of geometry. As a first step in the error analysis, a fully diffuse enclosure was investigated. When all $\rho_i^m = 0$, the exchange factors, ϕ_{kj}, reduce to conventional shape factors, F_{kj}; additional simplification results because all of the surfaces are plane so that all $F_{kk} = 0$.

The preliminary results for δA_k lying at the centroid of A_1 indicate that local excitation may be used as the basis for making experimental measurements of nodal interchange factors. The simple error analysis confirms intuition by showing that single point excitation is acceptable for "open" systems such that $F_{\delta A_k, A_i} \approx F_{A_j, A_i}$. However, for closely coupled systems, single point excitation can lead to errors of about 50 percent in interchange factor measurement. It is apparent that successive (repeated) excitation at several locations on the exciting surface are needed to simulate area-to-area interchange. The procedure of point excitation and measurement is described below. The mathematical basis for the procedure is presented in the next section.

Consider an enclosure of nodal areas $A_1, A_2, \cdots, A_N$ which emit and reflect in an arbitrary manner:

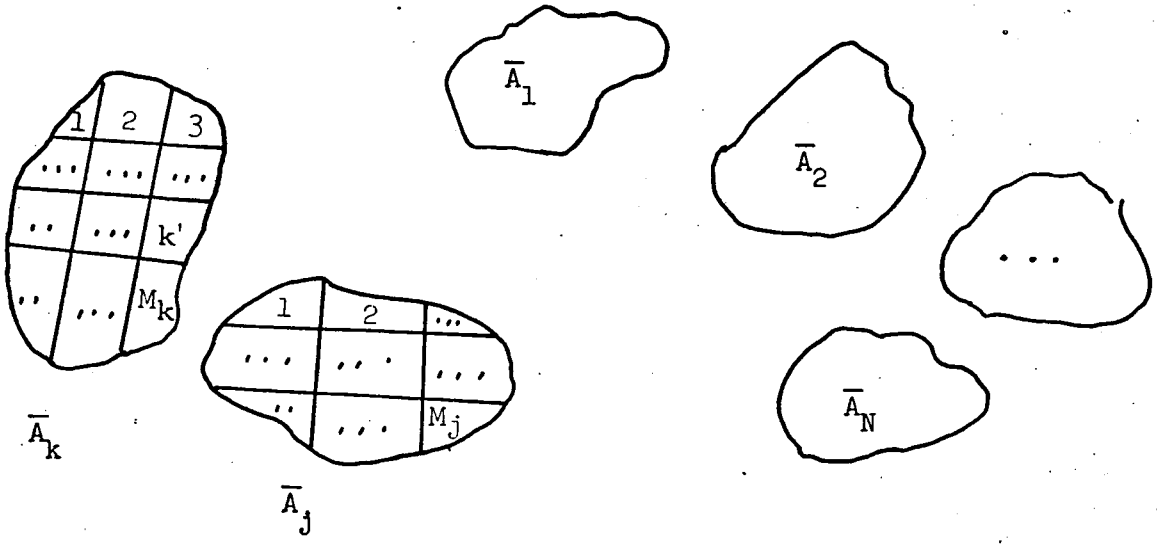

Each nodal area, $\bar{A}_j$, is subdivided into a number of elemental areas $\Delta A_{j'}$: e.g.

$$\bar{A}_k = \sum_{k'=1}^{M_k} \Delta A_{k'}$$

The interchange factor $\mathcal{F}_{ki}$ requires finding $\tilde{G}_k^{(i)}$ and $\tilde{J}_{oi}$. The nodal irradiation $\tilde{G}_k^{(i)}$, may be found by measuring point irradiation on $\bar{A}_k$ caused by point excitation on $\bar{A}_i$ and taking a double sum over k' and i' as follows:

1) Excite the element $\Delta A_{i'=1}$ on $\bar{A}_i$ and measure the point irradiation $\tilde{G}_{k'}^{(i'=1)}$, $k' = 1, 2, \cdots, M_k$, on $\bar{A}_k$. Take the area weighted sum of these to find

$$\tilde{G}_k^{(i'=1)} = \frac{1}{\bar{A}_k} \sum_{k'=1}^{M_k} \tilde{G}_{k'}^{(i'=1)} \Delta A_{k'}$$

2) Measure the point excitation $\tilde{J}_{0i'=1}$ at $A_{i'=1}$ in the absence of re-reflection from other surfaces.

3) Repeat steps 1) and 2) for $i' = 2, 3, \cdots, M_i$.

4) Take the sum of all $\tilde{G}_k^{(i')}$ to obtain the nodal irradiation $\tilde{G}_k^{(i)}$,

$$\tilde{G}_k^{(i)} = \sum_{i'=1}^{M_i} \tilde{G}_k^{(i')} = \frac{1}{\bar{A}_k} \sum_{i'=1}^{M_i} \sum_{k'=1}^{M_k} \tilde{G}_{k'}^{(i')} \Delta A_{k'}$$

5) Take the area weighted sum of all $\tilde{J}_{oi}$' to obtain the nodal excitation $\tilde{J}_{oi}$.

$$\tilde{J}_{oi} = \frac{1}{\bar{A}_i} \sum_{i'=1}^{M_i} \tilde{J}_{oi} \Delta A_{i'}$$

Observe that if the point excitation is constant at all $\Delta A_{i'}$, then

$$\tilde{J}_{oi} = \tilde{J}_{oi'}$$

This last condition eliminates the need to measure all $\tilde{J}_{oi'}$ and permits a single measurement to suffice. It does not eliminate the need to excite all of the locations $\Delta A_{i'}$. When $\tilde{G}_k^{(i)}$ and $\tilde{J}_{oi}$ are known, values may be used in Equation 1 to obtain the node-to-node interchange factor.

This discussion is general insofar as the excitation of a point may be considered as either monochromatic or total. However, it is not intended that point excitation be used if full node excitation is practical. Specifically,

point excitation appears to be necessary for measuring thermal interchange parameters, while nodal area excitation appears to be both more efficient and accurate for measuring solar interchange factors.

Relationship Between Local and Nodal Radiation Fluxes

Radiative transfer among surfaces separated by nonabsorbing, non-scattering media is governed by the linear Fredholm integral equation of the second kind. Inasmuch as the equation is linear, intuition indicates that superposition of forcing functions may be used to advantage in implementing the experimental measurement of radiative fluxes. The analysis which follows shows how a succession of points excited one at a time on an area $\bar{A}_i$ is equivalent to exciting the entire area $\bar{A}_i$ at once in creating a radiant flux incident at another area $\bar{A}_k$. The analysis is performed for an enclosure of diffusely reflecting surfaces in order to minimize the notational difficulties associated with more realistic surfaces.

An enclosure containing N surfaces is shown in Figure 3. Each surface may be subdivided into a finite number of elemental areas,

$$\bar{A}_j = \sum_{j'=1}^{M_j} \delta A_{j'} \tag{6}$$

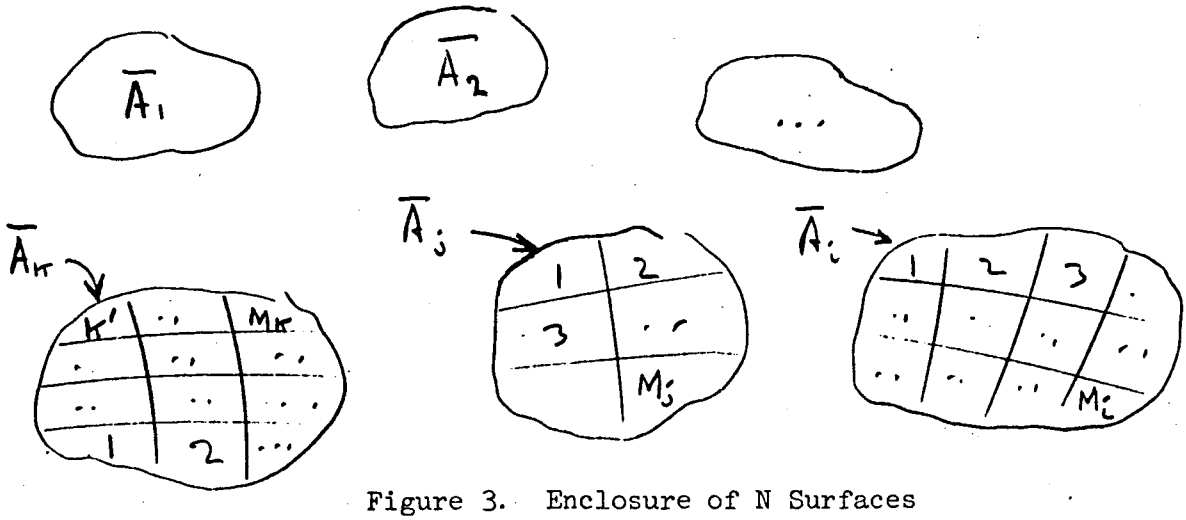

Figure 3. Enclosure of N Surfaces

A lower case index is used to identify a nodal area, $\bar{A}_j$, ($j = 1, 2, \ldots, N$), while the same index with a prime refers to an element of the nodal area, $\delta A_{j'}$, ($j' = 1, 2, \ldots, M_j$). Differential areas are identified with the index of the node,

$$\bar{A}_j = \int_{\bar{A}_j} dA_j \tag{7}$$

The radiosity equation at any point dA_a may be expressed as

$$J(dA_a) = J_o(dA_a) + \rho(dA_a) \sum_{j=1}^{N} \int_{\bar{A}_j} J(dA_j)\, K(dA_a, dA_j)\, dA_j, \tag{8}$$

where

$J_o(dA_a)$ = point excitation at dA_a

$K(dA_a, dA_j)$ = shape factor kernel relating dA_a and dA_j

$\rho(dA_a)$ = diffuse reflectance of dA_a.

J_o and K are assumed known everywhere in the enclosure and J must be found. The solution of Equation 8 may be expressed in terms of a resolvant, $R(dA_a, dA_j|\lambda)$, which is postulated as known. (In practice, the resolvant will be found experimentally). λ is a parameter which is related to reflectance. The solution has the form

$$J(dA_a) = J_o(dA_a) + \sum_{j=1}^{N} \int_{\bar{A}_j} J_o(dA_j)\, R(dA_a, dA_j|\lambda) dA_j \quad , \tag{9}$$

The irradiation at a point dA_k is

$$G(dA_k) = \sum_{j=1}^{N} \int_{\bar{A}_j} J(dA_j)\, K(dA_k, dA_j) dA_j \tag{10}$$

Equation 9 may be used with Equation 10 to obtain

$$G(dA_k) = \sum_{j=1}^{N} \int_{\bar{A}_j} \left[J_o(dAj) + \sum_{p=1}^{N} \int_{\bar{A}_p} J_o(dA_p)\, R(dA_j, dA_p|\lambda) dA_p \right] K(dA_p, dA_j) dA_j, \tag{11}$$

In keeping with the experimental procedure for measuring radiant interchange, it is assumed that only the surface $\bar{A}_i$ is excited and that the excitation is uniform over the surface. Equation 11 reduces to

$$G(dA_k;\bar{A}_i) = \sum_{j=1}^{N} \int_{\bar{A}_i}\int_{\bar{A}_i} J_o(dA_i)\, R(dA_j,dA_i|\lambda)\, K(dA_k,dA_j)\, dA_i dA_j \qquad (12)$$

The functional notation, $G(dA_k;\bar{A}_i)$, is used to denote that the irradiation at the point dA_k is due solely to excitation of the nodal area $\bar{A}_i$. The integration over $\bar{A}_i$ may be decomposed according to Equation 6:

$$\int_{\bar{A}_i} J_o(dA_i)\, R(dA_j,dA_i|\lambda)dA_i = \sum_{i'=1}^{M_i}\int_{\delta A_{i'}} J_o(dA_{i'})\, R(dA_j,dA_{i'}|\lambda)dA_{i'}, \qquad (13)$$

where $dA_{i'}$ is a point lying in the elemental area $\delta A_{i'}$. Equation 13 provides the basis for superposition by defining a partial irradiation $G(dA_k;\delta A_{i'})$ as

$$G(dA_k;\delta A_{i'}) = \sum_{j=1}^{N} \int_{\bar{A}_j}\int_{\delta A_{i'}} J_o(dA_{i'})\, R(dA_j,dA_{i'}|\lambda)\, K(dA_k,dA_j)dA_i dA_j \qquad (14)$$

The complete irradiation of Equation 12 is recovered by summing the partial irradiations over $\bar{A}_i$,

$$G(dA_k;\bar{A}_i) = \sum_{i'=1}^{M_i} G(dA_k;\delta A_{i'}) \qquad (15)$$

The mean nodal irradiation required for interchange factor computations is defined as

$$G_k^{(i)} = \frac{1}{\bar{A}_k}\int_{\bar{A}_k} G(dA_k;\bar{A}_i)dA_k \qquad (16)$$

Once more, the integral may be decomposed as

$$G_k^{(i)} = \frac{1}{\bar{A}_k} \sum_{k'=1}^{M_k} \int_{\delta A_{k'}} G(dA_{k'};\bar{A}_i)dA_k \tag{17}$$

An elemental mean value defined as

$$G_{k'}^{(i)} = \frac{1}{\delta A_{k'}} \int_{\delta A_{k'}} G(dA_k';\bar{A}_i)dA_k \tag{18}$$

and used with Equation 15 define an elemental irradiation at $\delta A_{k'}$, caused by an elemental excitation at $\delta A_{i'}$:

$$G_{k'}^{(i')} = \frac{1}{\delta A_{k'}} \int_{\delta A_{k'}} G(dA_{k'};\delta A_{i'},)dA_k \tag{19}$$

Equations 15 and 19 may be combined in Equation 17 to obtain

$$G_k^{(i)} = \frac{1}{\bar{A}_k} \sum_{k'=1}^{M_k} \sum_{i'=1}^{M_i} G_k^{(i')} \delta A_{k'} \tag{20}$$

This double summation over the excitation area and the irradiated area is the formal relationship suggested by intuition.

Turning next to the excitation of the nodal area, $\bar{A}_i$, the quantity required for experimental evaluation of interchange factors is

$$J_{oi} = \frac{1}{\bar{A}_i} \int_{\bar{A}_i} J_o(dA_i)dA_i \tag{21}$$

$$= \frac{1}{\bar{A}_i} \sum_{i'=1}^{M_i} \int_{\delta A_i} J_o(dA_{i'},)dA_i \tag{22}$$

If the local excitation, $J_o(dA_{i'})$, is uniform over all of $\overline{A}_i$, then

$$J_{oi} = J_o(\delta A_{i'}) = J_o(dA_{i'}) \tag{23}$$

This result is intuitively apparent and is included to show that the local excitation need be measured only once, so long as it is maintained constant during the experiment.

4.2 EQUIPMENT SURVEY: THERMAL FACTORS

The analysis and discussion in preceding sections have shown how local excitation and local irradiation measurements may be used to obtain empirical data for radiative interchange factors. This section describes the findings of an equipment survey which demonstrates the feasibility of using readily available hardware to obtain thermal (IR) and solar radiation interchange factors in a shirtsleeve environment based on the local-to-local technique.

Thermal Factors

The components required to obtain radiative interchange factors from a model spacecraft include the following:

1) An excitation source

2) A diffuse excitation target

3) A diffuse irradiation target

4) An irradiation detection system

These components would be used in a manner similar to that described by Bobco (Reference 1) for obtaining local solar irradiation data. The principal differences are the waveband of the radiative excitation and the use of an excitation target to simulate surface emission. The implementation of the local-to-local technique for IR interchange factors requires the use of an IR beam of radiant energy focused on a small diffusely reflecting excitation target. The target radiosity, $J_{oi'}$, must be measured by a remote viewing radiation detector for use as a reference value. A second diffusely reflecting target placed on some surface of interest is also viewed by the remote

detector to obtain the partial irradiation, $G_{k'}^{(i)}$, at that point. The irradiation is found by measuring the radiosity of the second target and dividing the value by the irradiation target reflectance, $\rho_{t'}(k)$

$$G_{k'}^{(i)} = J_{k'}^{(i)} / \rho_{t'}(k)$$

The radiation interchange factor script-F, is shown to be proportional to the ratio

$$G_{k'}^{(i')} / J_{oi'}$$

This last result may be used to remark that the reflectance of the excitation target, $\rho_t(i)$, is arbitrary and its magnitude may be unknown so long as it is Lambertian (diffuse). The magnitude of the irradiation target, $\rho_{t'}(k)$, must be known quantitatively, but it is arbitrary, as well; however, practical considerations indicate that both targets should be highly reflective, $\rho_t(i) \approx \rho_{t'}(k) \rightarrow 1.0$ in order to obtain consistent data.

The discovery that target reflectance is constrained only by the requirement of diffuseness allowed most of the current feasibility study to be concerned with IR sources, transfer optics, radiometers, and associated electronics equipment. The purpose of the study was to obtain a list of optimum components. The "first-order" results reported in Reference 5 show that off-the-shelf hardware is, indeed, available for implementing the local-to-local technique successfully. Additional studies showed that marked improvements would result by modifying the transfer optics and using a state-of-the-art (rather than off-the-shelf) detector with commercially available equipment. The analysis and discussion in support of this conclusion are presented following a formal problem statement.

Problem Statement

Consider two diffusely reflecting elemental areas δA_1 and δA_2 separated by a distance L_{12} where the areas are on the order of 1-inch diameter and the separation distance is on the order of 0.5 meter. A pencil of IR energy

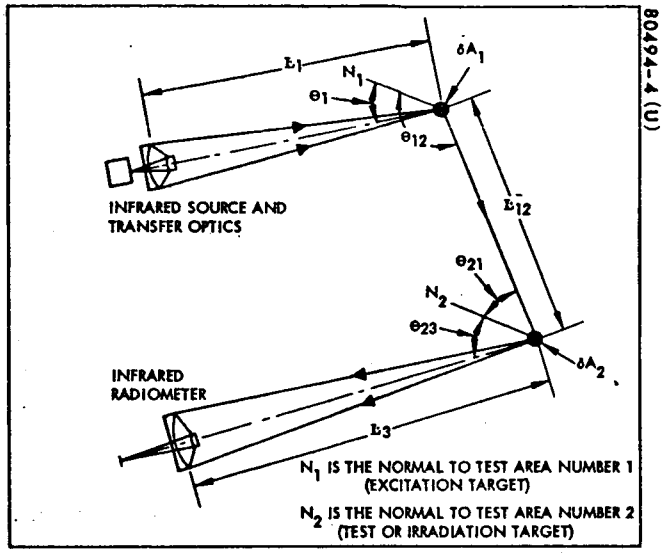

Figure 4 Geometry of Interchange Factor Measurement Experiment

irradiates δA_1 from a source of distance L_1, with an angle of incidence ϕ_i. An IR radiometer views δA_2 from a distance L_3 to detect energy which originates at the source. The geometry is shown schematically in Figure 4. The problem of interest is to determine the availability of equipment for application of the local-to-local method.

Summary of System Characteristics

The "first-order" feasibility of the remote excitation/remote detection technique was established by the equipment survey reported in Reference 5. It was established that off-the-shelf hardware was available for all major components (with the exception of diffuse targets), but system performance was only slightly better than marginal. The weakest components in the system were identified as the transfer optics and the thermistor bolometer detector. A preliminary design analysis of the transfer optics showed that the signal-to-noise ratio could be increased by an order of magnitude by using custom made f/2 transfer optics in place of the off-the-shelf f/5.5 component. An additional order of magnitude improvement was obtained by using a zinc-doped germanium (Ge:Zn) detector in place of the more common germanium immersed thermistor bolometer. A summary of equipment characteristics is shown in Table 1 and a discussion of the improved components follows.

TABLE 1. COMPARISON OF PRELIMINARY AND IMPROVED EQUIPMENT CHARACTERISTICS FOR THERMAL FACTOR MEASUREMENTS

Equipment	Preliminary (Reference 5)	Improved
Source	1100°C(a)	1100°C(a)
Transfer optics	(b)	(c)
Speed	f/5.5	f/2
Transmittance	72 percent	76 percent
Transmitted power	0.1 watt	1.2 watts
Detector	Thermistor bolometer	Ge:Zn
Radiometer	Barnes 8 inches(a)	Barnes 8 inches(a)
Amplifier	PAR:HR-8(d)	PAR:HR-8(d)
System NEPD	4.9×10^{-12} w/cm^2	2.8×10^{-13} w/cm^2
Nominal signal-to-noise ratio	14	7,500
Time for one data point	~2 minutes	~4 seconds

(a) Barnes Engineering Company
(b) Warner and Swasey Model 30
(c) Custom made
(d) Princeton Applied Research Corporation

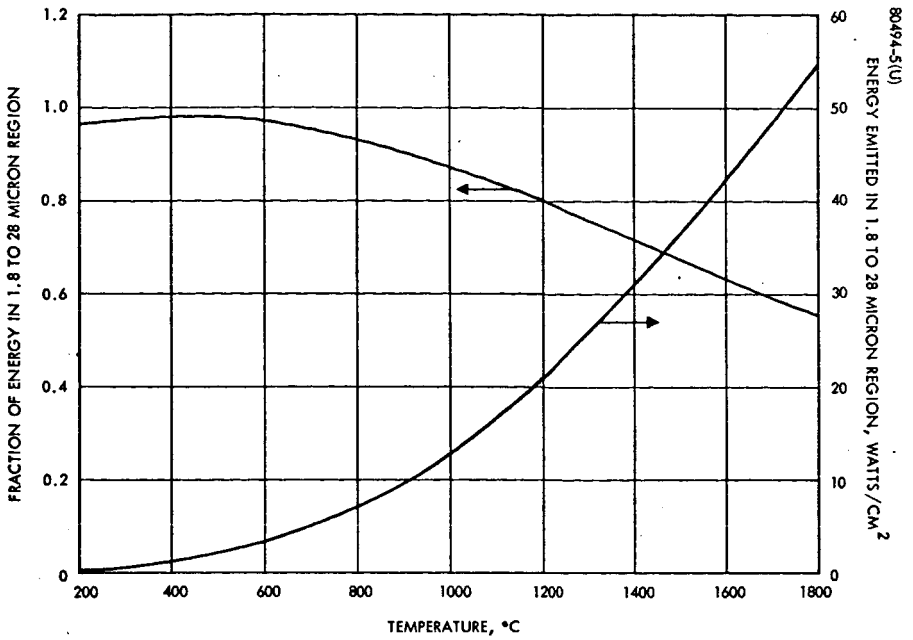

Figure 5. Energy Emitted in 1.8 to 28-Micron Region and Its Fraction of Total Energy for Blackbody as Function of Temperature

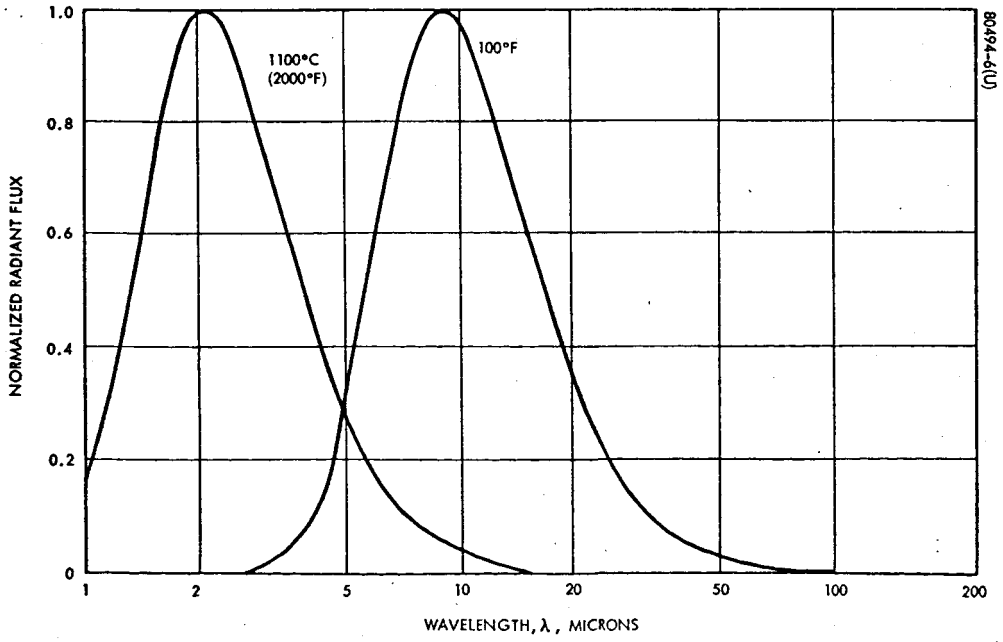

Figure 6. Radiant Flux as Function of Blackbody Temperature and Wavelength

Sources

In the present discussion, radiant sources are considered as being distinct from the transfer optics (auxiliary equipment) needed to irradiate a target area. There are several obvious radiant energy sources for this long-wave region: Nernst glowers, glow bars, and blackbodies. From these spectrally continuous sources, the blackbody was chosen since it can be operated at temperatures as high or higher than a glow bar or Nernst glower, and has both a larger active area and higher emittance than the other candidates. Figure 5 shows that, as the temperature of the blackbody increases, a smaller fraction of the total energy is in the region of interest. However, since the Plankian curves do not cross, more energy is always obtained in the region of interest. Above 1800°C more energy must be discarded than is used, and the rate at which the available energy increases with temperature becomes smaller. Thus, the real concern, as shown above and in Figure 6, is the spectral match. (This aspect is discussed in detail below.) If a flat response detector is used, the 1100°C source would weight the 2-micron region unduly, whereas at more realistic spacecraft temperatures of 100°F, the 9-micron region would be the spectral interval of interest. This effect can be counterbalanced by using a detector that does not have a flat response or a filter, or both.

Detectors

The most critical component in the excitation/detection system is believed to be the detector in the radiometric collector. Several doped germanium detectors (Ge:Cu, Ge:Cd, Ge:Zn) have a biased response which would tend to "shift" the 1100°C curve to the longer wavelengths. The apparent emissive power of a lower temperature source may be obtained by considering the arithmetic product of a high temperature source (viz. 1100°C) and the spectral response of an appropriate germanium detector. Figure 7 shows three different cases: the Ge:Cu and an 1100°C source approximate a 1000°F blackbody; the Ge:Zn and 1100°C source approximate a 680°F blackbody; and an 1100°K source and the Ge:Zn approximate a 400°F blackbody. This last combination may be improved additionally with an appropriate long-wave bandpass filter to approximate a 220°F blackbody excitation (OCLI, Optical Coatings Laboratories, Inc., has a proven capability for providing such components). Thermistor bolometers,

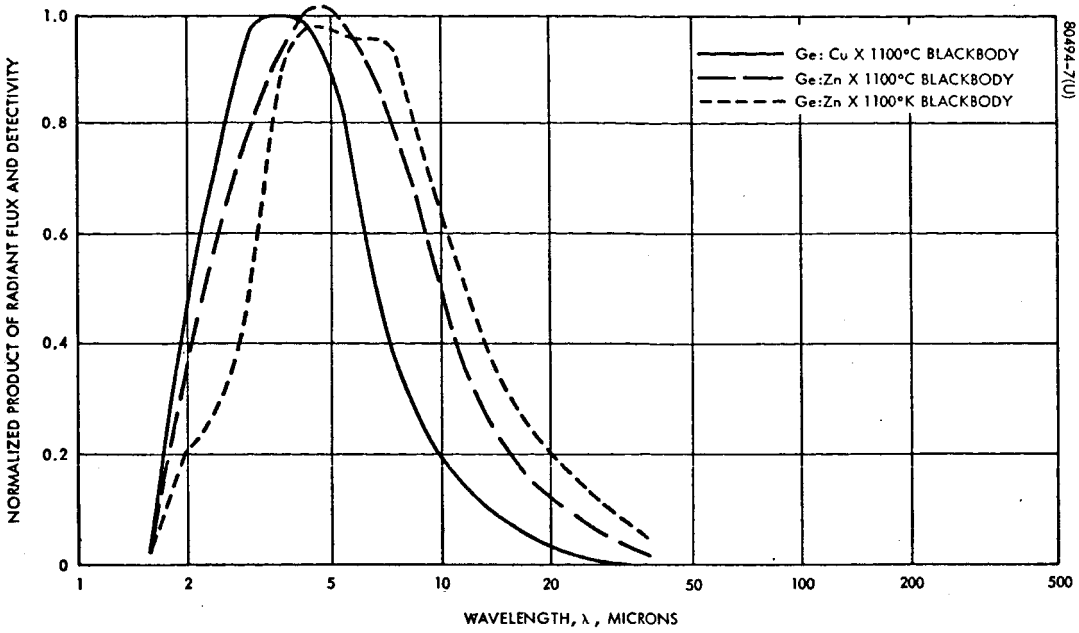

Figure 7. Product of Radiant Flux Emitted by Blackbody and Spectral Response of Two Different Detectors

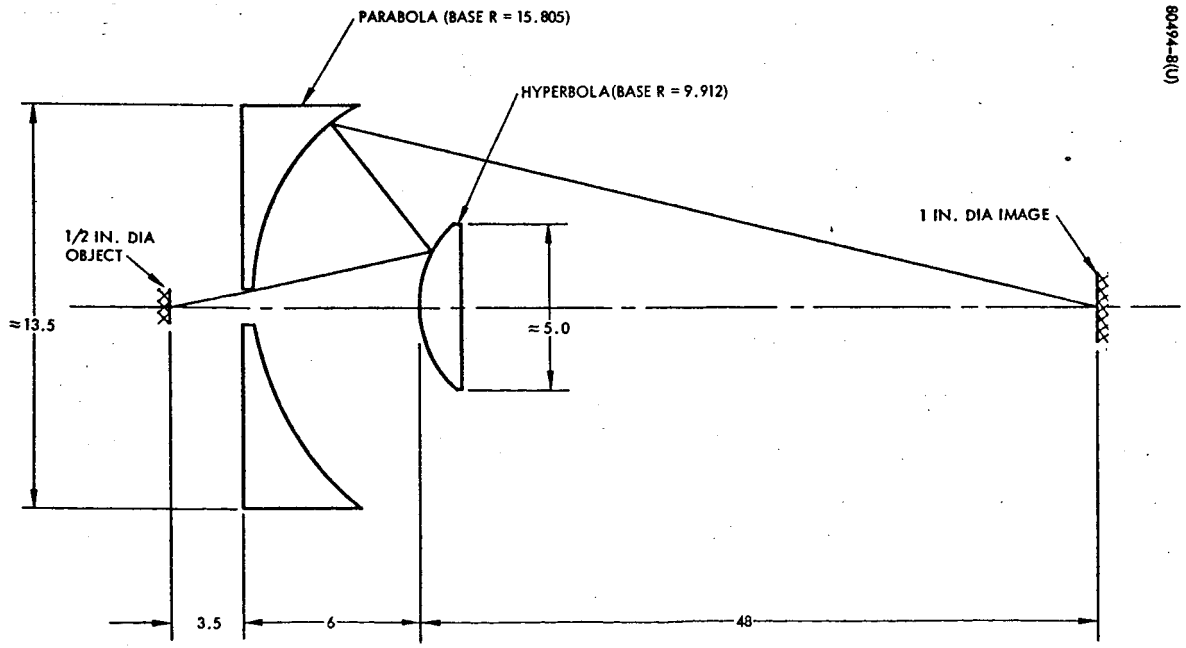

Figure 8. Schematic of Transfer Optics

which were considered as common and readily available detectors do not either ease the spectral mismatch or provide an adequate signal-to-noise ratio. The Ge:Zn detector is recommended as the best choice although it is not a common detector. For either the 1100°C or the 1100°K sources, the Ge:Zn detector in a Barnes 8-inch radiometer would provide a typical NEPD of about 4×10^{-13} watt/cm^2.

Auxiliary Equipment

Ancillary equipment required to perform a successful IR interchange measurement includes source transfer optics, a radiometric collecting device, signal processing equipment, and targets. The Barnes 8-inch radiometer with interchangeable detectors and built-in electronics is recommended as the best choice among all currently available detection systems. However the off-the-shelf f/5.5 transfer optics described in Reference 5 "throw away" too much of the source energy. In an attempt to improve upon the f/5.5 system, new transfer optics were analyzed and the f/2 system shown in Figure 8 is believed to be most appropriate.

As was suggested in Reference 5, the PAR lockin amplifier (Model HR-8) is recommended to integrate the signal. This amplifier would be locked in phase with a chopper on the blackbody source.

Signal-to-Noise Calculations

This section summarizes the analytical considerations which led to the choice of equipment described above. Using the above equipment and the setup of Figure 4, the following is obtained for the 1100°C blackbody

$$B_s = W r_s^2 = 20(0.635)^2 = 8.1 \text{ watts/steradian}$$

With the improved f/2 transfer optics

$$P_1 = B_s T \Omega$$

where the solid angle is simply $\Omega = 2\pi(1 - \cos \theta)$ and for an f/2 system $\theta = 14$ degrees or $\Omega = 0.188$.

Ray tracing analysis yields an obscuration of 16 percent and using 95 percent reflectance for the mirrors gives a transmittance

$$T = 0.84(0.95)^2 = 0.76$$

therefore

$$P_1 = 8.1(0.76)0.19 = 1.17 \text{ watts}$$

The power incident at the irradiation target is

$$P_2 = \frac{\rho P_1 \cos \theta_{12} \cos \theta_{21} \Omega_{12}}{\pi}$$

where

ρ = reflectance of surface 1

$\cos \theta_{12}$ and $\cos \theta_{21}$ are defined in Figure 4

Ω_{12} = angular subtense of surface 2 as seen from surface 1 when it is perpendicular to the line of sight from surface 1 to 2.

Assuming nominal case angles of 45 degrees and an average reflectance of 50 percent,

$$P_2 = 1.88 \times 10^{-4} \text{watt}$$

The Barnes 8-inch radiometer subtends an 8-milliradian field of view, so that a 1-inch-diameter target fills the field at L_3 = 125 inches. The radiant flux collected by the radiometer is

$$G_3 = 2.11 \times 10^{-10} \text{ watt/cm}^2$$

This flux can be improved if both targets have reflectances greater than 0.5, but the discussion below shows that diffuse target reflectances of about

0.50 to 0.70 are reasonable for infrared applications. Using a highly sensitive Ge:Zn detector in the Barnes 8-inch radiometer set for a 3-millisecond response time (50-Hz system bandwidth) provides an NEPD of 4×10^{-13} watt/cm^2. The radiometer may be modified so that it can be phase-locked to a Princeton Applied Research amplifier with an equivalent noise bandwidth of 2.5×10^{-3} Hz to provide an overall or system NEPD of 2.8×10^{-13} watt/cm^2.

The signal-to-noise ratio for the system described above is

$$S/N = G_3/NEPD = 7.5 \times 10^4$$

The signal-to-noise ratio is increased by about four orders of magnitude above the preliminary result reported in Reference 5, but for longer working distances, say 144 inches, the diameter of the source would have to be reduced by a factor of slightly more than 3 to keep its image smaller than the 1 inch-diameter target; the signal-to-noise ratio would decrease to 5.6×10^3. Furthermore, if the two targets can not "see" each other directly, the signal-to-noise would be cut drastically. The signal-to-noise also has a direct bearing upon the time required to obtain a single data point; typically, an experimenter would like to take data points faster than once every 6 minutes ($\Delta f = 2.5 \times 10^{-3}$). A more reasonable Δf is 0.25 Hz allowing a sample rate of one data point every 4 seconds and giving a basic signal-to-noise of 7,500 instead of 75,000. Another benefit of this large signal-to-noise ratio is the option to lower the source temperature to eliminate spectral mismatch. For example, the source temperature could be lowered to 500°C and with a Δf of 0.25 Hz still have a signal-to-noise ratio of 750. At this source temperature, one would be approximating a 100°F spacecraft surface quite closely.

Excitation and Detection Targets: Thermal Factors

The concept of remote excitation and detection is based on the use of diffusely reflecting targets. The property of diffuseness has a spectral dependence in that surfaces which appear to be diffuse reflectors for visible or solar radiation may be strongly bidirectional or even specular to infrared

radiation. Surface roughness appears to be one of the key mechanical requirements for a diffusely reflecting surface in that the rms asperity should be of the same magnitude as the wavelength of incident radiant energy.

Herold and Edwards (Reference 7) demonstrated the validity of diffuse reflection of long-wave radiation by testing six different rough surfaces. They presented the following summary: "...very rough sintered bronze and glass beaded surfaces were quite diffusing to infrared radiation. The wire-screen surface showed highly bidirectional behavior, but little specularity in reflection was found. The sandblasted aluminum specimen showed increasingly specular-like reflection at longer wavelength ..." Three sintered bronze surfaces were prepared from particles which had minimum to maximum diameters of 2.5 to 12, 12 to 25, and 25 to 50 microns. The glass bead projection screen had particles about 0.1 millimeter diameter and the screen was woven from 51-micron strands on 260-micron centers. The aluminum was sandblasted with 280 grit abrasive; probably the "smoothest" of the six specimens. The roughest sintered specimen had a directional reflectance which varied from about 0.62 to 0.90 in the 2.5 to 7.5 micron waveband. The other specimens had lower reflectances with the sandblasted aluminum having the lowest values of 0.50 to 0.70 for the same waveband. Unpublished bidirectional reflectance data taken by TRW Systems for NASA/MSC under Contract NAS9-5073 in September 1966 show that sandblasted aluminum prepared with 36 grit abrasive is very diffuse in the waveband 0.50 to 22 microns. The magnitude of directional reflectance is the same as the range reported in Reference 7. Both excitation and detection targets should have high reflectances, but the magnitude need be known only for the irradiation target for use as a divisor to obtain the irradiation to excitation ratio, $G_k^{(i)}/J_{ok}$.

Aluminized sintered bronze surfaces made from particles in the size range 25 to 50 microns are recommended for use as targets for infrared (thermal) radiation interchange measurements.

A variety of techniques may be used to hold the targets in position on a model. Double-backed, pressure-sensitive tape is suitable for most applications. In some instances, the reflective surface may be bonded to a thin disk magnet which can be held in place by using a second magnet behind the

location of interest on the model. If ferromagnetic sheet metal is used for model fabrication, the second magnet is not required.

The size of the target is dictated by the model scale, the area of a nodal surface on the model, and the minimum power required to create a detectable signal. It is apparent that a target should have an area which is much smaller than the area of a node so that the optical properties of the node are not changed by the introduction of the target. At the same time, an excitation target should be large enough so that the flux reflected from it creates a detectable signal at the irradiation target. The irradiation target may be much smaller than the excitation target insofar as all that is required is an area which fills the field of view of the detection instrument. It should be observed that reciprocity may be used to advantage in instances where a node is too small to accommodate an excitation target. Finally, the target should be sufficiently large so that it can be handled without difficulty by a technician when moving it from one location to another.

In consideration of all the restraints on target size, it is believed that the minimum size of an excitation target should be 0.5 inch diameter and for an irradiation target, 0.25 inch diameter. If these targets are too large for a complete scale model, it may be necessary to use partial models of a larger scale in which only selected nodes are reproduced.

Spectral Considerations

The experimental procedure described above for measuring thermal interchange factors relies on the use of an infrared beam of moderately high power density (approximately 13 watts/cm^2). A commercially available blackbody source which is capable of providing this flux operates at a temperature of 1100°C (2012°F). The Planckian distribution of this blackbody source shows a peak at 2.11 microns and 98 percent of the energy lies in the 1 to 16 micron waveband. This distribution of radiant energy does not correspond to the "thermal" waveband used to measure spectral and total emittance. The thermal waveband spans the 1 to 30 micron interval and the spectral energy distribution may be taken as that of a blackbody at about 100°F with a peak at

9.3 microns and 90 percent of the energy in the 4.6 to 32 micron interval. The Planckian curves are shown in Figure 6. In consideration of this apparent spectral mismatch, it is necessary to examine the magnitude of errors which may arise when testing nongray surfaces such as white paints ($\alpha^* \approx 0.2$, $\epsilon \approx 0.9$).

The spectral analysis starts with the expression for spectral net flux of an arbitrary surface in an enclosure containing N nodal surfaces

$$q_{k,net}(\lambda) = \sum_{j=1}^{N} \mathcal{F}_{kj}(\lambda) \left[E_k(\lambda,T_k) - E_j(\lambda,T_j)\right], \frac{\text{power}}{\text{unit area-micron}} \qquad (24)$$

$\mathcal{F}_{kj}(\lambda)$ is the spectral radiant interchange factor (dimensionless) and $E_k(\lambda,T_k)$, $E_j(\lambda,T_j)$ are spectral blackbody emissive fluxes. The net spectral exchange between two surfaces, A_k and A_i, is

$$q_{k,i}(\lambda) = \mathcal{F}_{ki}(\lambda) \left[E_k(\lambda,T_k) - E_i(\lambda,T_i)\right] \qquad (25)$$

The total net flux is obtained by integrating overall wavelengths,

$$q_{ki} = \int_0^\infty q_{ki}(\lambda)\, d\lambda \quad , \quad \text{power/unit area} \qquad (26)$$

The total radiant interchange factor is then

$$\mathcal{F}_{ki} = \frac{\int_0^\infty \mathcal{F}_{ki}(\lambda) \left[E_i(\lambda,T_k) - E_i(\lambda,T_i)\right] d\lambda}{\sigma\left(T_k^4 - T_i^4\right)} \qquad (27)$$

where

$$\sigma T^4 = \int_0^\infty E(\lambda,T)\, d\lambda \qquad (28)$$

It is necessary to specify the temperatures T_k and T_i in order to evaluate Equation 27. The Planckian difference, $[E_k(\lambda,T_k) - E_i(\lambda,T_i)]$, represents the weighting function required to define an average value of $\mathcal{F}_{ki}$ appropriate to the Stefan-Boltzmann difference, $\left(\sigma T_k^4 - \sigma T_i^4\right)$. According to Wiens' Law, the blackbody flux peak occurs at

$$\lambda_{max}\, T = 5216\,\mu\text{-}^\circ R$$

however, it can be shown that the peak of the Planckian difference is shifted to a shorter wavelength. In the limit $T_k \rightarrow T_i$, the Planckian difference peaks at

$$\lambda'_{max}\, T = 4338\,\mu\text{-}^\circ R$$

For purposes of comparison, when $T = 560^\circ R$,

$\lambda_{max} = 9.314$ microns
$\lambda'_{max} = 7.746$ microns

The spectral distribution of the Planckian difference $(E_k - E_i)$ tends to resemble a blackbody spectral distribution at the higher temperature T_i. In consideration of this shift, and as a convenience to computation, it will be assumed that Equation 27 may be approximated as

$$\mathcal{F}_{ki} = \frac{\int_0^\infty \mathcal{F}_{ki}(\lambda)\, E_i(\lambda,T_i)\, d\lambda}{\sigma T_i^4} \qquad T_i > T_k \qquad (27a)$$

In this form, the thermal radiant interchange factor is defined in a manner analogous to thermal emittance:

$$\epsilon = \frac{\int_0^\infty \epsilon(\lambda)\, E(\lambda,T)\, d\lambda}{\sigma T^4}$$

Before proceeding, it should be noted that neglecting the ultraviolet shift may introduce errors in the conventional computation of radiant interchange factors if either surface A_k or A_i has a pronounced change of spectral reflectance in the immediate vicinity of the peak in $(E_k - E_i)$. A more detailed examination of the ultraviolet shift is beyond the scope of the present study.

The last step in preparing an analytical relationship between total and spectral radiant interchange factors requires elucidation of $\mathcal{F}_{ki}(\lambda)$. The analysis of Section 2.0 shows that in an enclosure of diffuse-plus-specular reflectors

$$\mathcal{F}_{ki}(\lambda) = \frac{\epsilon_k(\lambda)\ \epsilon_i(\lambda)}{\rho_k^d(\lambda)}\ \beta_{ki}(\lambda) \qquad (29)$$

where $\beta_{ki}(\lambda)$ is the spectral interreflection kernel relating A_k and A_i in terms of enclosure geometry and surface properties. Equations 27a and 29 may be combined to yield

$$\mathcal{F}_{ki} = \frac{1}{\sigma T_i^4} \int_0^\infty \frac{\epsilon_k(\lambda)\ \epsilon_i(\lambda)}{\rho_k(\lambda)}\ \beta_{ki}(\lambda)\, E(\lambda,T_i)\, d\lambda \qquad (30)$$

Equation 30 is taken to represent the ideal or "true" value of the thermal radiant interchange factor and will serve as a base of comparison in this spectral analysis. The interreflection kernel, $\beta_{ki}(\lambda)$, is a function of both geometry and the spectral bidirectional reflectances of an enclosure.

The algorithm for obtaining the total interchange factor by empirical means is

$$\mathcal{F}'_{ki} = \frac{\tilde{\epsilon}_k \, \tilde{\epsilon}_i \, \tilde{G}_k^{(i)}}{\tilde{J}_{oi}} \tag{31}$$

where the total hemispherical emittances $\tilde{\epsilon}_k$ and $\tilde{\epsilon}_i$ are assumed known and the total hemispherical fluxes $\tilde{J}_{oi}$ and $\tilde{G}_k^{(i)}$ must be measured. These four total parameters may be expressed in terms of their spectral precedents as

$$\tilde{\epsilon}_k = \frac{1}{\sigma T_k^4} \int_0^\infty \tilde{\epsilon}_k(\lambda) \, E(\lambda, T_k) \, d\lambda \tag{32a}$$

$$\tilde{\epsilon}_i = \frac{1}{\sigma T_i^4} \int_0^\infty \tilde{\epsilon}_i(\lambda) \, E(\lambda, T_i) \, d\lambda \tag{32b}$$

$$\tilde{J}_{oi} = \int_0^\infty \tilde{J}_{oi}(\lambda) \, d\lambda \tag{32c}$$

$$\tilde{G}_k^{(i)} = \int_0^\infty \tilde{G}_k^{(i)}(\lambda) \, d\lambda \tag{32d}$$

The empirical method requires exciting only the A_i node with a known flux, $\tilde{J}_{oi}$, and measuring the flux incident at A_k to obtain $G_k^{(i)}$.

Equations 31 and 32 apply to the case of a noise-free environment. In the presence of stray radiation, Equation 31 becomes

$$\mathcal{F}'_{ki} = \frac{\tilde{\epsilon}_k \tilde{\epsilon}_i \left[\tilde{G}_k - \sigma T_n^4\right]}{\left[\tilde{J}_i - \epsilon_t \sigma T_n^4\right]} \tag{33}$$

The radiosity $\tilde{J}_i$ includes signal plus noise measured from a target in an isolated location (not on the spacecraft model) and ϵ_t is the target emittance. The irradiation $\tilde{G}_k$ is measured on the model and includes the signal plus noise caused by surroundings at a temperature T_n. The correction for noise may be done by chopping the signal or making a measurement first of signal plus noise and second noise alone, or suppressing the noise ($T_n \to 0°$). In the present study, the noise is eliminated by chopping the signal so that the radiometer detects only $\tilde{J}_{oi}$ and $\tilde{G}_k^{(i)}$, both of which are total rather than spectral fluxes. As a result, it is not necessary to consider the spectral character of the noise.

The excitation flux which a radiometer detects is influenced by the spectral reflectance of a target, $\rho_t(\lambda)$, and the spectral response of the optics and the detector, $R(\lambda)$. The excitation is provided by a collimated beam of radiant energy with a spectral distribution $E_s(\lambda,T_s)$ corresponding to a blackbody source at a temperature T_s. These factors require that Equation 32c be expressed as

$$J_{oi} = C_{s,i} \int_0^\infty \rho_t(\lambda)\, E_s(\lambda,T_s)\, R(\lambda)\, d\lambda \tag{34}$$

In the manner of Reference 1, it is convenient to introduce an apparent source spectrum

$$\mathcal{S}(\lambda,T_s) = E_s(\lambda,T_s)\, R(\lambda) \tag{35a}$$

and apparent source flux

$$\mathcal{S}(T_s) = \int_0^\infty \mathcal{S}(\lambda,T_s)\, d\lambda \tag{35b}$$

The discussion and analysis of Section 2.0 shows that the irradiation measured from a second diffuse target with a spectral reflectance is related to the excitation by the expression

$$\tilde{G}_k^{(i)}(\lambda) = \frac{\tilde{J}_{oi}(\lambda)\ \beta_{ki}(\lambda)}{\rho_t'(\lambda)} \tag{36}$$

where $\beta_{ki}'(\lambda)$ is the spectral interreflection kernel. The analytical and experimental interchange kernels are related as

$$\beta_{ki}(\lambda)/\rho_i(\lambda) = \beta_{ki}'(\lambda)/\rho_t'(\lambda) \tag{36a}$$

Combining Equations 35 and 36 into Equation 32d gives

$$\tilde{G}_i^{(i)} = C_{s,i} \int_o^\infty \frac{\rho_t(\lambda)}{\rho_t'(\lambda)}\ \beta_{ki}(\lambda)\ \mathcal{S}(\lambda,T_s)\ d\lambda \tag{37}$$

The final expression for an experimentally determined total thermal radiant interchange factor is found from Equations 31, 34 and 37 as

$$\mathcal{F}_{ki}' = \frac{\tilde{\epsilon}_k \tilde{\epsilon}_i \int_o^\infty \frac{\rho_t(\lambda)}{\rho_t'(\lambda)}\ \beta_{ki}'(\lambda)\ \mathcal{S}(\lambda,T_s)\ d\lambda}{\int_o^\infty \rho_t(\lambda)\ \mathcal{S}(\lambda,T_s)\ d\lambda} \tag{38}$$

Equation 38 must be compared with Equation 30 to obtain insight to any potential spectral shortcomings of the experimental procedure.

It is necessary to specify both surface properties and geometry in order to proceed with the spectral analysis. An enclosure of diffuse-plus-specular reflecting surfaces is examined here in order to use available spectral reflectance data and to avoid computational complications inherent in bidirectional interreflection data. A three nodal surface enclosure is postulated for additional convenience. This simple model leads to interreflection kernels

$$\frac{\beta_{12}}{\rho_1} = \frac{\beta'_{12}}{\rho'_t} = \left[\frac{\phi_{12}\,(1 - \rho_3^d\,\phi_{33}) + \rho_3^d\,\phi_{13}\phi_{32}}{1 - \gamma}\right]_\lambda \tag{39}$$

$$\begin{aligned}\gamma = {} & \rho_1^d\,\phi_{11} + \rho_2^d\,\phi_{22} + \rho_3^d\,\phi_{33} + \rho_1^d\,\rho_2^d\,(1 - \rho_3^d\,\phi_{33})(\phi_{12}\,\phi_{21} - \phi_{11}\,\phi_{22}) \\ & + \rho_1^d\,\rho_3^d\,(1 - \rho_2^d\,\phi_{22})(\phi_{13}\,\phi_{31} - \phi_{11}\,\phi_{33}) \\ & + \rho_2^d\,\rho_3^d\,(1 - \rho_1^d\,\phi_{11})(\phi_{23}\,\phi_{32} - \phi_{22}\,\phi_{33}) \\ & + \rho_1^d\,\rho_2^d\,\rho_3^d\,(2\phi_{12}\,\phi_{23}\,\phi_{31} + \phi_{11}\,\phi_{22}\,\phi_{33})\end{aligned} \tag{40}$$

All of the reflectances ρ_j^d and exchange factors ϕ_{jm} have a spectral dependence, but the functional notation is omitted for convenience. In all circumstances, the term γ in the denominator is less than unity and for most spacecraft geometries $\gamma^2 \ll 1$ so that to a good approximation

$$\frac{\beta_{12}}{\rho_1} = \frac{\beta'_{12}}{\rho'_t} = \left[\phi_{12} + \rho_3^d\,(\phi_{13}\,\phi_{32} - \phi_{33})\right](1 + \gamma) \tag{41}$$

Equation 41 is introduced in Equations 30 and 38 to obtain

$$\mathcal{G}_{12} = \frac{1}{\sigma T_2^4}\int_0^\infty \epsilon_1\,\epsilon_2\left[\phi_{12} + \rho_3^d\,(\phi_{13}\,\phi_{32} - \phi_{33})\right](1 + \gamma)\,E_2\,d\lambda \tag{42}$$

and

$$\mathcal{F}'_{12} = \frac{\tilde{\epsilon}_1 \, \tilde{\epsilon}_2 \int_0^\infty \rho_t \left[\phi_{12} + \rho_3^d \, (\phi_{13} \, \phi_{32} - \phi_{33})\right](1 + \gamma) \, \mathcal{S} \, d\lambda}{\int_0^\infty \rho_t \, \mathcal{S} \, d\lambda} \tag{43}$$

Equations 42 and 43 provide a great deal of insight to potential sources of spectral mismatch between computed measured values of thermal interchange factors. One observation which should be made is that the apparent spectral distribution of the beam, $\mathcal{S}(\lambda)$, does not influence the emittances $\tilde{\epsilon}_1$ and $\tilde{\epsilon}_2$; the influence is restricted to the interreflection terms only. Another observation which should be made is that Equation 42 does not correspond to the usual engineering formulation for the thermal radiant interchange factor; the engineering formulation would be

$$\mathcal{F}''_{12} = \tilde{\epsilon}_1 \, \tilde{\epsilon}_2 \left[\tilde{\phi}_{12} + \tilde{\rho}_3^d \, (\tilde{\phi}_{13} \, \tilde{\phi}_{32} - \tilde{\phi}_{33})\right](1 + \tilde{\gamma}) \tag{44}$$

where the tilde denotes that surface properties are defined in the manner of Equations 32a and 32b.

Additional insight requires further restriction and specification of the surface properties in order to obtain numerical results. On the one hand, it may be assumed that all surfaces are purely specular so that the interreflection kernel is

$$\frac{\beta_{12}}{\rho_1} = \frac{\beta'_{12}}{\rho'_t} = \phi_{12} = F_{12} + \rho_3 \, F_{12(3)} \tag{45}$$

On the other hand, if all surfaces are assumed to be plane and diffuse

$$\frac{\beta_{12}}{\rho_1} = \frac{\beta'_{12}}{\rho'_t} = (F_{12} + \rho_3 F_{13} F_{32})(1 + \gamma) \tag{46}$$

In both instances, the nominal spectral dependence of the interreflection kernel is coupled with a geometrical factor. Insofar as both $F_{12(3)}$ and $F_{13}F_{32}$ are less than unity, there are many instances in which the spectral dependence of β/ρ is very slight. The single (but not uncommon) instance in which a strong spectral dependence may exist is when

$$F_{12(3)} \gg F_{12}$$

or

$$F_{13} F_{32} \gg F_{12}$$

For the sake of discussion, Equation 45 will be used for the remaining analysis; that is, the comparison of interchange factors will be made in terms of the following expressions:

$$\mathcal{G}_{12} = \frac{1}{\sigma T_2^4} \left\{ F_{12} \int_0^\infty \epsilon_1 \epsilon_2 E_2 \, d\lambda + F_{12(3)} \int_0^\infty \epsilon_1 \epsilon_2 \rho_3 E_2 \, d\lambda \right\} \tag{47}$$

$$\mathcal{G}'_{12} = \tilde{\epsilon}_1 \tilde{\epsilon}_2 \left\{ F_{12} + \frac{F_{12(3)}}{\int_0^\infty \rho_t \mathcal{S} \, d\lambda} \int_0^\infty \rho_t \rho_3 \mathcal{S} \, d\lambda \right\} \tag{48}$$

$$\mathcal{G}''_{12} = \tilde{\epsilon}_1 \tilde{\epsilon}_2 \left[F_{12} + \tilde{\rho}_3 F_{12(3)} \right] \tag{49}$$

Meaningful quantitative results may be obtained by specifying the spectral properties of the target reflectance, ρ_t, and A_1, A_2, A_3. The equipment feasibility study reported above shows that the target reflectance should be high ($\rho_t \rightarrow 1$) and diffuse. It will be assumed that either sandblasted aluminum (coarse grit) or aluminized sintered metal specimens (Reference 7) may be suitable targets. Spectral data for a variety of aluminum surface finishes (Reference 8) indicate that there reflectance is both high ($\rho_t > 0.7$) and constant (gray) for wavelengths in the region of concern $1.0 < \lambda < 30\ \mu$. This last observation of aluminum grayness will be used to eliminate ρ_t from Equation 48.

A variety of thermal control surface finishes exhibit a strong variation in the near infrared waveband, $1.0 < \lambda < 10\ \mu$, these include white paint, second surface mirrors (including metallized plastic films), and oxidized metals. An inorganic white paint developed at Hughes Aircraft Company has a change in spectral reflectance from $\rho_\lambda = 0.85$ at $\lambda = 1.0\mu$ to $\rho_\lambda = 0.11$ at $\lambda = 5.0\ \mu$. In consideration of the availability of spectral data for this white paint as well as its dramatic change in reflectance in the spectral region of interest, all of the surface properties appearing in Equations 47, 48, and 49 were taken as those of Hughes inorganic white paint. Spectral data for this white paint are shown in Figure 9.

The spectral response of a detection system, $R(\lambda)$, depends on several components within the system. An ideal radiation detection instrument for thermal design measurements would have a flat response, $R(\lambda) = 1.0$, for all wavelengths; most real infrared detection instruments have a response which approaches zero at either end of a finite waveband. For example, a Ge:Cd detector operating at 20°K has a useful range of about 1.0 to 26 μ with a maximum detectivity at about 12 μ which is approximately 2 orders of magnitude larger than at either end of the range (Reference 9). An immersed thermistor bolometer has a useful waveband which starts at about 2μ with a detectivity which is relatively constant from about 4 to 16 μ. The detectivity increases by a factor of 5 between 2 and 4μ. (The upper limit of the useful waveband is not available in Reference 9.) The useful waveband of any detector may be decreased by other components in a detection system and contribute to the

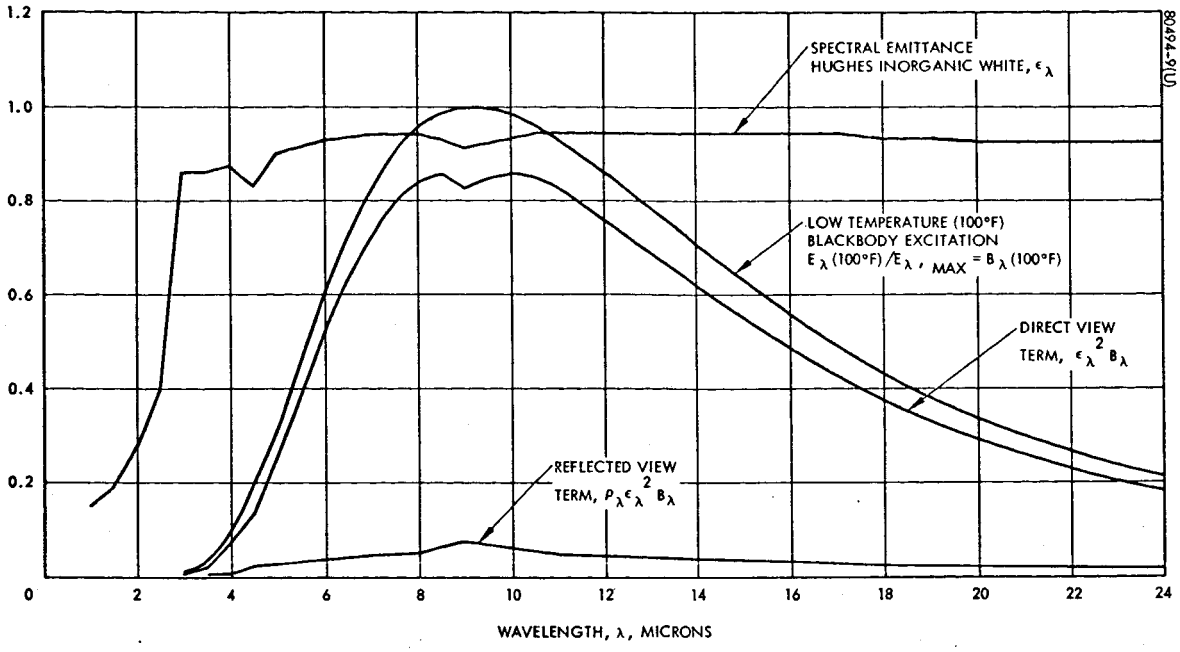

a) Excited by 100°F Blackbody

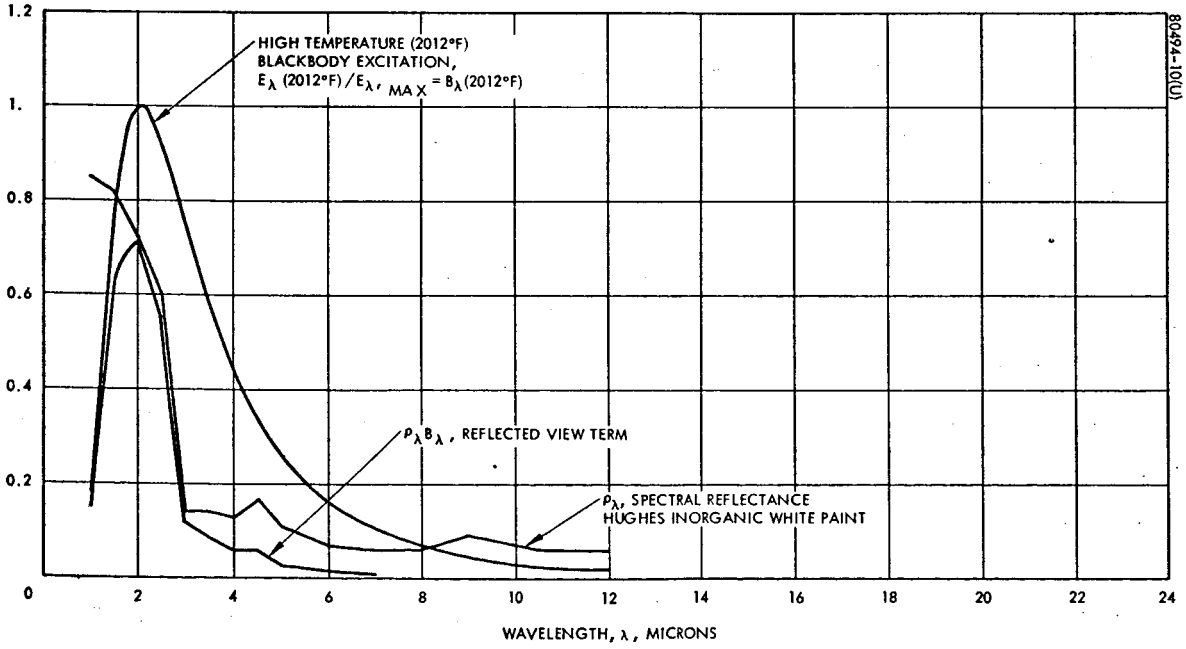

b) Excited by 2012°F Blackbody

Figure 9. Graphical Construction of "True" Spectral Interreflection Terms for White Painted, Three-Surface Enclosure

spectral response of the system. Notwithstanding other possible spectral influences, it is reasonable to assume that the apparent source spectrum, $S(\lambda)$, of an 1100°C blackbody viewed by a Ge:Cd detector would approximate a blackbody at a temperature in the range 0 to -50°F, while the use of a thermister bolemeter would resemble a blackbody of temperature about 1200°F. These considerations suggest that it is conservative to use $R(\lambda) = 1.0$ for the present comparison and to assume a useful detection waveband $1.0 < \lambda < 24$ for the numerical results which follow.

The spectral analysis for white paint was completed within the framework of assumptions described above by performing a graphical integration of the several terms in Equations 47 and 48. The curves used in the integration are shown in Figure 9. The engineering formulation of Equation 49 is based on $\epsilon_1 = \epsilon_2 = 1 - \rho_3 = 0.927$. The numerical results are presented below:

Integration factor (Equation 47): $\mathcal{F}_{12} = 0.87\ (F_{12} + 0.07\ F_{12(3)})$

Measurable factor (Equation 48): $\mathcal{F}'_{12} = 0.86\ (F_{12} + 0.29\ F_{12(3)})$

Engineering factor (Equation 49): $\mathcal{F}''_{12} = 0.86\ (F_{12} + 0.073\ F_{12(3)})$

Although these results were obtained for an enclosure of specular surfaces they indicate the magnitude of potential spectral mismatch for a fully diffuse enclosure as well; however, for a three-surface diffuse enclosure, the geometrical factor is $F_{13}\ F_{32}$ instead of $F_{12(3)}$.

Discussion

The comparison of total or integrated factors with measurable and engineering factors shows, first, good agreement between integrated and engineering factors and, second, the strong geometrical dependence of potential spectral mismatch between total and measurable factors. The mismatch arises because a blackbody at 1100°C (2012°F) is used to simulate blackbody emission at room temperature. The mismatch is termed "potential" because it occurs only in the presence of surfaces which undergo a large change in spectral reflectance in the waveband $1.0 < \lambda < 7.0$ microns and then only if geometrical relationships permit.

The numerical results for Hughes inorganic white paint are conservative because of the assumption $R(\lambda) = 1.0$. If a thermistor bolometer response were used, the apparent source spectrum would reach its peak at about 3.1 μ and have very little intensity for $\lambda < 2.0$ μ. The spectral reflectance of Hughes inorganic white paint shows a large decrease between 1.0 and 3.0 μ so that the measured apparent total reflectance would be closer to 0.14 than the value 0.29 quoted above. Although such a decrease does not eliminate the potential mismatch, it mitigates the mismatch to a large extent. The shift of peak intensity from about 2.1 to 3.1 μ would not correct the potential mismatch of other surface finishes such as second surface mirrors which have restrahlen bands in the interval 3.0 to 10 μ. The Ge:Zn response with a lower temperature source and a bandpass filter could shift the peak intensity to even higher wavelengths and eliminate the potential spectral mismatch

A CO_2 laser operating at about 10.6 μ may be used to detect and perhaps correct spectral mismatch. The detection may be accomplished by making two independent measurements, one using an 1100°C blackbody source, the other using a CO_2 laser. If the two measurements yield comparable values, then the probability of a mismatch is small. If the two measured values are dissimilar, then additional laser measurements may be required at other wavelengths to obtain a more complete spectral sample of the interreflection term, $G_k^{(i)}/J_{oi}$. H_2O lasers operating at both 18 and 28 μ are available for this application and lasers have been fabricated to operate at 118 μ (H_2O) and 338 μ (HCN), also. An acceptable mean value of the interreflection term could be computed as

$$\frac{\tilde{G}_k^{(i)}}{\tilde{J}_{oi}} = \sum_{j=1}^{m} a_j \left[\frac{\tilde{G}_k^{(i)}}{\tilde{J}_{oi}}\right]_j$$

where the spectral weighting factors a_j are related to the blackbody emissive power associated with a finite waveband.

Conclusions

The analysis of spectral interreflection phenomena has disclosed the existence of a potential spectral mismatch arising from the use of a blackbody source operating at 1100°C to simulate blackbody emission at room temperature. The mismatch will occur only when two conditions are satisfied: 1) strongly nongray surfaces are included in an enclosure, and 2) the radiative coupling between two nodal surfaces, A_i and A_k, is dominated by reflection from a nongray surface A_w rather than a direct view between A_i and A_k. Tentative criteria for the existence of a mismatch are

$$1)\quad \frac{\rho_w^*}{\rho_w} > 2 \qquad \text{or} \qquad \frac{\rho_w^*}{\rho_w} < 0.5$$

$$2)\quad F_{ki} + \sum_{j=1}^{m} F_{kj}\, F_{ji} \leq \sum_{w=1}^{n} F_{kw}\, F_{wi}$$

where ρ_w^* and ρ_w are conventional solar and thermal reflectances and $j = 1, 2, \cdots, m$ enumerate the nongray surfaces in the enclosure.

The use of a blackbody source at 1100°C is believed to be acceptable for most spacecraft applications, but an exploratory experimental study is required to establish the importance of a potential spectral mismatch. If such a study shows that a serious loss of accuracy arises from the use of a high temperature blackbody source, the situation may be corrected by making additional measurements with two or three infrared lasers.

Interchange Without Direct View: $F_{ki} = 0$

A possibility exists in which radiative interchange occurs between two surfaces which do not have a direct view of each other; that is $F_{ki} = 0$. For this case, the radiative exchange occurs by virtue of reflection from other surfaces; a simple illustration of such a geometry is shown in Figure 10.

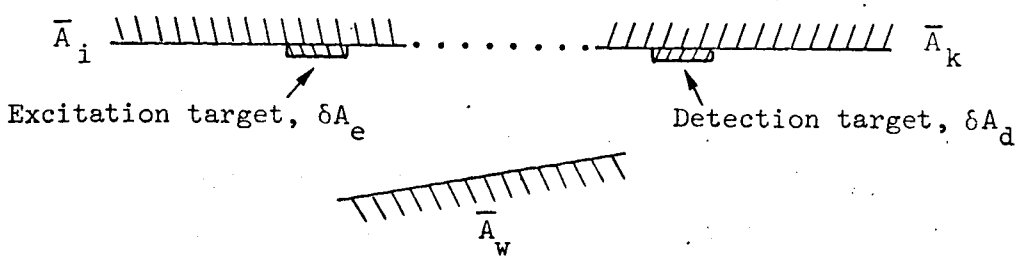

Fig. 10. Nodes $\bar{A}_i$ and $\bar{A}_k$ are coplanar, $F_{ki} = 0$; radiant interchange occurs by reflection at $\bar{A}_w$ so that $\mathcal{F}_{ki} \neq 0$.

If the area $\bar{A}_w$ is a diffuse reflector, the excitation signal incident at the detection target may be too low to provide an adequate signal-to-noise ratio when using off-the-shelf equipment. Under these circumstances, it will be necessary to either modify the experimental procedure or the equipment in order to obtain the flux data, $\tilde{G}_k^{(i)}/\tilde{J}_{oi}$. The analysis which follows develops a modified algorithm by considering an enclosure containing N diffuse-plus-specular reflecting nodal areas.

The irradiation of a surface $\bar{A}_k$ is

$$G_k = \sum_{j=1}^{N} J_j \, \phi_{kj} \tag{50}$$

while the radiosity is known to be expressed in terms of the excitation and an interchange kernel

$$J_j = \sum_{w=1}^{n} J_{ow} \, \beta_{jw} \tag{51}$$

It was shown in Section 2.0 that when only one surface, $\bar{A}_i$, is excited, then

$$J_j^{(i)} = J_{oi} \, \beta_{ji} = \delta_{ji} \, J_{oi} + \rho_j^d \, G_j^{(i)} \tag{52}$$

where δ_{ji} is the Kronecker delta. Combining Equations 50 and 52 yields

$$\frac{G_k^{(i)}}{J_{oi}} = \sum_{j=1}^{N} \phi_{kj} \left[\rho_j^d \frac{G_j^{(i)}}{J_{oi}} + \delta_{ji} \right] \tag{53}$$

The flux ratios $\left(G_j^{(i)}/J_{oi}\right)$ are measured quantities while the exchange factors, ϕ_{kj}, and reflectances ρ_j^d are presumed known. The Kronecker delta is included for analytical completeness, but in an application of local-to-local excitation and detection, it would not be part of this algorithm because the excitation and irradiation targets do not coincide.

The formulation is similar for an enclosure of bidirectional reflecting surfaces:

$$\frac{\tilde{G}_k^{(i)}}{\tilde{J}_{oi}} = \sum_{j=1}^{N} F_{kj} \left[\tilde{\rho}_{jk} \left[\frac{\tilde{G}_j^{(i)}}{\tilde{J}_{oi}} \right] + \delta_{ji} \right] \tag{54}$$

The apparent hemispherical-directional reflectance, $\tilde{\rho}_{jk}$, must be used instead of the hemispherical reflectance which appears in Equation 52. The bidirectional result follows from the analysis of Section 2.0 by observing the following relationships:

$$\mathcal{g}_{jk}^{(i)} = E_i \, \eta_{\substack{jk \\ i}} = \delta_{ji} \, \mathcal{g}_{oik} + \sum_{w=1}^{N} r_{wjk} \, \mathcal{g}_{wj}^{(i)} \, F_{jw} \tag{55}$$

$$\mathcal{g}_{jk}^{(i)} = \delta_{ji} \, \mathcal{g}_{oik} + \tilde{\rho}_{jk} \, \tilde{G}_j^{(i)} \tag{56}$$

$$\tilde{G}_k^{(i)} = \sum_{j=1}^{N} \mathcal{g}_{jk}^{(i)} \, F_{kj} \tag{57}$$

Ordinarily the directional reflectance, ρ_{kw}, is not the same as the apparent hemispherical-directional reflectance, $\tilde{\rho}_{kw}$:

$$\text{Apparent directional reflectance:} \quad \tilde{\rho}_{kw} = \frac{\sum_{j=1}^{N} r_{jkw}\, \vartheta_{jk}\, F_{kj}}{\sum_{j=1}^{N} \vartheta_{jk}\, F_{kj}} \tag{58}$$

$$\text{Directional hemispherical reflectance:} \quad \rho_{kw} = \sum_{j=1}^{N} r_{jkw}\, F_{kj} \tag{59}$$

The directional-hemispherical reflectance ρ_{kw} is a surface property which is easily measured while $\tilde{\rho}_{kw}$ must be computed in terms of bidirectional properties and geometry. The error in using ρ_{kw} in place of $\tilde{\rho}_{kw}$ is believed to be small and is justified in the interest of experimental convenience.

Radiation Loss to Space

A radiation heat balance on an external nodal area of a spacecraft requires accounting for heat loss to space as well as the exchange between pairs of surfaces. The experimental procedures developed above do not lend themselves to a case in which the "space node" is distributed in several geometric locations. This case is shown schematically in Figure 11.

Figure 11. Hypothetical Enclosure in Which Nodal Area for Space Occupies Multiple Locations

This case is both common and important so that it is necessary to find the thermal coupling term, $\mathcal{G}_{k,space}$ in order to make the experimental procedure fully effective.

Despite the difficulty of measuring the flux ratio implicit in $\mathcal{G}_{k,space}$, it is possible to obtain the space coupling term from other measurements. The analysis which follows is based on an enclosure of N nodal areas and space which is designated as the (N+1) node. The net gray heat flux at the k^{th} node may be expressed as

$$q_{k,net} = J_k - G_k = \frac{\epsilon_k}{\rho_k} (E_k - J_k) \tag{60}$$

which leads to the results

$$\sum_{i=1}^{N+1} \mathcal{G}_{ki} = \frac{\epsilon_k}{\rho_k} \tag{61}$$

$$\mathcal{G}_{ki} = \frac{\epsilon_k \epsilon_i}{\rho_k^d} \beta_{ki}, \qquad i = 1, 2, \cdots, N+1 \tag{62}$$

Alternately, the net heat flux may be written as

$$q_{k,net} = \epsilon_k (E_k - G_k) = \epsilon_k \left(E_k - \sum_{j=1}^{N} J_j F_{kj} \right) \tag{63}$$

which leads to the result

$$\sum_{i=1}^{N+1} \mathcal{G}_{ki} = \epsilon_k \tag{64}$$

$$\mathcal{G}_{ki} = \epsilon_k \epsilon_i \sum_{j=1}^{N+1} F_{kj} \beta_{ji}, \qquad i = 1, 2, \cdots, N+1 \tag{65}$$

Equations 62 and 65 give identical results with the single exception for $i = k$; in this instance, it may be established that

$$\underset{(Eq.65)}{\mathcal{F}_{kk}} = \underset{(Eq.62)}{\mathcal{F}_{kk}} - \frac{\epsilon_k^2}{\rho_k} \tag{66}$$

The β_{ki} and β_{ji} terms in Equations 62 and 65 would be replaced by appropriate flux ratios when the experimental algorithm is invoked (cf. Equation 65 above and Equation 54).

Either Equation 61 or 64 may be used to find the radiant interchange factor from A_k to space, A_{N+1}:

$$\text{From Equation 61:} \quad \mathcal{F}_{k,N+1} = \frac{\epsilon_k}{\rho_k} - \sum_{i=1}^{N} \mathcal{F}_{ki} \tag{67}$$

$$\text{From Equation 64:} \quad \mathcal{F}_{k,N+1} = \epsilon_k - \sum_{i=1}^{N} \mathcal{F}_{ki} \tag{68}$$

Equations 67 and 68 will yield identical results only when the proper value of $\mathcal{F}_{kk}$ is used in each case. When Equation 67 is used, the measured interchange factors are found as

$$\mathcal{F}_{ki} = \frac{\epsilon_k \epsilon_i G_k^{(i)}}{J_{oi}}, \qquad i \neq k \tag{69}$$

$$\mathcal{F}_{kk} = \frac{\epsilon_k^2}{\rho_k}\left[1 + \frac{\rho_k G_k^{(k)}}{J_{ok}}\right], \qquad i = k \tag{70}$$

When Equation 68 is used, $\mathcal{F}_{ki}$ is given by Equation 69, while

$$\mathcal{F}_{kk} = \frac{\epsilon_k^2 \, G_k^{(k)}}{J_{ok}} , \qquad i = k \tag{71}$$

Ordinarily, $G_k^{(k)}/J_{ok}$ will be the parameter measured for thermal factors when the excitation target is different from the irradiation target. The measurements will yield $J_k^{(k)}/J_{ok}$ only when the two targets coincide as in the case of solar factor measurements which requires only an irradiation target.

With the use of Equations 67, 69 and 70 or 68, 69 and 71, there is no difficulty in evaluating the space coupling term from experimental measurements.

Comparable expressions result from real surface enclosures. That is, the use of hemispherical fluxes yield the following analogy to Equations 60, 61, 69 and 70:

$$q_{k,net} = \tilde{J}_k - \tilde{G}_k \tag{72}$$

whereby

$$\sum_{i=1}^{N+1} \mathcal{F}_{ki} = \frac{\tilde{\epsilon}_k}{\tilde{\rho}_k} \tag{73}$$

$$\mathcal{F}_{ki} = \frac{\tilde{\epsilon}_k \, \tilde{\epsilon}_i}{\rho_k} \frac{\tilde{J}_k^{(i)}}{\tilde{J}_{oi}} \tag{74}$$

$$\tilde{J}_k^{(i)} = \tilde{\rho}_k \, \tilde{G}_k^{(i)} \qquad k \neq i \tag{75}$$

$$\tilde{J}_k^{(k)} = \tilde{J}_{ok} + \tilde{\rho}_k \, \tilde{G}_k^{(k)} \qquad k = 1 \tag{76}$$

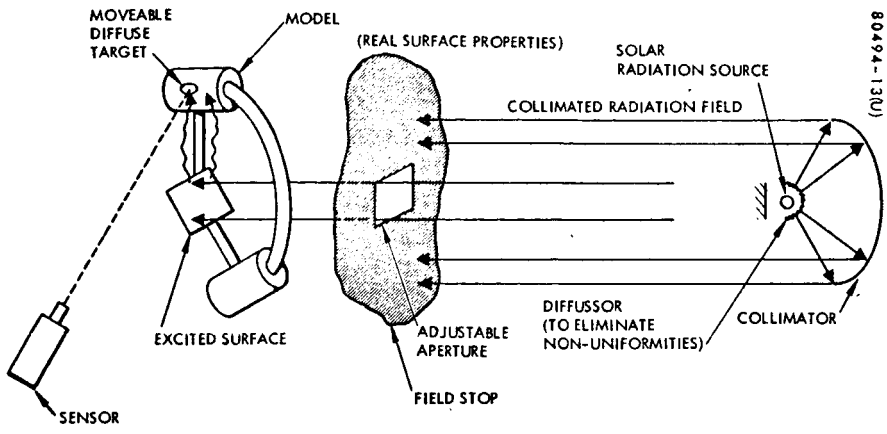

Figure 12. Schematic Representation of Setup for Experimental Determination of Radiant Interchange Factors

The real surface analogy to Equations 63, 64, 69 and 71 is obtained by employing a tilde over any given parameter to designate a hemispherical value.

4.3 SOLAR FACTORS IMPLEMENTATION

The analysis of Section 4.1 applies equally well for the measurement of solar interchange factors with one important exception: the real surface, $\overline{A}_i$, must be excited rather than a diffusely reflecting target, δA_i,. The reason for this is that solar excitation is strongly dependent upon incident and emergent directions unlike thermal excitation which tends to be diffuse. The solar interchange measurements may be carried out on a local-to-local basis, but it appears to be more convenient and accurate to use full surface excitation as shown in Figure 12.

The feasibility and accuracy of solar interchange measurements was established in Reference 1. The only problems which remain relate to optimizing the procedure and the equipment. For example, greater operational flexibility can be obtained by bringing the measurements indoors and using an artificial light source instead of the sun. A brief investigation of the availability of equipment (sources and sensors) is reported below.

An outgrowth of the IR feasibility study has been the realization that the use of a source chopper with a lock-in amplifier may be adapted to solar interchange measurements as well. It appears that Barnes 8-inch radiometer and the PAR lock-in amplifier may be used for both IR and solar measurements. Solar measurements would require the use of a light source having solar spectral properties and the substitution of a different detector in place of the interchangeable Ge:Zn package.

Solar Factors

Source

The source would be a Varian Associates xenon illuminator which contains built-in "transfer optics." With this source stopped down to a 2-degree beam angle at a working distance of 100 inches, it will illuminate a 3.4-inch circle with 1 watt of energy (Figure 13).

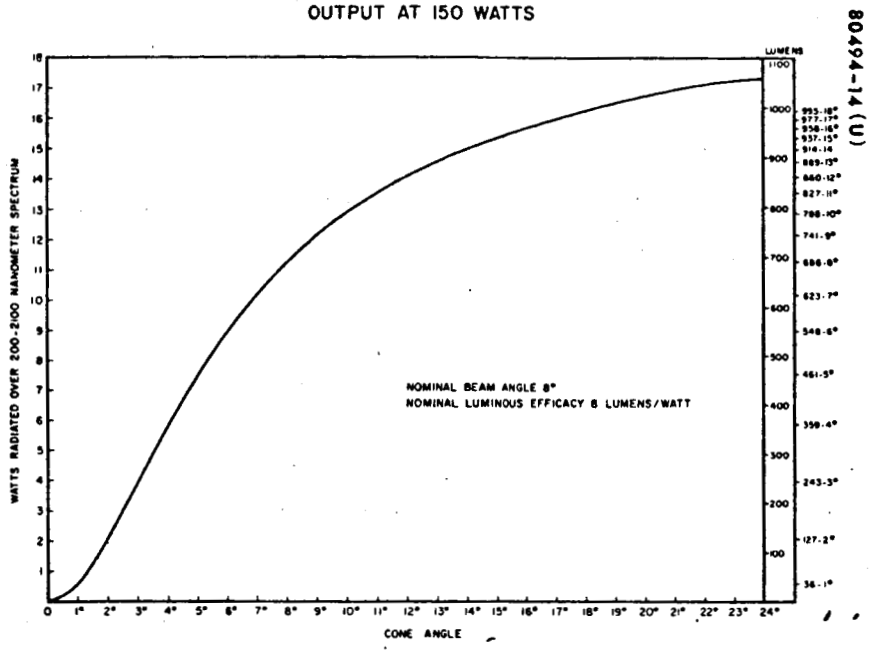

Figure 13. Beam Distribution and Total Radiant Flux

Detector

The only other change would be to exchange a PbS detector for the Ge:Zn used for IR measurements. The PbS detector has an NEPD when used with the xenon lamp of approximately 7×10^{-13} watt/cm^2. Assuming the same geometry as in Figure 12 and assuming the second surface was only 1 inch in diameter approximately the same PD would be obtained. That is

$$PD = 2 \times 10^{-10}$$

or a signal-to-noise = 285 for a Δf of 50 Hz or for the case of $\Delta f = 0.25$ Hz, then the

$$S/N = 4000$$

Again this allows sufficient latitude for radically different geometries and/or working distances.

Alternately, the Spectra Pritchard Model 1970-PR photometer used in Reference 1 may be used for solar factor measurements. The off-the-shelf Model 1970-PR uses an S-11 photomultiplier tube as the detector, but a better spectral match can be obtained by substituting either S-1 or S-14 photomultiplier tubes. The photometer may be used with a digital voltmeter and a constant source to obtain signal-plus-noise data and separate measurements may be taken to obtain noise alone (Reference 1). If a source chopper is employed, the photometer may be phase-locked to the PAR amplifier to obtain signal data with a single measurement.

Solar Irradiation Targets

The specification of a diffuse target for use in solar interchange measurements is much less restrictive than for infrared measurements (see above). Targets which are used for infrared measurements should be suitable for solar measurements, as well. However, occasions may arise in which more highly reflective targets are needed for solar measurements. A high reflectance ($\rho^* = 0.89$) white paint was used as a target finish for the experiments

described in Reference 1 (Alcoa A 14 $A\ell_2O_3$ in Sylvania PS-7 potassium silicate). As a first approximation, the diffuseness of a solar target may be checked by visual inspection. Forty percent of solar energy is contained in the visible waveband (0.4 to 0.7 micron) so that any tendency for a target to become specular in the near infrared (0.7 to 3.0 microns) is apt to produce only a second-order influence. The seriousness of near IR specularity will depend upon the spectral response of a detection system; for example, an S-11 photomultiplier tube does not detect energy above 0.7 micron, so target specularity in the near IR would be unnoticed.

Target size considerations and mounting techniques are essentially the same as those discussed in the section on thermal factor targets.

5.0 FACILITY DESIGN

The principal goal of an experiment is to obtain reliable data. In this regard it is necessary that the data be repeatable as well as capable of interpretation. The experimental determination of radiant interchange factors from model spacecraft will yield reproducible data so long as 1) surface excitation and signal detection are measured on a relative (rather than absolute) basis, and 2) the geometrical orientation of radiant source, model, and detection system can be reproduced. Inasmuch as the experimental algorithm developed in Section 2.0 and the spectral analysis in Section 4.2 provide a rational basis for interpreting data, the remaining discussion of laboratory facility requirements will emphasize the facilities and hardware needed to perform an experiment.

5.1 GEOMETRICAL REQUIREMENTS

The phenomena of solar and thermal radiant transport are strong functions of geometry. If experimental results must be reproducible, then it is necessary that all spatial coordinates defining model orientation, source location and detector location be known. This requirement can be met by using a model mounting fixture that has three rotational degrees of freedom relative to a laboratory reference frame. The source must be mobile and have translational degrees of freedom within the laboratory reference coordinate system and at least two degrees of rotational freedom relative to a point in the laboratory coordinate system. The detector should have the same degrees of freedom as the source.

Figure 14 is a schematic representation of all the elements needed to obtain geometrical reproducibility. A model is shown mounted in an indexed

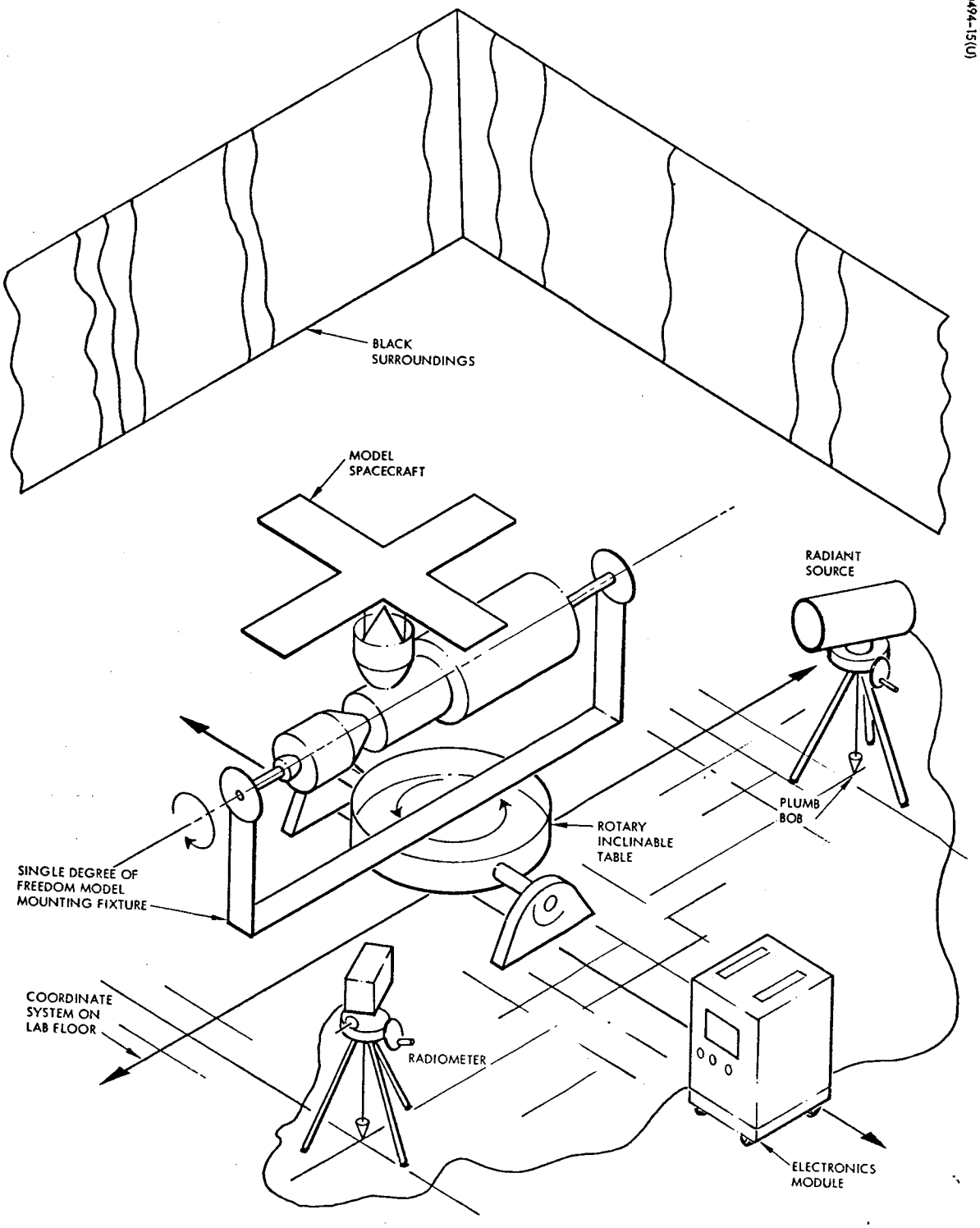

Figure 14. Schematic Representation of Facility for Measuring Radiation Interchange Factors With Model Spacecraft

fixture which permits "rolling" about a model axis. The fixture is mounted to a commercially available rotary inclinable table to permit both "pitching" and "yawing" of the model. The holding (roll) fixture would not be available as off-the-shelf hardware, but could be designed and fabricated without difficulty.

A planar coordinate system scribed on the laboratory floor would provide an inexpensive and convenient means of locating the radiant source and detector relative to the rotary inclinable table. In Figure 14, the source and detector are shown mounted on tripods. The use of tripods provides mobility for the source and detector and a plumb bob suspended from each tripod serves to identify a precise location in the laboratory. Heavy duty tripods are commercially available with indexed heads for mounting and aiming source and detector equipment.

5.2 SPATIAL AND ENVIRONMENTAL REQUIREMENTS

The floor space required for a radiant interchange measurements laboratory should be large enough to allow 360 degrees rotation of the rotary table with a model mounted in place and a minimum of 4 feet clearance on all sides. In addition to the minimum clearance, the floor space should be sufficient to allow the source or detector to be located at least 10 feet from the model in a working zone. A square room about 25 feet on a side with the rotary table at the center would satisfy the last requirement and would be suitable for any model with a maximum dimension of less than about 15 feet.

The measurements laboratory should have black walls, floor, and ceiling to minimize stray radiation. The room should be air-conditioned to minimize water vapor and CO_2 concentration and to avoid problems of volumetric absorption of radiant energy. Care should be exercised to avoid introducing extraneous and random sources of stray radiation such as electronic and electromechanical equipment, soldering irons, incandescent and fluorescent lamps, etc.

6.0 CONCLUDING REMARKS AND RECOMMENDATIONS

The study reported here has examined techniques for measuring radiant interchange factors appropriate to the thermal design of spacecraft. The technique which appears to be most promising is an outgrowth of the method for measuring local solar irradiation of model spacecraft described in Reference 1. The conceptual details presented in Sections 2.0 and 4.0 demonstrate the feasibility of the remote excitation/remote detection method. However, it is not reasonable to expect that the method can be mechanized immediately into a full-blown production procedure for measuring radiant interchange factors. An intermediate period of equipment procurement and familiarization is required to develop operational procedures as well as to evaluate the accuracy of the method. The following sections describe two additional study phases which should be pursued to perfect a procedure for the empirical determination of radiant interchange factors.

6.1 PHASE A: EXPLORATORY MEASUREMENTS AND PROTOTYPE DEMONSTRATION

A 9- to 12-month program should be undertaken with the following goals:

1) Procure equipment needed to measure thermal and solar radiant interchange factors.

2) Perform exploratory experiments on simple configurations to develop operating techniques.

3) Compare experimental results with analytical predictions.

4) Optimize the operating techniques by automating the procedures, improving the accuracy and eliminating restrictions.

5) Document the operating procedures, prepare a complete set of drawings and specifications for the prototype system.

6) Prepare a detailed definition of facility requirements for a maximum automated laboratory for measuring radiant interchange factors.

These goals were identified, originally, in NASA RFP BG721-13-8-11P September 1967, which preceded the present study. Experience gained during the course of this study continues to support the need for such an exploratory study.

The emphasis in this next phase should be placed on the measurement of thermal radiant interchange factors. The measurement of solar interreflection phenomena, discussed in Reference 1 is sufficiently advanced so that very little additional effort is required to meet the goals itemized in the preceding paragraph. On the other hand, the application of infrared technology to the purposes of spacecraft thermal design is certain to lead to problems which can not be anticipated and must be solved by trial-and-error evolution. The solar interchange studies can be initiated as the thermal studies approach completion.

The most important and expensive item of equipment needed for measuring thermal interreflection factors is a radiometer. It will be necessary either to purchase an expensive, high quality instrument or to devote a great deal of time and effort to develop inexpensive components for the purpose of measuring radiant flux. The first possibility appears to be more appropriate to a program of exploratory measurement. The development or invention of flux sensors should be deferred until after the measurement concept has been proved by a demonstration or carried on as a parallel, independent effort. A radiant source, as well as signal processing electronics for the radiometer, will also be needed for exploratory measurements. A three-degree-of-freedom support fixture will not be needed for holding models during this study inasmuch as source-to-model-to-detector orientation can be fixed for the convenience of the experimenter. Simple holding fixtures such as ring stands or optical bench supports can be used for early experiments.

An experiment should be performed using analytically simple models. The model surfaces should be plane and reflect either perfectly diffusely or perfectly specularly. The models should be designed to investigate the following:

1) The accuracy of the remote excitation concept for gray enclosures.

2) The magnitude of a spectral mismatch for a nongray enclosure when surfaces are closely coupled by a direct view ($F_{ij} \neq 0$), and when surfaces are coupled only by a reflection ($F_{ij} = 0$).

Two geometries which satisfy these conditions and which would be simple to fabricate are shown in Figure 15. The execution of the experiment would provide the experience and insight needed to suggest improvements for optimizing test procedures. The accuracy of test results would be determined by comparing experimental data with analytically derived values.

6.2 PHASE B: RADIANT INTERCHANGE MEASUREMENTS — APPLICATION TO SPACECRAFT MODELS

The last phase of this program should be a 6- to 9-month study which culminates with the measurement of radiant interchange factors on a complex spacecraft model having real directional/bidirectional surface properties. This study should have the following goals:

1) Fabricate and test three different enclosure geometrics all of which have one or more real (directional/bidirectional) surfaces: two models models should be geometrically simple and the third should have the complexity of an AAP spacecraft.

2) Compute radiant interchange factors appropriate to the three different enclosures.

3) Correlate the results of analysis and experiment and perform error analysis to explain any differences between analytical predictions and experimental measurements.

4) Document all findings, update operating procedures, and identify additional applications.

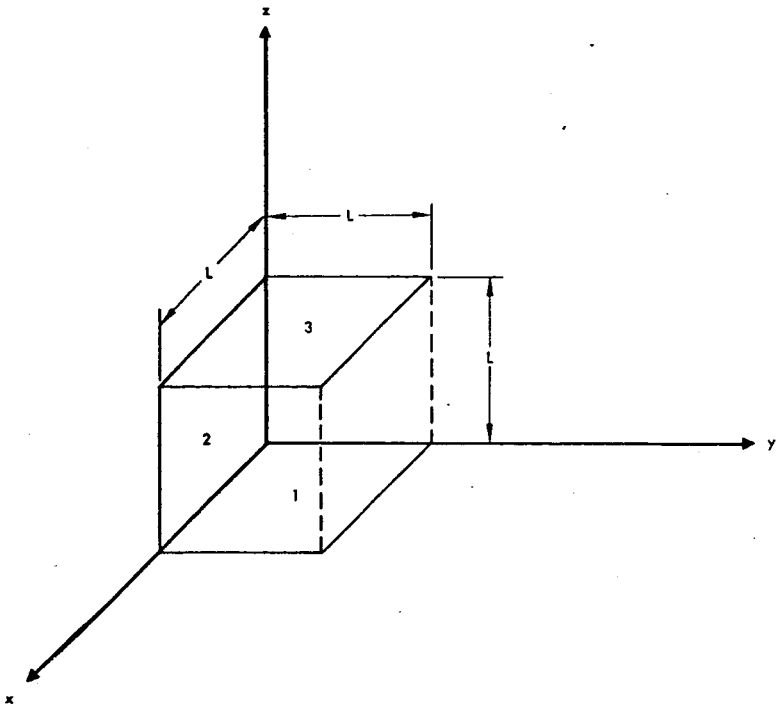

$F_{12} \approx 0$
$F_{13} \approx 0$
SPECTRAL MISMATCH AT A_2

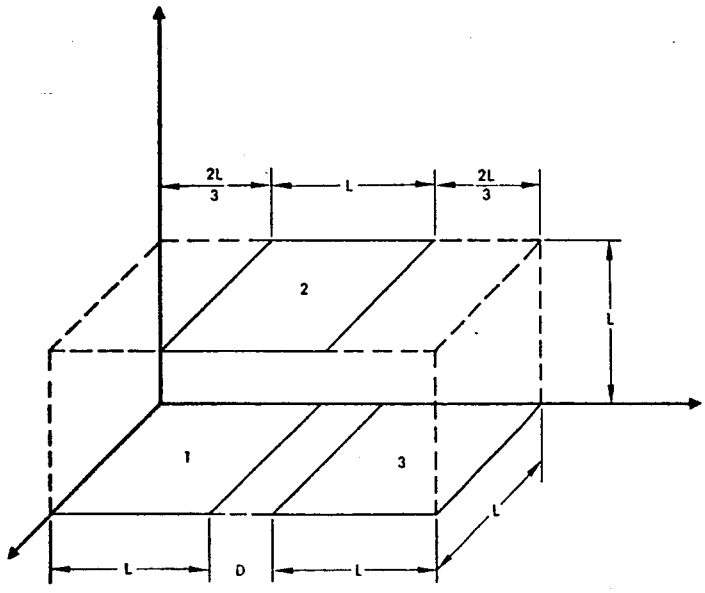

$F_{12} \approx 0$
$F_{13} = 0$
SPECTRAL MISMATCH AT A_2

Figure 15. Model Geometries for Exploratory Test Program.

A_1 and A_3 should be either bare metal or black painted and A_2 should be either a second surface mirror or white painted.

5) Deliver all equipment and models to NASA.

On completion of this second recommended phase, the thermal designer will have a useful tool available for solving difficult problems of radiative exchange. The use of breadboard models tested in a shirt-sleeve environment will serve to make thermal design more of a science and less of an art. The measurement of radiative interchange phenomena will provide the designer with a convenient means of visualizing problems and optimizing problem solutions.

7.0 NOMENCLATURE

A_k = radiating surface area of k^{th} node, square feet

$C_{s,k}$ = solar incidence factor of k^{th} node (ordinarily, the ratio of the projection of the directly irradiated area to the geometric area), nondimensional

E_k = blackbody emissive power, power/ft^2

F_{kj} = conventional shape factor, nondimensional

$\mathcal{F}_{kj}$ = radiation interchange factor, nondimensional

G_k = irradiation at A_k; radiant flux incident at A_k, power/ft^2

$G_k^{(i)}$ = irradiation at A_k due to excitation originating at A_i, power/ft^2

I_{kj} = emergent radiant intensity at A_k directed toward A_j, power/ft^2/ster

J_k = radiosity (diffuse emergent flux) of A_k, power/ft^2

$\tilde{J}_k$ = apparent radiosity (hemispherical emergent flux) of a nondiffuse surface, A_k, power/ft^2

$J_k^{(i)}$ = $\delta_{ki}J_{oi} + \rho_k^d G_k^{(i)}$, partial radiosity of A_k due to excitation at A_i, power/ft^2

J_{oi} = excitation flux of A_i; the component of emergent flux which originates at A_i before accounting for interreflections, power/ft^2

$\mathcal{J}_{kj}$ = πI_{kj}, pseudo-radiosity of A_k, power/ft^2

$\mathcal{J}_{okj}$ = directional excitation flux originating at A_k and directed toward A_j, power/ft^2

N = an integer designating the number of nodal surfaces in an enclosure

$q_{k,net}$ = net radiant heat flux at A_k, power/ft^2

q_{kj} = radiant flux exchanged between A_k and A_j, power/ft^2

r_{jkw} = bidirectional reflectance of A_k for radiation arriving from A_j and redirected toward A_w, nondimensional

S = solar constant; 442 Btu/hr-ft^2

$\mathcal{S}$ = simulated solar constant detected by a radiometer, power/ft^2

T = absolute temperature, $^\circ$R

α_k = hemispherical absorptance of A_k, nondimensional

$\tilde{\alpha}_k$ = apparent hemispherical absorptance of A_k, nondimensional

α_{kj} = directional absorptance of A_k for radiation arriving from A_j, nondimensional

β_{kj} = $J_k^{(j)}/J_{oj}$, the interreflection kernel which designates the influence of excitation at A_j on the partial radiosity of A_k, nondimensional

$\beta_{\substack{kj \\ iw}}$ = the interreflection kernel which designates the contribution to $\mathcal{J}_{kj}$ of directional excitation $\mathcal{J}_{oiw}$, nondimensional

δ_{kj} = δ_k^j = Kronecker delta

ϵ_k = hemispherical emittance of A_k, nondimensional

$\tilde{\epsilon}_k$ = apparent hemispherical emittance of A_k, nondimensional

$\tilde{\epsilon}_{kj}$ = directional emittance of A_k for radiant flux directed toward A_j

$\eta_{\substack{kj \\ i}}$ = $\sum_{w=1}^{N} \epsilon_{iw}\beta_{kj}$, interreflection kernel which designates the contribution to $\mathcal{J}_{\substack{kj \\ iw}}$ of hemispherical excitation at A_i

θ = polar angle measured relative to a surface normal vector, degrees or radians

λ = wavelength, microns

ρ_k = hemispherical reflectance of A_k

ρ_k^d = diffuse component of ρ_k

ρ_k^m = specular (mirror) component of $_k$

ρ_{kj} = hemispherical directional reflectance of A_k toward A_j for uniform hemispherical incidence

$\tilde{\rho}_{kj}$ = apparent hemispherical directional reflectance of A_k toward A_j

σ = Stefan-Boltzmann constant

ω = solid angle, steradians

8.0 REFERENCES

1. Bobco, R. P., "An Experimental Technique for Measuring Local Solar Irradiation With a Model Spacecraft," AIAA Paper No. 68-770, AIAA 3rd Thermophysics Conference, Los Angeles, Calif., June 24-26, 1968.

2. Bevans, J. T., et al, "Prediction of Space Vehicle Thermal Characteristics," Air Force Flight Dynamics Laboratory Technical Report, AFFDL-TR-65-139, Aug. 1965, Wright-Patterson Air Force Base, Ohio.

3. Viskanta, R., "Analysis and Experiment of Radiant Heat Exchange Between Simply Arranged Surfaces," Air Force Flight Dynamics Laboratory Technical Report, AFFDL-TR-67-94, July 1967, Wright-Patterson Air Force Base, Ohio. (Also AD 655335.)

4. Morse, P. M. and Feshback, H., Methods of Theoretical Physics, Part I, 1953, Chapter 8, McGraw-Hill Book Co., Inc., New York, N.Y.

5. "Radiation Interchange Factors: First Quarterly Report 7 June through 1 Sept. 1968," Hughes Aircraft Co. Space Systems Division, SSD 80339M, Sept. 1968, El Segundo, Calif.

6. Bobco, R. P., "Comment on Radiative Exchange Among Non-Lambert Surfaces," by Sarofim, A. F. and H. C. Hottel, Journal of Heat Transfer, Trans. ASME, Ser. C, Vol. 88, No. 1, Feb. 1966, p. 43.

7. Herold, L. M. and Edwards, D. K., "Bidirectional Reflectance Characteristics of Rough, Sintered Metal, and Wire-Screen Surface Systems," AIAA J., Vol. 4, No. 10, Oct. 1966, pp. 1802-1810.

8. Edwards, D. K., et al, "Basic Studies on the Use and Control of Solar Energy," University of California, Los Angeles, Dept. of Engineering, Rept. No. 60-93, Oct. 1960, pp. II-1 to II-61.

9. Wolfe, W. L., (editor), Handbook of Military Infrared Technology, ONR, Dept. of Navy, Washington, D. C., 1965, pp. 491, 498.

APPENDIX

AN EXPERIMENTAL TECHNIQUE FOR MEASURING LOCAL SOLAR IRRADIATION WITH A MODEL SPACECRAFT*

*Aerospace Technology Research Report, December 1967

AN EXPERIMENTAL TECHNIQUE FOR MEASURING LOCAL SOLAR IRRADIATION WITH A MODEL SPACECRAFT

R. P. Bobco, Senior Staff Engineer
Hughes Aircraft Company
Space Systems Division, Thermophysics Department
Los Angeles, California

Abstract

An experimental process is described which is capable of yielding quantitative information on the local solar exposure of spacecraft models. The technique uses models which are geometrically and reflectively similar to some prototype of interest and tests them in a shirtsleeve environment. In addition to the model, the process requires a collimated radiant field which simulates the solar spectrum, a diffusely reflecting target which is small relative to any model surface, a remote radiation detector with a narrow field of view, and a fixture for holding the model in some desired orientation relative to the radiant source. The experimental method does not require any knowledge of shape factors, solar incidence factors, bidirectionsl reflectances, or interreflection coefficients. An analytically tractable model was tested using the sun as the radiant source and a photometer as a detector. A comparison between analytical predictions and experimental results indicates that local solar irradiation on a model may be measured with an accuracy that is comparable to the measurement of surface reflectance. The ease and accuracy of the process recommend its use as an engineering thermal design tool.

Nomenclature

C_{sk} = solar incidence factor from sun to surface δA_k

F_{kj} = shape factor δA_k to δA_j

G_k^* = solar irradiation at δA_k, power/unit area

g_k^* = nondimensional irradiation at δA_k

$I(\vec{r}_k, \vec{\Omega}_{kj})$ = intensity at δA_k emerging toward δA_j, power/unit area/steradian

$J_{k,\lambda}$ = monochromatic radiosity at δA_k, power/unit area/micron

K = instrument constant

$q_{k,net}^*$ = net solar flux at δA_k, power/unit area

R_λ = spectral response of a radiation detector

$\vec{r}_k$ = vector locating δA_k in some reference frame

S = solar constant at zero air mass, power/unit area

$\tilde{S}$ = solar constant at local surface air mass, power/unit area

V_k = meter numeric due to signal from radiation leaving δA_k

$\tilde{V}_k$ = meter numeric due to signal-plus-noise from radiation leaving δA_k

v_k = $\tilde{V}_k - V_k$

α_k^* = solar absorptance of δA_k

β_{ij} = radiant transfer function (interreflection coefficient) δA_i to δA_j

θ_k = angle of incidence measured from surface normal at δA_k

λ = wavelength, microns

ρ_k^* = diffuse (or hemispherical) reflectance at δA_k

ρ_{ikj}^* = bidirectional reflectance at δA_k for energy arriving from δA_i and reflected toward δA_j

τ_λ = monochromatic transmittance of atmospheric air mass

$\vec{\Omega}_{kj}$ = direction vector from δA_k to δA_j

Ω_{jk} = solid angle subtended by δA_j as seen from δA_k

Ω = solid angle

Introduction

The rational thermal design of spacecraft requires detailed quantitative information on the solar and thermal radiant exchange among spacecraft surfaces. These data are required almost at the outset of design so that frequently gross simplifications are made in order to compute various radiation coefficients rapidly. Typical simplifying assumptions include specification of semigray surfaces, diffuse emission, diffuse or specular reflection, and uniformity of radiation over arbitrarily large areas. Even if computer programs were available for more realistic radiation processes, virtually no data are presently available for engineering materials and properties such as directional emittance, bidirectional reflectance, or even the relative proportions of diffuse and specular components of reflectance if the combined reflectance model is chosen. After preliminary design has been completed, it is possible to refine analytical

predictions either by using a mean-to-local algorithm or test data from space-solar simulator tests of prototype spacecraft or thermal similitude models.[1, 2]

This paper reports the results of a study to develop an experimental breadboard technique for obtaining solar heating data in support of analytical design. The study was motivated by the difficulty and uncertainty of making any type of radiative exchange computation, especially for solar heating of geometrically complex spacecraft in the presence of irregular shadow patterns and nonplane surfaces. A procedure was developed 1) using scale models of spacecraft having real surface finishes wherever feasible, and 2) employing a shirtsleeve environment for both test personnel and models. Simple measurements which are both rapid and accurate yield the nondimensional local solar irradiation anywhere on the spacecraft surface. This measured value must be multiplied by the product of local solar absorptance and solar constant, $\alpha^* S$, to obtain the net solar flux at a location. The method does not require computation of solar incidence factors, shape factors, or interreflection coefficients.

Analytical Background

An arbitrary enclosure irradiated by a collimated beam of solar energy is shown in Fig. 1. The direct solar irradiation is discontinuous insofar as some of the surfaces cast shadows on other surfaces; however, by virtue of interreflections among the several surfaces, even regions which lie in a pronounced shadow may be irradiated by indirect solar energy. The solar energy incident on an elemental area δA_k located at $\vec{r}_k$ (relative to some reference frame) may be found by solving the intensity integral equation:[3]

$$I(\vec{r}_k, \vec{\Omega}_{kj}) = \rho^*_{skj} \frac{S}{\pi} C_{sk} + \int_{2\pi} \rho^*_{ikj} I(\vec{r}_i, \vec{\Omega}_{ik}) \cos\theta_k \, d\omega_k \qquad (1)$$

where ρ^*_{skj} is the bidirectional reflectance for solar energy. When the intensity is known elsewhere in the enclosure, the irradiation at δA_k is

$$G^*_k = \sum_{i=1}^{n} \int_{\Omega_{ik}} I_i \cos\theta_k \, d\omega \qquad (2)$$

and the absorbed solar flux is

$$q^*_{k,net} = \sum_{i=1}^{n} \int_{\Omega_{ik}} \alpha^*_k I_i \cos\theta_k \, d\omega \qquad (3)$$

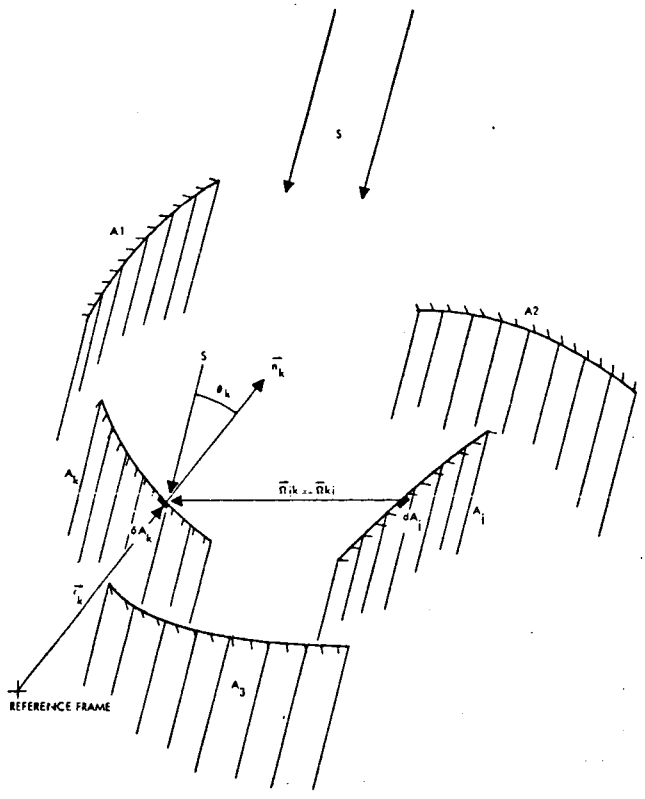

Figure 1. Enclosure of Arbitrary Complexity Irradiated by Collimated Solar Energy

The directional solar absorptance is implied by the coefficient α^*_k in the integrand of Eq. (3). A solution of Eq. (1) and evaluation of Eq. (3) still falls beyond the state of the art of thermal analysis because design data for bidirectional reflection and directional absorption are not available. However, it is possible to measure the irradiation G^*_k of Eq. (2) with comparative ease.

Consider the case where the element δA_k is covered by a diffusely reflecting material with a solar reflectance ρ^*_t, while all other surfaces in the enclosure retain their real bidirectional reflection properties. So long as $\delta A_k \ll A_k$, it will not have a first-order influence on the intensity at any other location in the enclosure even though ρ^*_t and ρ^*_k may be different. As a result, the irradiation G^*_k will remain unchanged. Additionally, the element δA_k will have a radiosity, as well as an intensity, inasmuch as it reflects diffusely:

$$J^*_k = \rho^*_t G^*_k \qquad (4)$$

Next, consider some radiation sensing device placed at a location remote from the enclosure. The detector must have a small field of view and be sensitive to reflected solar energy. If the element δA_k is "viewed" by the detector (Fig. 2), the irradiation of the detector is

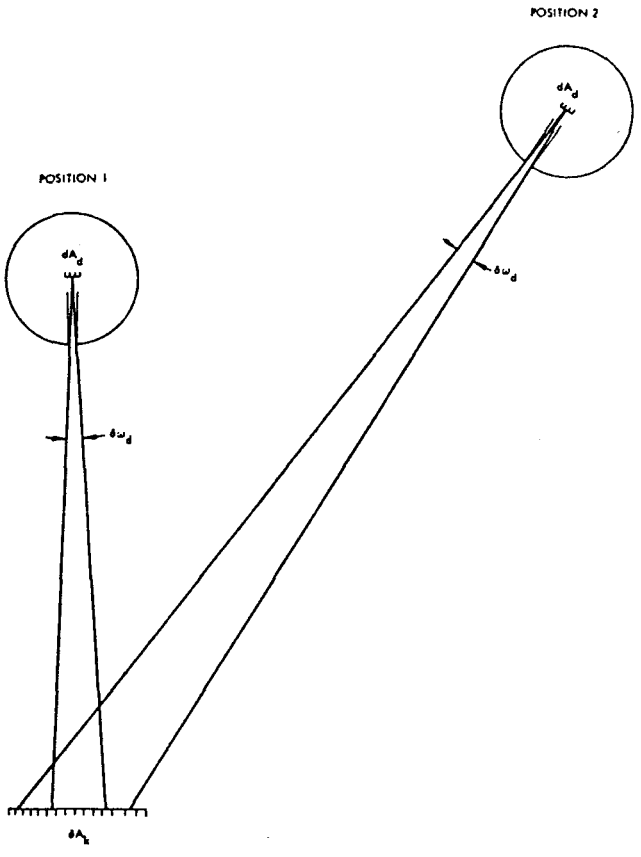

Figure 2. Elemental Area δA_k Viewed by Small Field Radiation Detector in Two Different Orientations

$$G_d^* = \int_{\delta\omega_i} I_k \cos\theta_i \, d\omega_i$$

$$= J_k^* \int_{\delta\omega_i} \frac{1}{\pi} \cos\theta_i \, d\omega_i \qquad (5)$$

Eq. (5) is true so long as δA_k completely fills the field of view and δA_k is a diffusely reflecting surface. It should be observed that when these conditions are met, the irradiation of the detector is independent of the sensor position relative to δA_k. The integral remaining in Eq. (5) is a shape factor and may be considered as an instrument constant. The detector output may be transformed into an electrical signal and from Eqs. (4) and (5) a meter-reading, V_k, is equivalent to

$$V_k = \rho_t^* G_k^* K \qquad (6)$$

where K is an overall instrument constant.

The irradiation, G_k^*, may be recovered from Eq. (6) by a simple calibration procedure. The calibration is made by irradiating an isolated target with a diffuse reflectance ρ_t^* with the same source used to irradiate the enclosure. In the absence of interreflections, the radiosity of the isolated target is

$$J_t^* = \rho_t^* S \cos\theta_t \qquad (7)$$

The orientation of the target may be chosen to provide normal solar incidence (i.e., $\cos\theta_t = 1$) so that the calibration meter reading is

$$V_t = \rho_t^* S K \qquad (8)$$

A nondimensional irradiation, g_k^*, may be defined as the ratio of the in situ-to-calibration measurements:

$$g_k^* = \frac{V_k}{V_t} = \frac{G_k^*}{S} \qquad (9)$$

Presumably, the magnitude of S is known from independent considerations.

The conceptual development above is based on the separation of thermal (i.e., long wave or IR) and solar radiation and the use of a detecting system which is filtered or otherwise insensitive to thermal radiation. The radiation source may be the sun itself or any artificial source which is 1) well collimated, 2) uniform, and 3) spectrally similar to the sun. It is not necessary either to duplicate the magnitude of the solar flux (i.e., $S = 442$ Btu/hr-ft^2) or to place the enclosure in a cold-walled vacuum chamber because enclosure surface temperatures are not germane to the measurements. The conceptual elements required to measure local irradiation are shown in Fig. 3. However, when measurements are made in a typical shirtsleeve environment, it is necessary to take proper account of stray radiation ("noise"). The noise correction requires two sets of measurements: First, irradiation and calibration measurements are made with both the primary source and the noise irradiating δA_k and the isolated target, respectively:

$$\tilde{V}_k = \rho_t^* K (G_k^* + \tilde{G}_k) \qquad (10)$$

$$\tilde{V}_t = \rho_t^* K (S + N) \qquad (11)$$

where $\tilde{G}_k$ is the irradiation due to stray radiation, N. Second, the primary source is removed and the measurements are repeated at δA_k and the isolated target:

$$v_k = \rho^* K \tilde{G}_k \qquad (12)$$

$$v_t = \rho^* K N \qquad (13)$$

From Eqs. 9 through 13, it follows that the desired nondimensional irradiation at δA_k is

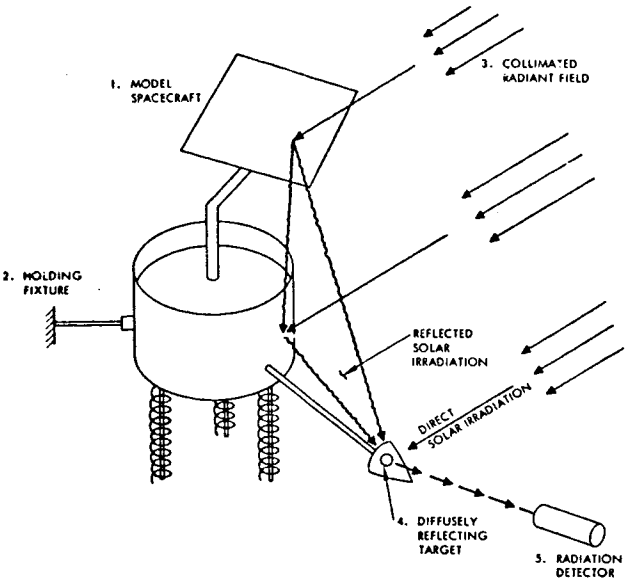

Figure 3. Schematic Representation of Experimental Process for Finding Local Solar Irradiation of Scale Model Spacecraft

$$g_k^* = \frac{\tilde{V}_k - v_k}{\tilde{V}_t - v_t} \qquad (14)$$

The remaining discussion describes a method of implementing this procedure as a useful engineering design tool.

Experimental Procedure

A feasibility study was conducted to establish the availability of hardware for sources and detectors. As a result, it was decided to use the sun as the radiant source, a photometer as the detector, and to construct a field stop to control and minimize the diffuse radiation coming from the sky. In Southern California the climate is reasonably constant, so the sun represents a dependable and inexpensive source of solar radiation. The sea level solar spectral distribution is a close approximation of the zero air mass distribution[4] so that there is no gross spectral mismatch.

The detector chosen was a Spectra Pritchard Model 1970-PR (Photo Research Corporation, Hollywood, California), which has a telescopic viewing system and a choice of functional fields of view ranging from 6 minutes to 2°. A photomultiplier tube with an S-11 spectral response is the photometric transducer. The output signal was measured with a digital voltmeter. The S-11 spectral response is limited to the waveband 0.30 to 0.66 micron; the implication of this response on spectral matching is discussed in a later section.

The analytical development of the procedure shows that the measurement is independent of target reflectance, ρ_t^*. However, in the interest of maximizing the meter reading for locations in deep shadows, a white target was chosen. A diffusely reflecting white paint was mixed for this purpose (Alcoa A14, Al_2O_3 in Sylvania PS-7 potassium silicate). Targets were fabricated by painting 7/8-inch diameter aluminum disks with a 5 to 10 mil thickness of the white paint. The target solar reflectance was measured as $\rho_t^* = 0.89 \pm 0.01$ using a Gier-Dunkle integrating sphere. The spectral reflectance of the targets is shown in Fig. 3. The aluminum disks were bonded to thin disk magnets (1-inch diameter x 1/8-inch thick) for use with sheet metal models.

Although theoretical considerations indicate that the magnitude of stray radiation was not important, experience showed that atmospheric changes could cause the signal-to-noise ratio to vary by a factor of two or three during several hours of testing. A hemispherical tent ("Blackhouse") was designed to act as a field stop to block out the view of the sky everywhere except in the vicinity of the solar disk. The tent was erected on a site in Placerita Canyon in the San Gabriel Mountains about 30 miles north of the Los Angeles International Airport. The tent is about 16 feet in diameter and consists of a fabric-covered steel framework mounted on rollers on a circular track (Fig. 4). Sliding panels on the front of the structure allow a variable aperture for solar irradiation of models mounted in the interior. The Blackhouse has the same degrees of freedom (azimuth and zenith) as an astronomical observatory dome. Signal-to-noise ratios (inside the Blackhouse) of 10 or more have been measured on typical days when the cloud cover has been 10% or less.

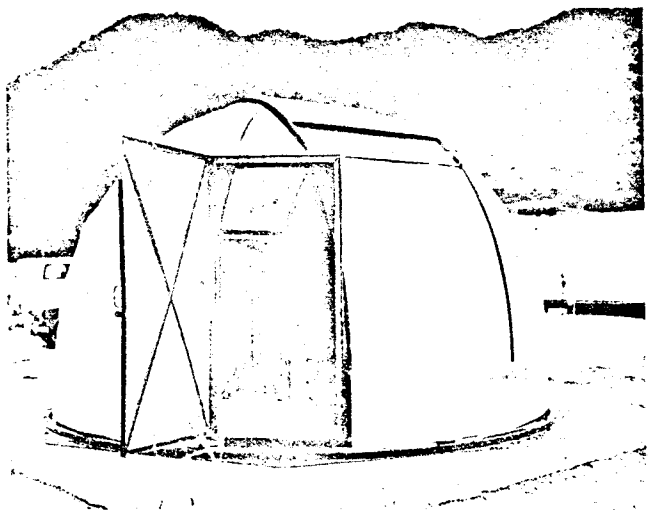

Figure 4. Blackhouse — Inexpensive Test Facility for Measuring Solar Irradiation on Spacecraft Models (Photo ES 4 67-18174)

An equatorial tracker was erected at the center of the Blackhouse base. The tracker serves as a mounting fixture for spacecraft models: a model may be mounted on the tracker at some orientation of interest, and that orientation will be maintained by an electric clock drive as the sun moves across the sky. Manual repositioning of the Blackhouse maintains a fixed view of the sun from the tracker.

With a model mounted on the tracker and the Blackhouse in the desired position, the test procedure followed a straightforward pattern consisting of the following steps:

1. Place the isolated target in the vicinity of the model and measure the combined noise and apparent solar constant.
2. Rotate the Blackhouse (in azimuth) until the solar disk has been obscured from the isolated target and the model.
3. Measure the noise incident on the isolated target.
4. Return the Blackhouse to the original position so that the solar disk directly irradiates the model.
5. Place the target at a location of interest on the model and measure the irradiation (noise plus signal).
6. Repeat Step 5 as necessary.
7. After 10 minutes (or the end of the test, whichever comes first), repeat Steps 1 through 3.
8. With the sun still obscured, place the target on the model at a location measured in Step 5 or 6 and measure the irradiation due to noise.
9. Rotate the Blackhouse so that the sun directly irradiates the model and the isolated target.
10. Repeat Step 1 as a check on atmospheric changes.
11. Continue with the measurements (Steps 5 through 10) until all locations of interest have been measured.

Under typical circumstances, two technicians can make a signal-plus-noise or noise measurement in less than 30 seconds.

The solar constant measurement is made with an isolated target located adjacent to a model. In practice, a specially designed alignment fixture is clamped to the model in a position such that there is no radiant interaction between the model and the fixture. A magnetic target is placed on the fixture table, aligned to normal incidence and the noise plus direct solar irradiation or the noise alone is measured. By using this technique, it is also possible to account for secondary noise interactions between the model and the black-walled interior of the Blackhouse.

The noise measurement techniques evolved during early shakedown tests of the facility. The requirement for "removing" the primary radiant source led to the technique of rotating the Blackhouse to obscure the solar disk. A variety of measurements were made during various atmospheric conditions, and it was established that the background radiation from the sky was virtually constant within about a 60° field of view around the sun. By rotating the Blackhouse about 30° to just barely obscure the solar disk, the noise was found to be within 2% or 3% of the noise magnitude measured when the solar disk occupied the center of the Blackhouse aperture.

Spectral Phenomena

For the sake of discussion, consider some unspecified ideal method for measuring local solar irradiation at an arbitrary location δA_k. The nondimensional solar irradiation of Eq. (9) may be expressed in terms of spectral (monochromatic) quantities as

$$\left\langle g_k^* \right\rangle = \frac{\int_0^\infty S_\lambda \, g_{k,\lambda} \, d\lambda}{\int_0^\infty S_\lambda \, d\lambda} \tag{15}$$

In the real case described previously, it is necessary to take into account the spectral reflectance of the target, $\rho_{t,\lambda}$, the distribution of solar energy, $\tilde{S}_\lambda$, for non-zero air mass, and the spectral response of the phototube, R_λ. Neglect noise and assume a phototube response which is non-zero only in a wave band $\lambda_1 \le \lambda \le \lambda_2$, so that the irradiation determined by photometric means is

$$g_k^* = \frac{\int_{\lambda_1}^{\lambda_2} \rho_{t,\lambda} \, R_\lambda \, \tilde{S}_\lambda \, g_{k,\lambda} \, d\lambda}{\int_{\lambda_1}^{\lambda_2} \rho_{t,\lambda} \, R_\lambda \, \tilde{S}_\lambda \, d_\lambda} \tag{16}$$

All of the factors in Eqs. (15) and (16) are known a priori, except for $g_{k,\lambda}$. In order to estimate the magnitude of errors, it is necessary to have some knowledge of $g_{k,\lambda}$. It is possible to develop insight as to the nature of $g_{k,\lambda}$ without specifying a geometry and merely assuming that all surfaces contributing to $g_{k,\lambda}$ are diffuse reflectors. For this case, it is shown in Ref. 1 that

$$G_{k,\lambda} = \left[S_\lambda C_{s,\lambda} + \sum_{j=1}^{n} J_{j,\lambda} F_{kj} \right] \qquad (17)$$

The spectral radiosity, $J_{j,\lambda}$, is known to have a solution of the form

$$J_{j,\lambda} = S_\lambda \rho_{j,\lambda} \left[C_{s,j} + \sum_{i=1}^{n} C_{s,i} \frac{\rho_{i,\lambda}}{\rho_{j,\lambda}} \beta_{ij,\lambda} \right] \qquad (18)$$

where $\beta_{ij,\lambda}$ is a transfer function which may be found by matrix inversion or the solution of an integral equation. Combining Eqs. (17) and (18),

$$G_{k,\lambda} = S_\lambda \left[C_{s,k} + \sum_{j=1}^{n} \rho_{j,\lambda} F_{kj} f(\lambda, \text{geom.}) \right] \qquad (19)$$

The form of Eq. (19) indicates that the spectral irradiation at δA_k is influenced primarily by the direct solar incidence and secondarily by the reflectance $\rho_{j,\lambda}$ at other surfaces. The potential for a spectral mismatch lies in S_λ and $\rho_{j,\lambda}$. A worst case would arise if δA_k lay in a shadow ($C_{s,k} = 0$) and had a good view of some surface A_j ($F_{kj} \to 1.0$). In such an instance,

$$G_{k,\lambda} \approx S_\lambda \rho_{j,\lambda} \qquad (20)$$

Eq. (20) may be used in Eqs. (15) and (16) to obtain a quantitative measure of a spectral mismatch arising from a photometric technique for measuring irradiation. From Eqs. (15) and (20), find

$$\left\langle g_k^* \right\rangle \approx \frac{\int_0^\infty S_\lambda \rho_{j,\lambda} \, d_\lambda}{S} \equiv \rho_j^* \qquad (21)$$

that is, the ideal irradiation at δA_k is strongly influenced by the solar reflectance of A_j. The corresponding expression for the photometric measurement is

$$g_k^* \approx \frac{\int_{\lambda_1}^{\lambda_2} \rho_{t,\lambda} \rho_{j,\lambda} R_\lambda \tilde{S}_\lambda \, d_\lambda}{\int_{\lambda_1}^{\lambda_2} \rho_{t,\lambda} R_\lambda \tilde{S}_\lambda \, d\lambda} \qquad (22)$$

Eqs. (21) and (22) provide a simple basis for estimating spectral mismatch.

Fig. 5 shows the spectral reflectance of several spacecraft thermal control surfaces and the response waveband of an S-11 phototube.[5] It is apparent that little or no error would arise from a gray reflecting surface. However, surfaces such as gold plate and white paints which have a strong spectral dependence are apt to influence the measurement of irradiation.

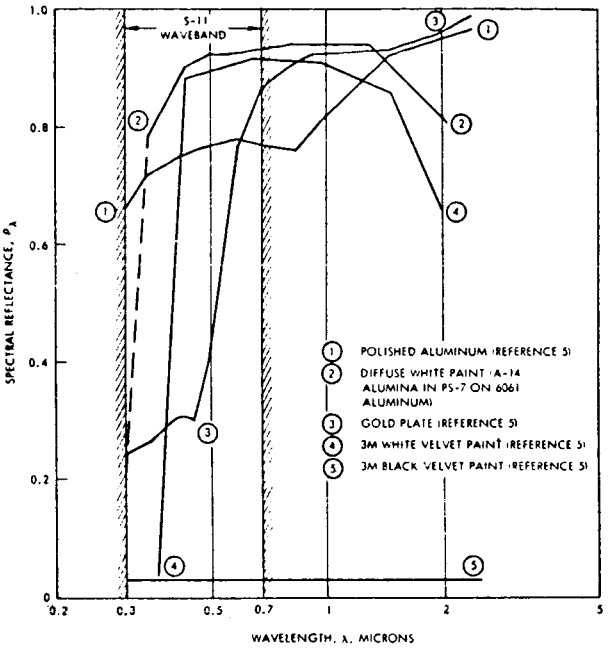

Figure 5. Spectral Reflectances of Typical Spacecraft Thermal Control Surface Finishes

The spectral solar flux was estimated from data given in Ref. 3 for an air mass $m \approx 1.2$ (an approximation for the latitude of Los Angeles during the spring and summer months). It was assumed that

$$\tilde{S}_\lambda = \tau_\lambda S_\lambda \qquad (23)$$

$$\tau_\lambda = 0.4, \quad 0.30 \le \lambda \le 0.40 \ \mu$$
$$\tau_\lambda = 0.7, \quad 0.40 < \lambda \le 0.70 \ \mu \qquad (24)$$

The approximate spectral distribution of solar flux, $\tilde{S}_\lambda$, is shown normalized to the peak value in Fig. 6; also shown is the spectral response, R_λ, of an S-11 photomultiplier tube[6] and the product

$$\tilde{\tilde{S}}_\lambda = \rho_{t,\lambda} R_\lambda \tilde{S}_\lambda \qquad (25)$$

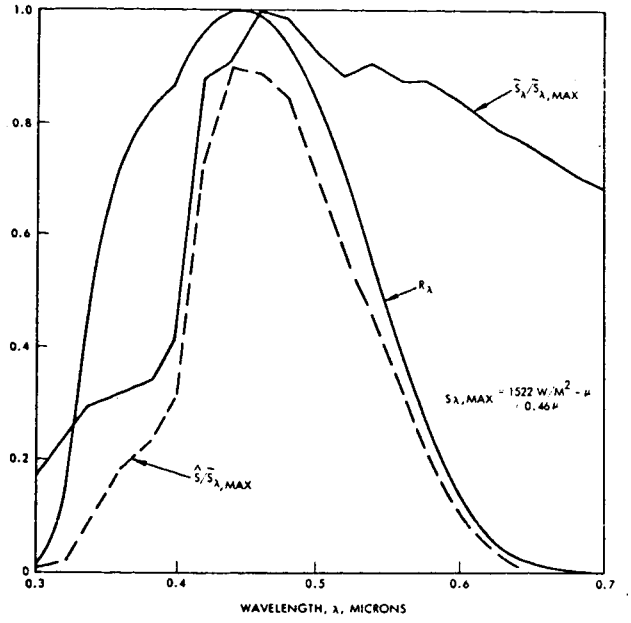

Figure 6. Approximate Solar Spectrum $\tilde{S}_\lambda$ for Air Mass ≈ 1.2; Spectral Response, R_λ, of S-11 Photomultiplier; Apparent Solar Spectrum, $\tilde{S}_\lambda = \tilde{S}_\lambda R_\lambda$, for Photometric Tests

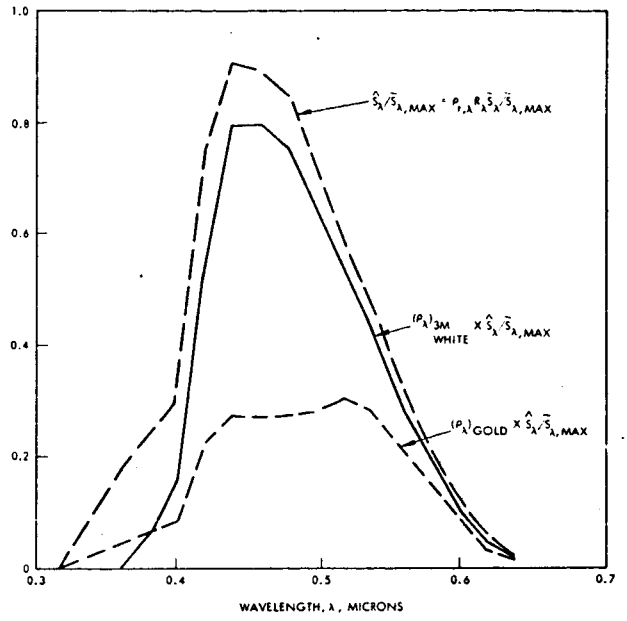

Figure 7. Reflection Spectra of 3M White Velvet Paint and Gold Plate Irradiated by Apparent (Photometric) Solar Spectrum

This last parameter represents the apparent spectral solar flux available for the experimental procedure described previously.

Eq. (22) was evaluated by graphical integration for the spectral reflectances of gold plate and 3M White Velvet paint using data from Fig. 5. The graphical construction is shown in Fig. 7, and the results are tabulated below:

Surface	Photometric Response, Eq.(21)	Solar Response[5]
3M White Velvet	0.79	0.79
Gold Plate	0.39	0.78

It appears that the spectral response of an S-11 photomultiplier tube imposes some restrictions on the use of certain materials when measuring solar irradiation. In practice, the restrictions are not so severe because:

1. Other materials may be used to simulate gold plate (e.g., aluminized mylar).
2. The irradiation implicit in Eq. (21) is based on a shape factor $F_{kj} \to 1.0$, a geometrical case which is improbable in spacecraft design.
3. Photomultiplier tubes or sensors may be used with a broader response waveband (e.g., S-1, S-14).

This discussion is intended to demonstrate that some caution must be exercised in applying the remote sensing procedure to measuring solar irradiation; proposed surface finishes should be screened before using them with a spectrally selective radiation detector.

Comparison of Analytical and Experimental Results

An experiment was performed to demonstrate the utility and accuracy of photometric measurements of solar irradiation. A model was constructed which was geometrically simple and had analytically tractable reflection characteristics. The model (Fig. 8) consists of three mutually orthogonal square planes which are, respectively, a diffusely reflecting white paint, a specularly reflecting polished aluminum, and a dull black paint. The white paint was identical to the paint used for the targets ($\rho^*_{white} = 0.89 \pm 0.01$), the aluminum surface was polished according to Hughes Aircraft Company Specification HP 9-29 ($\rho^*_{al} = 0.15$), and the black surface was painted with 3M Black Velvet ($\rho^* = 0.02$). Although the plates were mutually orthogonal, they did not intersect; the plates were separated for reasons of analytical tractability. The analysis of Ref. 1 showed that a simple algorithm could be used to solve for local radiant phenomena with accuracies comparable to more sophisticated computations. However, the simple algorithm lost accuracy in the immediate vicinity of corners or edges. Surface intersections were eliminated on the model to avoid any problems arising from analytical shortcomings.

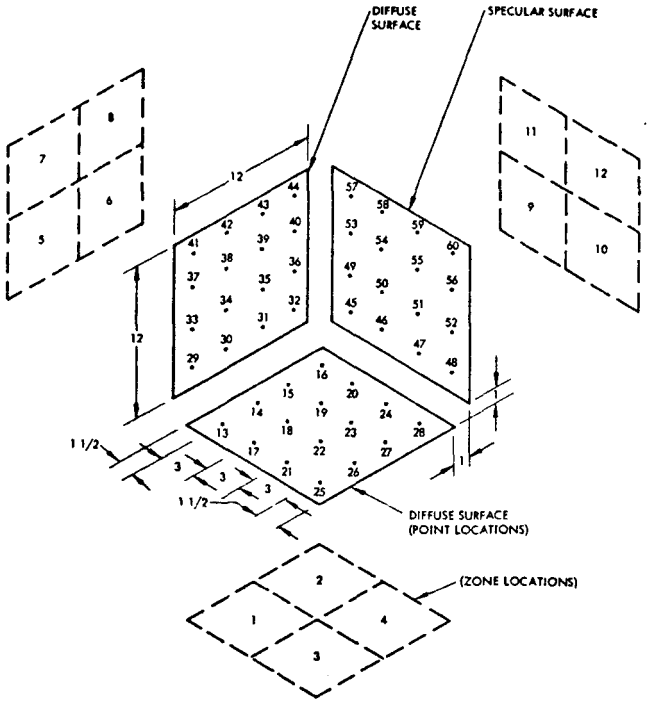

Figure 8. Schematic Representation of Three Mutually Orthogonal Square Plates Used as Test Model

Zones shown in exploded view; point locations in isometric perspective; all plates of equal size and spatially separated along edges

Calculations were made to obtain the non-dimensional solar irradiation at 16 locations on each surface (see Fig. 8). The zones are shown numbered consecutively from 1 to 12, while the locations at which both calculations and measurements were made are numbered 13 to 60, inclusive. No calculations were made for locations in the 1-1/2 inch strip adjacent to a plate edge which was closest to another plate; these strips were avoided to obtain further assurance of valid analytical results. The algorithm used for computation was

$$g_k^* = C_{s,k} + \sum_{i=1}^{8} \rho_i^* \, \bar{g}_i^* \, \varphi_{ki}$$

$$k = 13, 14, \ldots, 60 \qquad (26)$$

$$\rho_i^* \, \bar{g}_i^* = \sum_{j=1}^{8} \rho_j^* \, \bar{C}_{s,j} \, \beta_{ij}^*$$

$$i = 1, 2, \ldots, 8 \qquad (27)$$

where

g_k^* = local nondimensional irradiation at any of the 48 positions on the three surfaces

$\bar{g}_i^*$ = mean value of irradiation in a zone on a diffusely reflecting surface

$C_{s,k}$ = local solar incidence factor

$\bar{C}_{s,j}$ = mean solar incidence factor

ρ^* = diffuse reflectance

φ_{ki} = exchange factor accounting for direct view plus specular reflection of A_i as seen from δA_k

β_{ij}^* = transfer function accounting for all diffuse and specular interreflections among zones

The exchange factors were all of the form

$$\varphi_{ki} = F_{ki} + \rho_m^* \, F_{ki(m)}$$

where ρ_m^* is the reflectance of the specular surface F_{ki} and $F_{ki(m)}$ are shape factors to zones and zone images, respectively. All shape factors were evaluated using CONFAC II.[7] The transfer functions were found by inverting the transfer matrix associated with script eff formulations.[8,9]

Computations and measurements were made for the case in which only one surface at a time was directly irradiated while the other two surfaces were parallel to the collimated input. This arrangement provided solar incidence factors

$$C_{s,k} = \bar{C}_{s,i} = 1.0$$

on the directly irradiated points and zones and

$$C_{s,k} = \bar{C}_{s,i} = 0$$

at the remaining locations and zones. Three sets of computations and measurements were made as follows:

1. White surface directly irradiated, black and aluminum surfaces dark
2. Black surface irradiated, aluminum and white surfaces dark
3. Aluminum surface irradiated, white and black surfaces dark

Analytical and Experimental Results

Measurements were made both in mid-June and early December 1967, to investigate repeatability with 1) extreme seasonal variations of solar irradiation and 2) the use of different operating personnel. Analytical predictions and experimental results are summarized in Table 1 for the case of normal solar incidence on the white

TABLE 1. COMPARISON OF ANALYTICAL AND EXPERIMENTAL RESULTS

Normal solar incidence on white surface; black and aluminum shaded; local nondimensional irradiation, g_k^*

Surface	Location	Analytical Value	Experimental Results		
			June (Nominal)	December (Nominal)	Maximum Deviation from Anal.
White	13	1.001	0.98	0.99	-0.02
	14	1.001	0.98	0.99	-0.02
	15	1.001	1.01	1.00	+0.01
	16	1.001	1.02	1.00	+0.02
	17	1.001	0.97	1.02	±0.03
	18	1.001	0.99	1.01	±0.02
	19	1.001	1.01	1.02	+0.02
	20	1.001	1.02	1.00	+0.02
	21	1.000	0.98	0.99	±0.03
	22	1.001	1.01	1.00	+0.03
	23	1.001	1.01	1.00	+0.04
	24	1.001	1.02	1.00	+0.03
	25	1.000	0.98	1.04	+0.04
	26	1.000	1.01	1.05	+0.05
	27	1.000	1.00	1.06	+0.06
	28	1.000	1.02	1.03	+0.03
Black	29	0.220	0.25	0.24	+0.04
	30	0.277	0.31	0.28	+0.03
	31	0.282	0.31	0.29	+0.03
	32	0.247	0.26	0.25	+0.02
	33	0.152	0.17	0.15	+0.02
	34	0.192	0.20	0.20	+0.01
	35	0.205	0.22	0.21	+0.02
	36	0.191	0.20	0.19	+0.01
	37	0.105	0.11	0.09	-0.02
	38	0.128	0.14	0.13	+0.02
	39	0.139	0.15	0.14	+0.01
	40	0.135	0.15	0.13	+0.02
	41	0.073	0.08	0.08	+0.01
	42	0.088	0.09	0.09	+0.01
	43	0.094	0.11	0.09	+0.02
	44	0.094	0.10	0.09	+0.01
Aluminum	45	0.221	0.23	0.22	+0.01
	46	0.276	0.30	0.28	+0.03
	47	0.275	0.30	0.28	+0.03
	48	0.220	0.22	0.22	±0.01
	49	0.147	0.15	0.14	-0.01
	50	0.181	0.18	0.20	+0.02
	51	0.181	0.18	0.19	+0.02
	52	0.147	0.15	0.14	-0.01
	53	0.097	0.09	0.11	+0.02
	54	0.113	0.10	0.11	-0.01
	55	0.113	0.11	0.13	+0.02
	56	0.096	0.10	0.09	±0.01
	57	0.064	0.06	0.07	+0.01
	58	0.072	0.07	0.07	-0.01
	59	0.072	0.07	0.07	-0.01
	60	0.064	0.06	0.06	-0.01

diffuse surface ($C_{s,\,black} = C_{s,\,alum} = 0$). Additional measurements were made for normal solar incidence on 1) the black surface, others shaded, and 2) the polished aluminum surface, others shaded, but the tabulations are omitted for the sake of brevity. Typical results for the case of normal solar incidence on the black surface follow:

Black:

Analytical	1.0003 to 1.0012
Experimental	1.00 to 1.03

White:

Analytical	0.0064 to 0.0017
Experimental	0.02 to 0.005

Aluminum:

Analytical	0.0078 to 0.0016
Experimental	0.02 to 0

For the case of normal solar incidence on the specular aluminum surface, the analysis predicts a nondimensional irradiation of unity at all locations on the aluminum surface and zero irradiation at all other locations. The experimental results at the aluminum surface varied from unity to 1.05 and at the other surfaces from zero to 0.03.

The experimental data summarized in Table 1 represent nominal values based on an average solar constant measured immediately before and immediately following measurements at four locations. The maximum deviation shown in Table 1 represents the worst case of analytical and experimental disagreement based either on a "before" or "after" measurement of the solar constant. The typical experimental results summarized above for normal incidence on the black and aluminum surfaces are based on nominal values.

Discussion

The good agreement of analytical and experimental results demonstrated the utility of photometric testing as a thermal design tool. It appears possible to measure local solar irradiation on complex surfaces with accuracies that are commensurate with those implicit in computing engineering radiation phenomena. That is, it is conservative to claim that

$$\left| \left(g_k^*\right)_{measured} - \left(g_k^*\right)_{computed} \right| \leq 0.05$$

A mean value for the absolute value of the maximum deviation listed in Table 1 is closer to 0.02 than 0.05, but either figure appears to be reasonable for thermal design applications.

The smallness of the deviation between analysis and experiment eliminates the motivation for a lengthy error analysis. However, experience accumulated here indicates that the sources of error, in their order of importance, are:

1. Short-term variations in the solar constant
2. The number of significant figures available for readout of noise and low-level irradiation
3. Instrumentation stability
4. Alignment of model surfaces to the precise orientation implicit in an analytical formulation
5. Placement of a target on the precise location implicit in an analytical formulation

These items are discussed below to establish a quantitative insight into their influence.

Solar Constant

It was not unusual to observe a 10% variation in the magnitude of the signal-plus-noise associated with a solar constant measurement during a 10-minute interval. In a number of instances, these variations could be correlated with the sound of a gust of air or the movement of a truck, both of which tend to stir up dust. On a few occasions, the passage of a jet airplane created a contrail; but, most often, the variation was attributed to unknown atmospheric disturbances. This particular source of error could be eliminated either by monitoring the sun and noise continuously during a test or moving to an indoor facility for testing. Inasmuch as the present technique is based on relative (not absolute) measurements, all variations in the reference irradiation have a first-order influence on model irradiation.

Instrumentation Readout

All of the measurements reported here were exploratory in nature, so that operating procedures were subject to a wide variety of improvisations. One degree of freedom which was overlooked was the total signal-plus-noise amplification available in the photometer and digital voltmeter electronics. Both electronic systems were set at an amplification level corresponding to a 0.000 to 0.100 millivolt readout. Typical signal-to-noise ratios for a solar constant measurement were 0.150/0.010, while for a model location measurement in a shaded location (e.g., No. 39 of Fig. 8 and Table 1) signal-to-noise ratio was 0.015/0.001. An additional four decades of electronic amplification and three decades of optical amplification were available for greater precision, but they were never utilized.

Instrumentation Stability

Although the electronics for both the photometer and voltmeter appeared to have satisfactory stability, a drift of ±0.001 in the meter reading

was not unusual over a 30-minute interval. This characteristic was discovered during the December tests, and thereafter the instrumentation was calibrated every 20 minutes.

Model Surface Orientation

Normal solar incidence on a given surface was obtained by visual inspection. It is believed that alignment errors of ±2° or less could be maintained during the course of a test. Orthogonality of the model surfaces as mounted on a holding fixture may have contributed an additional error of ±2°. If these errors are cumulative, the effect would be to underestimate the directly irradiated surface reading by about 0.002 times the meter reading; at the "shaded" surfaces, a direct input of about 0.07 times the meter reading would be superimposed on the reflective input to such a surface.

Target Placement

The 48 locations identified in Fig. 8 were marked with pencil on the model test surfaces. During a test, the magnetic targets were placed on the small pencil marks and the photometer focused on the center of the target. It is estimated that a 0.50-inch location error may have occurred using this procedure. Detailed measurements over a directly irradiated surface showed that a 0.50-inch location error could lead to a measurement error of ±0.002 in the meter output.

All sources of error identified here can be eliminated or at least minimized if circumstances should require greater accuracy. However, it is questionable whether greater accuracy is required for thermal design when the nondimensional irradiation is used in Eq. (3) as

$$q^*_{k,\,net} = \alpha^*_k \, g^*_k \, S$$

and typical limits of accuracy for solar absorptance, α^*_k, are ±0.01 and for the solar flux are ±2%.[10, 11] The importance of such errors is further minimized if a heat balance is used to solve for temperature in the form

$$T_k \approx \left(\frac{\alpha^*_k \; S \; g^*_k}{\epsilon_k \; \sigma} \right)^{1/4}$$

Conclusions

A simple experimental process has been developed for measuring the solar energy incident on systems of surfaces which are arbitrarily complex, both geometrically and in reflective properties. The accuracy of the process is on a par with the state of the art of other thermal design measurements and computations, and the process accuracy may be improved as necessary to meet changing requirements. The process permits testing to take place in a shirtsleeve environment which is comparable to breadboard development and testing of electronic systems.

The essential features of the irradiation measurement process include the use of a collimated, uniform radiant source with specified spectral properties, a model with geometric and reflective similarity to some prototype of interest, a small diffusely reflecting target which may be placed at any location of interest on the model, a remote viewing radiation sensor with a suitable spectral response, and appropriate readout and recording equipment. The process was developed and verified by using the sun as a radiant source, and off-the-shelf hardware (a photometer and digital voltmeter) for remote sensing and readout. A simple, analytically tractable model was constructed, analyzed, and tested to obtain quantitative insight to the accuracy of the process. In particular, this study demonstrated the following:

1. There is no spectral sensitivity to measuring local solar irradiation so long as surface properties are screened relative to the spectral response of the sensor

2. There is no apparent error associated with seasonal variations when the sun is used as the radiant source

3. No special skills are needed by operating personnel when off-the-shelf hardware is used

The real merit of the process lies in its application to geometrically complex systems with real surface properties. Fig. 9 shows a model of a helix antenna proposed for use on a space vehicle as an example of an analytically intractable configuration. The antenna was mounted on a proposed spacecraft model, and the shadow patterns and local irradiation values were established for half a dozen vehicle-to-sun orientations in about 3 days of testing, including setup. As a result of these tests, it was possible to compute local temperatures, thermal stress, and a variety of associated phenomena in a fraction of the time and with far greater precision than would have been possible from analytical considerations alone.

Finally, it is worth remarking that the process described here may be used to measure local solar interreflection factors as well as local irradiation. The mathematics supporting the interreflection factor application, together with a description of process modifications, are too lengthy to describe here and will be the subject of a future publication.

Acknowledgments

This study was carried out under Hughes Aircraft Company's general research sponsorship. The author gratefully acknowledges the assistance of Messrs. L. J. Nolte and R. J. Wensley, who first conceived the notion of

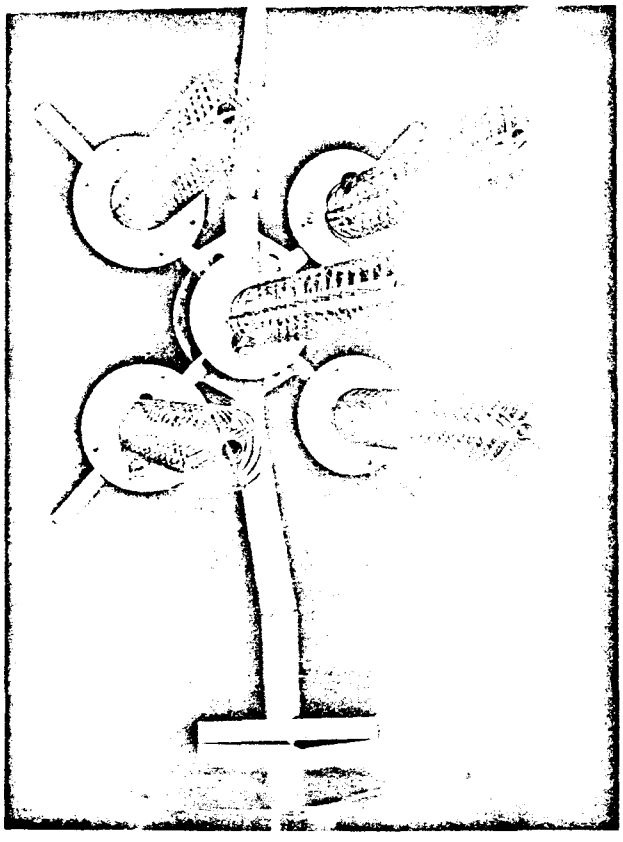

Figure 9. Helix Antenna as Example of Analytically Intractable Configuration Which is Easily Tested (Photo ES 4 67-18192)

solar-thermal bench testing; D. W. Thomas, A. F. Beardsley, and W. H. May, who helped develop the experimental details; and Miss Anne DiFiore, who programmed the analytical formulation.

References

1. Bobco, R. P., Allen, G. E., and Othmer, P. W., "Local Radiation Equilibrium Temperatures in Semigray Enclosures," J. Spacecraft, Vol. 4, No. 8, August 1967, pp. 1076-1082.

2. Vickers, J. M. F., "Thermal Scale Modeling," Astronaut. Aeron., Vol. 3, No. 5, May 1965, pp. 34-39.

3. Bevans, J. T. and Edwards, D. K., "Radiation Exchange in an Enclosure with Directional Wall Properties," Trans. ASME, Ser. C., J. Heat Transfer, Vol. 87, No. 3, August 1965, pp. 388-396.

4. Gast, P. R., "Thermal Radiation-Solar Radiation" Ch. 16, Sec. 3, Handbook of Geophysics, revised edition, 1961, The MacMillan Co., New York.

5. Blair, P. M., Jr., Comparison of Absorptance of Spacecraft Thermal Control Surfaces under Solar, Xenon Arc, and Mercury Xenon Arc Illumination, Hughes Aircraft Co., Culver City, Calif., Rept. TM-863, June 1966.

6. RCA, Electron Tube Handbook, Photosensitive Device Section, HB3, Radio Corporation of America, Harrison, New Jersey.

7. Toups, K. A. A General Computer Program for the Determination of Radiant Interchange Configuration and Form Factors — CONFAC II, North American Aviation, Inc., Downey, Calif., SID Rept. 65-1043-2, October 1965.

8. Ishimoto, T. and Bevans, J. T., "Method of Evaluating Script F for Radiant Exchange within an Enclosure," AIAA J., Vol. 1, No. 6, June 1963, pp. 1428-1429.

9. Bobco, R. P., "Radiation Heat Transfer in Semigray Enclosures with Specularly and Diffusely Reflecting Surfaces," Trans. ASME, Ser. C., J. Heat Transfer, Vol. 86, No. 1, February 1964, pp. 123-130.

10. Edwards, D. K., et al., "Integrating Sphere for Imperfectly Diffuse Samples," J. Opt. Soc. Am. (Applied Optics), Vol. 51, November 1961, pp. 1279-1288.

11. Johnson, F. S., "The Solar Constant," J. Meteorol. Vol. II, No. 6, December 1954, pp. 431-439.